NTNU – Trondheim
Norwegian University of
Science and Technology

Friction Factor Model and Interpretation of Real Time Data

Christine Frafjord

Petroleum Geoscience and Engineering
Submission date: May 2013
Supervisor: Pål Skalle, IPT
Co-supervisor: S. Ahmad Mirhaj, Aker

Norwegian University of Science and Technology
Department of Petroleum Engineering and Applied Geophysics

i. Acknowledgement

Several sources of information have been used to make present report. I would like to thank my academic advisor, Professor Pål Skalle, for guidance during the work on the report. I am thankful for the help from Professor Sigbjørn Sangesland. I would also like to thank Professor Bernt Aadnoy, who inspired me to work with his torque and drag model. Lastly, thanks to Statoil for providing selected data available through Discovery Web for Department of Petroleum Engineering and Applied Geophysics (IPT).

ii. Summary

The interest in torque and drag issues has over the last years increased when the complexity of wells drilled has become higher. The petroleum industry continually expands the extended reach drilling envelope, which forces the industry to find new methods and tools to better interpret friction because of the central role it has in achieving successful wells. The importance of model friction is further elaborated in chapter 2.

Present report contains an investigation of the theory in Aadnoy`s friction model in terms of possibilities and limitations. The theory has been used as foundation to build an Excel calculation tool to model friction. To study the model, three field cases have been applied with the friction model. Excel program which is applied in this work can be provided by the author of the present report to readers if requested.

Even though the limitations listed in chapter 6 do exist, the model has been shown to be applicable to get an indication on the downhole situation. By comparing the result from two different well sections in the same well, it was possible to evaluate high borehole friction because of hole cleaning issues. However, one important issue detected during present work, is that the modeled friction factor is highly sensitive to changes in hook load measurements in shallow sections with small inclination and little drillpipe downhole. This is an issue that demands awareness during application of the model because it is a source of risk to get misleading results.

For future work, the model should be improved in a more powerful tool than Excel with added features built in to it to reduce constrains in the model, which are mentioned in chapter 6. As continuation of present work the analytical model should also be further investigated by using real wells with more quantitative data and qualitative measured data.

Table of content

Acknowledgement …….. i

Summary…… ii

1 Introduction 1

1.1 Motivation 1

1.2 Approach 2

Part A: Review of basic theory 3

2 Review on work with torque & drag models and today`s applications 3

3 Physical principles behind the friction model and methodology of model friction factor 6

3.1 Relevant activities during drilling of a well 6

3.1.1 Reaming 6

3.1.2 PRS test 7

3.1.3 Tripping 9

3.1.4 Drilling 9

3.2 Wellbore trajectory 10

3.3 Buoyancy factor 10

3.4 Friction factor 11

3.5 Drag 14

3.5.1 Drag in straight sections 14

3.5.2 Drag in curved sections 15

3.6 Torque 16

3.6.1 Torque in straight sections 16

3.6.2 Torque in curved sections 17

3.7 Combined axial and rotational motion 17

3.8 Method to model friction with selected model 18

3.8.1 Input data to the friction model 22

3.8.2 Methodology of the friction modeling demonstrated with example 6.4 from the book Mechanics of Drilling 23

3.8.3 Quality control 29

3.8.4 Concerns in calculations 29

Part B: Application field data to verify model of friction factor 31
4 Field data background 31
4.1 Field data of well C47 31
4.2 Field data of well A12/A12 T2 37
4.3 Field data of well A5 39
5 Results of selected friction model 43
5.1 Drag results from the 17 ½" section and the 12 ¼" section of well C47 43
5.2 Drag results for the 17 ½" section of well A12/A12 T2 46
5.3 Drag results for the 17 ½" section of well A5 48
6 Evaluation of selected friction model 50
6.1 Evaluation of result from well C47 50
6.1.1 Compare modeled and expected friction factor of well C47 50
6.1.2 Compare the friction factor in the 17 ½" section and the friction factor in the 12 ¼" section of well C47 54
6.1.3 Compare friction factor for POOH and RIH in the 17 ½" section for well C47 55
6.2 Evaluation of result from well A12/A12T2 and well A5 55
6.2.1 Evaluation of the friction model to model shallow sections 55
6.2.2 Reliability test 1 of the of the friction model: Compare observed and estimated hook load of well A12/A12 T2 56
6.2.3 Reliability test 2 of the of the friction model: Evaluation of estimated hook load for well A12/A12 T2 and well A5 58
6.2.4 Evaluation of modeled friction factor for cases with torque during reaming in the 17 ½" section of well A12/A12 T2 59
6.3 Limitations reported in literature 63
6.3.1 Tortuosity and micro-tortuosity 64
6.3.2 Local variations 65
6.3.3 Hydrodynamic viscous drag 65
6.3.4 Perfect vertical wellbore 67
6.4 Limitations due to accuracy in field data detected through present work 67
6.4.1 Friction loss in the hoisting system affecting the accuracy of the measured load 69
6.4.2 Accuracy with depth 71
6.4.3 Buckling 75
6.5 Future improvements 77

7 Conclusion 78
8 Nomenclature 79
8.1 Parameters 79
8.2 Abbreviation 80
9 References 82
A Appendix 87
A.1 Friction calculation 87
A.2 Projected height principle 88
A.3 Example of drillstring design calculations 89

1 Introduction

1.1 Motivation

Torque & drag forces play an important role when planning and operating a well. Torque & drag forces can be used to decide success or failure of a well, and matters especially when wells are long and complex. For instance, high drag and torque forces are critical limitations in extended reach drilling (ERD) because they hinder to reach drilling targets (Gihselin 2009). Therefore, when the number of extended reach wells (ERW) is steadily increasing, also the focus on torque & drag forces is increasing (McCormick 2011). The general definition of an ERW is a well with a step-out ration, which is horizontal displacement divided by true vertical depth (TVD) at total depth (TD), equal to one or higher (Allen et al. 1997).

It is essential to apply a torque & drag model to obtain a successful well. Models are applied to analyze friction, in terms of a friction factor, to estimate how it affects hook load and torque. The friction factor is maybe the most uncertain factor in the calculations. The reason for this is that it is not a measured parameter, but a "fudge factor" with many factors added to the term. Factors included to the friction factor include mud system lubricity, pipe stiffness, cuttings beds, hydraulic piston effects and tortuosity (K&M Technology Group 2003). To get an accurate model, it is therefore important and challenging to find appropriate friction factors for different situations. During drilling the friction factor is given in terms of resistance and moment (torque) to overcome crushing of the rock.

The model has to be of high quality, and also be easy to apply. A reliable and accurate model has to model realistic forces, contact loads and bending moment, and at the same time be as user friendly as possible. In the past several attempts to develop a good model have been done, and still some confusion remains over the validity of the models used to characterize the well operations. First out was the well known 2D (two-dimensional) model to Johansick (1984), which is still commonly applied in the industry today. Another relevant model is an analytical 3D (three-dimensional) model developed by Aadnoy et al. (2010). The 3D model can be either applied as a fully 3D model, when both inclination and azimuth are changed, or be applied more simplified as a 2D model if the azimuth is negligible in the well path. The 3D model is relatively new and less familiar to the industry, even though it has been investigated. Once was an investigation of Mirhaj et al. (2010), where the analytical model was compared with other torque & drag models by studying the application on ERW. The conclusions were made on the importance of doing a precise friction modeling, and that the different models actually gave a close match.

In present work another investigation is going to be performed on the Aadnoy`s friction model, not to compare it with other models, but to evaluate if it is applicable in a real world to detect specific downhole problems. The object is to check the validity and limitations in the model. Because friction factor is one of the most important parameters in the torque & drag modeling, the main goal is to model friction factors for different situations to investigate if it can be used as an indicator on the downhole condition. This is the driving force for issues questioned in present report; What are the applications for the today`s accepted torque & drag model? Do the friction model give expected results; why, how? Because the friction factor is a fudge factor, the modeled outputs additionally need to be compared with torque and drag observations. How reliable are the results from the model? It is also interesting to discuss how to improve the model to get even better results? The main purpose of present report is to do an analytical approach to torque & drag issues by investigating professor Aadnoy`s theory of the mathematical model for friction.

1.2 Approach

First a literature review on the basic theory behind torque and drag will be studied in the first part, part A, in present report. To enable practical application of the theoretic model, a manual friction model in Excel is going to be developed with Aadnoy's analytical model as a foundation. In the next part in present report, part B, the friction model developed in Excel will be evaluated by applying field data to the model and evaluate different aspects, including:

- Do real well application of the model to:
  - Compare the modeled results to expected results
  - Compare modeled results from different example wells
- Study the model potential and check limitations with the model to evaluate the validity and accuracy. Also improvements to the model will be suggested.

Three real well applications of the model will be performed; one on well C47 in the Gullfaks Field and two wells, well A12/A12 T2 and well A5, in the Gudrun Field.

Part A: Review of basic theory

2 Review on work with torque & drag models and today`s applications

Before proceeding with defining basic principles for well friction, a short review on previous work with torque & drag models, and the driving force for focusing on torque & drag will be presented in the following section.

Johansick (1984) was one of the first to contribute to the work of understanding friction in the well by developing a torque & drag model with basic equations for friction in deviated wellbores. Sheppard et al. (1987) continued the work by putting the theory into a standard differential form. In 1993 British Petroleum (BP) completed the well known well in the Wytch Farm Field in England, which became a milestone in the evolution of ERD. This well was drilled 10,1 km horizontally from an onshore platform to the target, and thereby became the longest ERW at that time. After the success of the Wytch Farm well the industry saw the opportunities for drilling to targets that was earlier seen as out of reach or that required big capital in development. ERW became a global trend, and in May 2008 a new record for ERD was set to 12,3 km measured for Maersk Oil in the Al Shaheen field in Qatar (Redlinger and McCormick 2011). This development was a driving force to gaining better understanding on forces downhole, and to improve methods and tools that minimize torque & drag, because they limit distant drilling objects and decides the success of the well (Allen et al. 1997; McCormick et al. 2011). Aadnoy and Andersen (2001) established analytical solutions to wellbore friction for different geometries (Aadnoy et al. 2010), where each section of the well profile, including straight, drop-off and build-up sections, have different equations. Further on, Aadnoy (2008) made the theory even simpler by generalize the equations for different sections of the wellbore and the movement of the pipe; either up or down. The model applied in present report is based on the work performed by Aadnoy et al., which will be further discussed in chapter 3.

Torque & drag models are applied to analyze torque & drag forces to help drilling as efficient as possible to planned drilling target. The main purposes of the models can be summarized by two statements; one, to give a valid and reasonable torque & drag prediction, and secondly, to enable application for real time analysis. The models have many functions in the planning phase, operation phase and post-analysis of a well, including helping and understanding, prediction and preventing drilling problems.

During the planning phase the models act as a support for decisions, including decisions on drillstring design and well path design with minimized torque & drag (Frafjord 2012). For instance torque & drag criteria can be applied when planning the most appropriate well path to ensure successful drilling operations to planned depth (Johancsik et al. 1984). An accurate torque & drag analysis makes it possible to optimize design of drillstring and well trajectory within the capability of a specific rig (Wolfson 2005). A challenge during this work is that when the ratio of displacement to TVD and drag forces is becoming large, it is difficult to maintain enough weight to push the drillstring down to ultimate depth (Wolfson 2005). Reaching for targets which was earlier seen as out of reach, results in challenging well designs modified to operate safely. Prediction is the main purpose of the analysis in the planning phase. Once a model is reliable, calculations can be done to foresee what the hook load and torque can be farther downhole.

During operation phase, torque & drag software are applied for supervision of the operation in real time by measure, monitor and record torque and hook load. The models are beneficial in mainly three processes in the operation phase; tripping, connection tests and drilling, which will be explained in this subchapter. Unexpected changes, such as changes in lithology, mud-system behavior, surge/swap effects and change in directional performance, can be detected by comparing observed data with calculated during tripping. In addition expected effects, like doglegs (DL), can be identified by comparing trips done earlier. Also during drilling, modeled data are compared with observed to find changes which are not expected, and used as early warning to downhole problems. The work in real time has an important role for decision support, where the drilling team can react immediately if something unplanned is happening. The risk of getting significant problems, such as issues with the hole-cleaning, differential sticking problems, or trouble with wellbore stability, can be reduced with the ability to react before problems affect the drilling operations. During connection tests, which usually involves pick up, rotating off-bottom, and slackoff, it is also common to do a comparison between measured and calculated hook load and torque to study trends to obtain good and early indication on poor hole cleaning (Rommetveit et al. 2007).

In the last mode, the post-analysis, torque & drag models are compared with observed data to detect the true causes of hole problems, which could not be explained during drilling (Mirhaj et al. 2010).

In practice torque & drag analysis is a combination of study of historical behavior, take advantage of experience, utilize engineering models and use of data analysis, to be able to see the data in the context of the drilling environment, and to identify developing trends and incidents. For this task it should be noted that in a real work all available real time

data, both surface and downhole, must be applied together to monitor and optimize the processes involved for drilling. This means that torque & drag need to be compared with other drilling data, such as flow rate, rate of penetration (ROP), formation and equivalent circulation density (ECD). In addition, torque & drag need to be put in a context with operational data, such as circulation and study of cutting out of the hole, to identify downhole problems accurately. An example is that bad hole cleaning can be suspected if high ROP is experienced with high torque & drag forces. Both the torque & drag model and the ROP model will be involved (Rommetveit et al. 2007). However, the focus in this report is on torque & drag trends and its vital role on reducing non-productive time (NPT) of a well operation.

3 Physical principles behind the friction model and methodology of model friction factor

This chapter contains an introduction to theory relevant to the friction model applied in present report. First is relevant drilling activities presented, including activities which will be applied with the friction model. The next part of chapter 3 is presenting the equations and the methodology of the two friction models; the 2D and the 3D model, which are based on the theory of Aadnoy et al. After explaining the methodology in general, an example from the book Mechanics of drilling (Aadnoy 2006) is applied with the model to better demonstrate the procedure to model friction factor. The same procedure is used in the field cases in part B of present report.

3.1 Relevant activities during drilling of a well

Activities which can be recognized from real time data, include:

- Reaming
- PRS test
- Tripping in without rotation, referred in present report as RIH
- Tripping out without rotation, referred in present report as POOH
- Drilling with no, or neglected, movements in axial direction.

The friction forces will be different during these operations, and they therefore need to be analyzed separately.

3.1.1 Reaming

Reaming operation is performed during drilling of a well by moving the pipe while maintaining or modify drilling parameters, such as string rotation and circulation, seen in Fig. 1. Reaming can be done while lowering the string or pulling the string, but is different from tripping because in tripping, rotation and circulation are stopped, meaning zero torque and revolutions per minute (RPM). Reaming is performed for instance to clean the hole, or to make the drilled hole smoothly larger to an exact hole size in plastic formations that slowly creep and reduce the wellbore diameter over time (TechDictionary 2008).

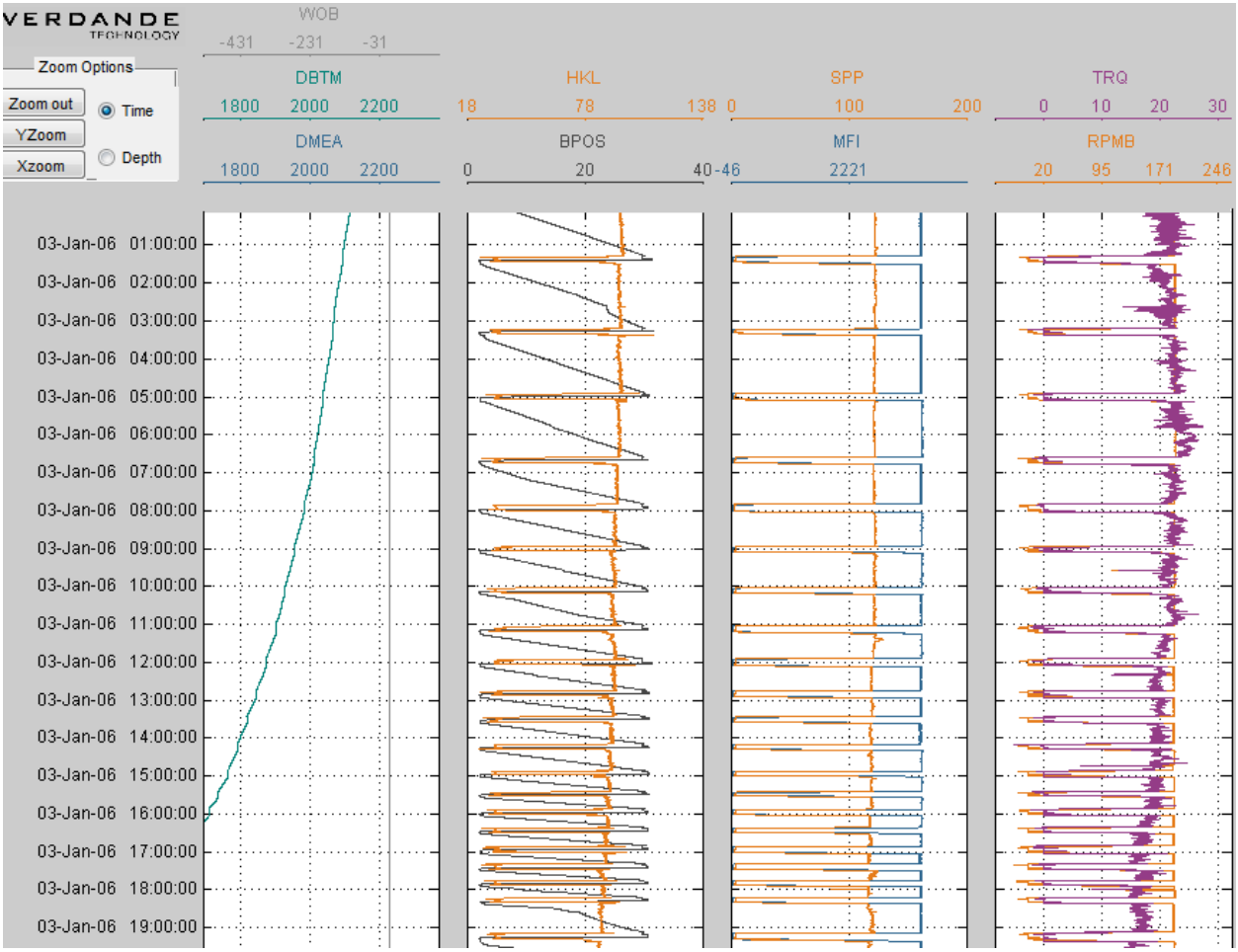

Fig. 1- Real time data of reaming out of hole (bit depth, DBTM, decreases in value with time) 3 January 2006 in the 17 ½" section of well C47 (Data from Statoil via Verande Technology).

3.1.2 PRS test

Pickup/rotate/slackoff test (PRS test) is a second operation that can be identified from the real time data. PRS tests are done to make torque & drag analysis more effective by maintaining a working understanding of the friction factor and by systematically gather drilling mechanics data. Friction factor check calculations are performed with PRS tests, where both sliding friction and rotating friction are monitored. The test is common to do at the casing shoe whenever tripping in or out after drilling every stand. The procedure for the test is to record hook load and torque when picking up the drillstring, rotating the stationary string and slacking off, and it is performed when pumping and then when not pumping (Rae et al. 2005).

In present report no PRS test was recognized and therefore analysis of PRS test could not be done. However, a PRS test performed during drilling of a well in the Captain Field in the UK sector of the North Sea have been presented and demonstrate below. Fig. 2 shows a graph for the test with 0,4 hour (24 min) drilling data, and completed stand at 4061,76 hours. The time interval for this test is approximately 10 min, and is marked out with the green lines in Fig. 2. Rotation mode ("R") is the first phase, followed by the same steps in a non-rotation mode ("NR"). Because the blue bit curve is showing decreasing depth and the light blue block position curve shows a lifting tendency, it means that the test is starting by picking up ("PO") the bit from the bottom as the first step. The indicated values from the black hook load curve is 290000 lbm, 19500 ft-lbf on the red torque curve and 1300 psi on the green pump pressure curve. A small overpull is experienced after picking up the bit, noted by slower block movement, increasing and then decreasing hook load, and fluctuating torque. Next step is stationary rotation ("S"), where 275000 lbm is recorded on the hook load graph, torque is still fluctuating and the pressure curve shows 1300 psi. After this, slackoff ("SO") is preformed where hook load is dropping to 235000lbm, torque to 18500 ft-lbf and pressure remains at 1300 psi. The second and last phase is pickup and slackoff without rotation ("NR"), with zero torque. The last values recoded in the PRS test, is the increase in hook load to 361000 lbm for pickup and the drop in hook load to 152 000 lbm for slacking (Rae et al. 2005).

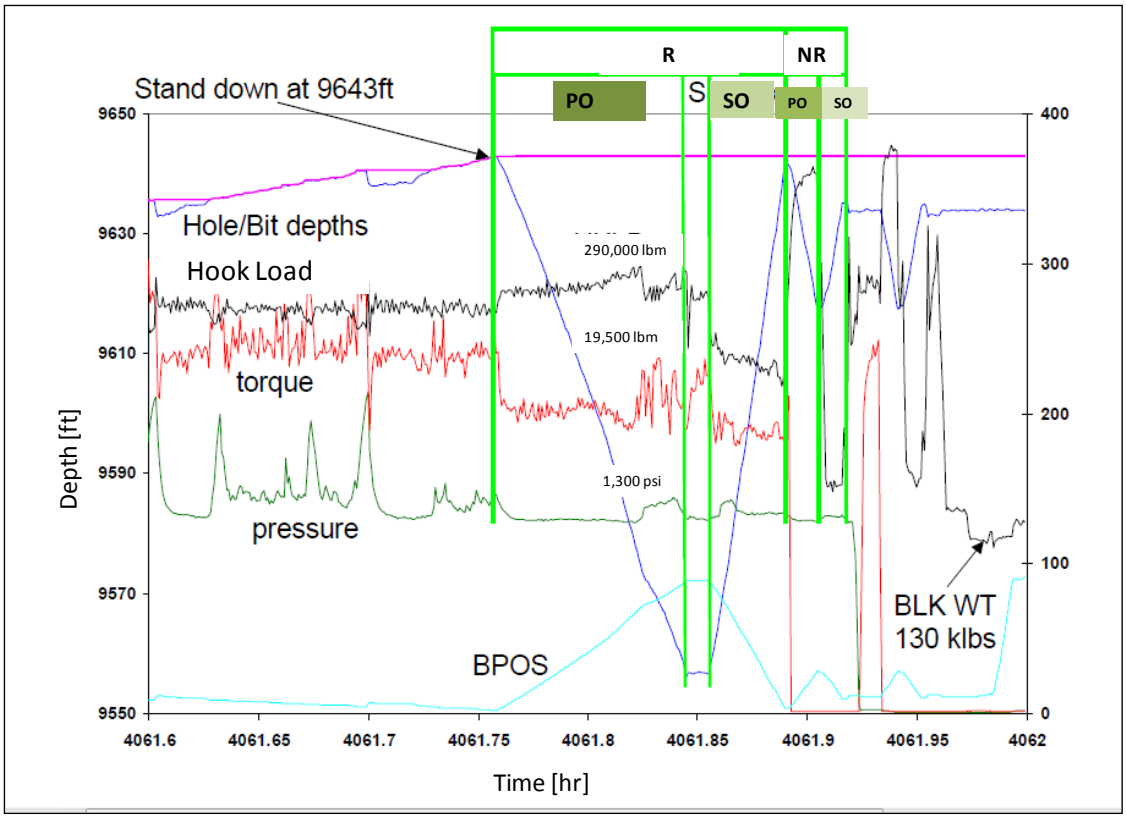

Fig. 2- Example of PRS test in a well in the Captain Field (Rae et al. 2005).

3.1.3 Tripping

Tripping is moving the pipe without rotation and circulation, and is often measured while the pipe is pulled out of hole and before making a connection. Measurements from operation without rotation are helpful to apply to analyze the downhole situation, because just here the full friction, which is acting in the axial movement and affecting the hook load, is on its maximum (Kucs et al. 2008).

One way of getting an indication on the resistance, or friction, when moving the pipe in the borehole, is by directly study the hook load during tripping operations and apply the theory in Aadnoy`s friction model. Measured hook load at the surface can indicate the friction, which is force (in terms of weight) needed to move the pipe up or down, by studying the deviation in tension when going in and out with the string. Eq. (1) to Eq. (3) demonstrate how the friction can be given by hook load for straight sections, but the same theory can be applied for curved sections. A more detailed derivation is presented in Appendix.

$$F_{up} = F_1 + \beta \Delta L w(\cos\alpha + \mu \sin\alpha) \tag{1}$$

$$F_{down} = F_1 + \beta \Delta L w(\cos\alpha - \mu \sin\alpha) \tag{2}$$

$$\frac{\Delta F}{2} = \left|\frac{F_{up} - F_{down}}{2}\right| = \frac{2\beta \Delta L w(\mu \sin\alpha)}{2} = \text{friction} \tag{3}$$

3.1.4 Drilling

Drilling is in this context to enlarge the borehole by rotating the string and bit on bottom of the borehole. The velocity in axial direction, ROP, is much smaller than the rotational speed, RPM, and the situation can therefore be seen as a case with drillstring rotation without axial movement.

3.2 Wellbore trajectory

This chapter describes properties of wellbore trajectory that are applied in the friction model in present report. Inclination, which is vertical projection, and azimuth, which is horizontal projection, are usually measured to describe the wellbore orientation. From these parameters, DL, which is absolute change in direction in an arbitrary plane, and dogleg severity (DLS), which is the derivative of DL, can be defined by Eq. (4) to Eq. (6).

$$\cos\theta = \sin\alpha_1 \sin\alpha_2 \cos(\phi_1 - \phi_1) + \cos\alpha_1 \cos\alpha_2 \tag{4}$$

$$\mathrm{DL}[^\circ] = \frac{\mathrm{DL}}{\pi} |\theta[\mathrm{rad}]| \tag{5}$$

$$\mathrm{DLS}[^\circ/\mathrm{m}] = \frac{\mathrm{DL}}{\Delta \mathrm{L}} |\theta[\mathrm{rad}]| \tag{6}$$

$\alpha_1$and α_2, and ϕ_1 and ϕ_2 are referring to two survey measurements of subsequently inclination and azimuth.

3.3 Buoyancy factor

The weight of the drillstring in a fluid filled well is the unit weight of the string in air multiplied with the buoyancy factor. The buoyancy factor is defined by Eq. (7) if there is a different fluid inside and outside of the pipe, and it is defined by Eq. (8) if there is equal fluid density inside and outside of the pipe.

$$\beta = 1 - \frac{\rho_0 A_0 - \rho_i A_i}{\rho_{\mathrm{pipe}}(A_0 - A_i)} \tag{7}$$

$$\beta = 1 - \frac{\rho_o}{\rho_{\mathrm{pipe}}} \tag{8}$$

3.4 Friction factor

Eq. (9) is expressing the general definition of the friction factor as a scalar number between zero and one.

$$\mu = \frac{F_F}{F_N} \tag{9}$$

It is common to refer to two different friction factors; static friction and dynamic friction, or kinetic friction, as illustrated in Fig. 3. As a force is applied to an object, the region for static friction last until the force is great enough to overcome the initial resistance to move the object. Kinetic friction is on the other hand valid for objects in movement, and is the one used in torque & drag models. Static friction on the other hand can be associated with differential sticking environment, which is a situation where the string is sucked into the borehole wall because of higher pressure in the wellbore than the pressure in the formation (Mason and Chen 2007). The static friction is in general larger than the dynamic, however in many wells static and dynamic friction can be difficult to distinguish.

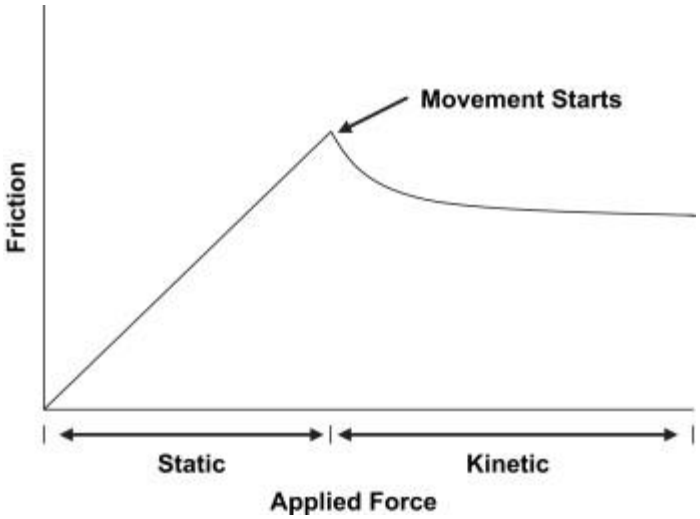

Fig. 3- Region for static and dynamic friction (Burrow 2009).

The friction factor is in general representing the roughness between two surfaces, for instance between the inside casing wall and the outside of the drillstring. However, usually the friction factor does not only include the true mechanical friction, but it has been practical to account for other effects with the friction factor because of a large number of variables in a drilling operation. The following list includes some of the parameters which are common to lump into the friction factor (Mason and Chen 2007):

- Pipe stiffness effects
- Viscous drag, which is defined as fluid resistance caused by to pipe movement
- Cutting beds, if present in the well
- Occurrence of lost circulation, which is leading to loss of lubricity
- Stabilizers/centralizers on the drillstring, which will affect string stiffness
- Tortuosity in the wellbore
- Hole cleaning issues
- Geometry of well

Modeling the listed parameters can be a complex task because they will vary over time and depth. Because the friction factor is a function of these parameters, also the friction factor will change depending on time and depth. For instance will there in general be a smaller friction factor in a casing then in an open hole. The friction factor will also vary from operation to operation, such as pulling out of hole (POOH), running in hole (RIH), rotation and no rotation. This is a reason for why it is necessary to perform individual torque & drag analysis for different situations. Table 1 and Table 2 show examples of how the friction factor varies, depending on mud type and whether the hole is open or cased.

Table 1- Experienced friction factors from over 100 wells drilled by conventional downhole assemblies (Gaynor et al. 2001).

Mud System	Actual Casing F.F.	Planning Casing F.F.	Actual Open Hole F.F.	Planning Open Hole F.F.
Water Based				
Generic	0.18	0.24	0.24	0.32
Polyseal / Barasilc	0.25	0.34	0.30	0.40
Thixal	0.22	0.29	0.27	0.36
Pure Oil Based				
Generic	0.10	0.13	0.12	0.16
Pseudo Oil Based				
Generic	0.15	0.20	0.17	0.23
XP07	0.17	0.23	0.17	0.23
Petrofree	0.14	0.19	0.18	0.24
Ecomul	0.16	0.21	0.20	0.27

Table 2- Ranges of friction factors for different fluid types and hole situations (Samuel 2010).

Fluid Type	Friction Factors	
	Cased Hole	Open Hole
Oil-based	0.16-0.20	0.17-0.25
Water-based	0.25-0.35	0.25-0.40
Brine	0.30-0.4	0.3-0.4
Polymer-based	0.15-0.22	0.2-0.3
Synthetic-based	0.12-0.18	0.15-0.25
Foam	0.30-0.4	0.35-0.55
Air	0.35-0.55	0.40-0.60

The friction factor plays a more significant role in ERW compared to a vertical well. Fig. 4 illustrates this, where the drillstring is forced against the side of the extended-reach wellbore, and in that way the friction becomes an important source of wear and energy losses in the tubular system. The drillstring is in general placed centrally in the borehole in a vertical hole, leading to negligible contact between the drillstring and the borehole wall, and consequently zero torque and drag. The middle sketch in Fig. 4 shows that during a build section the drillstring is pressed against the top side of the borehole wall and is in tension or compression, leading to varying degree of torque & drag forces. The right picture in Fig. 4 presents a tangential section of the hole where the entire drillstring is in contact with the low side of the borehole wall, and can be in some tension or compression. The friction is a critical factor not only in drilling operation, but also during completion and workover operations, and in casing/liner hanger jobs the release of setting tools can be significantly affected by torque & drag conditions (Aadnoy et al. 2010; Xie et al. 2012; Bennetzen et al. 2010). Torque & drag forces can be minimized by reducing the friction factor, and in that way increase the ability to drill farther and deeper wells.

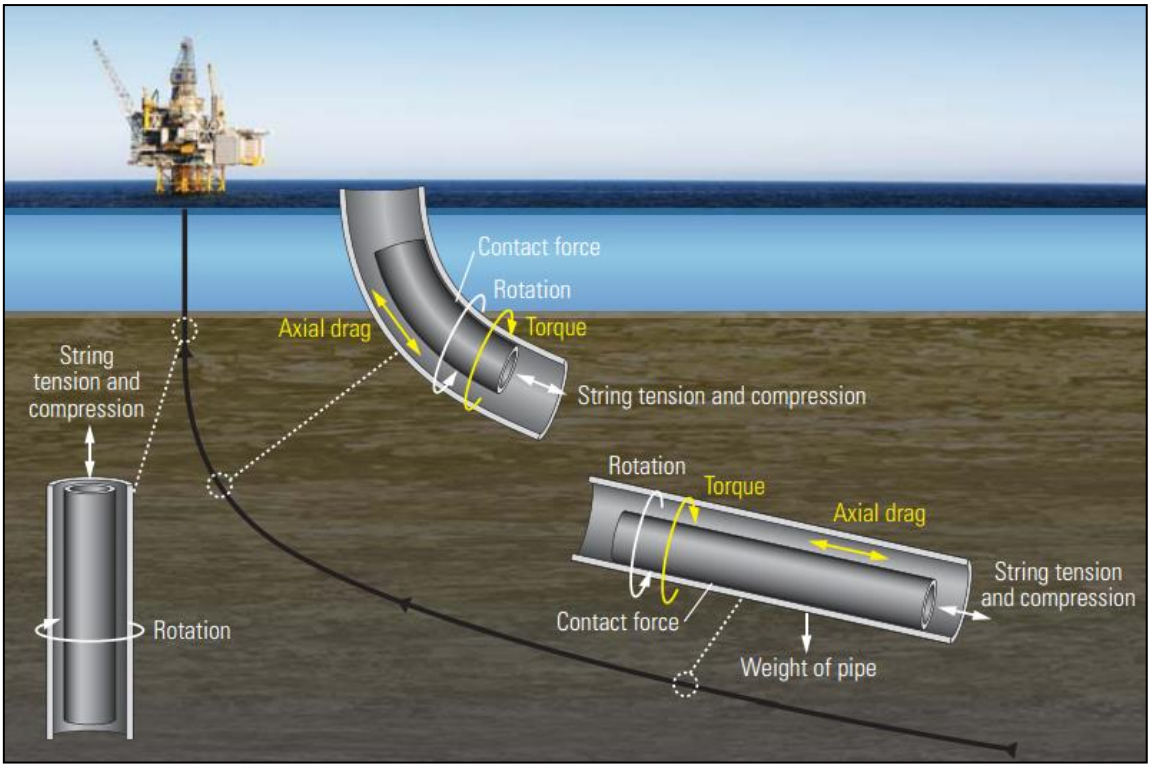

Fig. 4- Side forces on the string in different wellbore orientations (Bennetzen et al. 2010).

3.5 Drag

Drag is explained as the incremental force needed to pull or lower the drillstring through the borehole (Landmark Wellplan user manual 2004). The magnitude of the drag, also associated as sliding friction forces or borehole friction, is depending on two factors; the normal contact force and the coefficient of friction between the contact surfaces, based on Coulomb`s friction model (McCormick et al. 2011). This force is required to overcome the axial friction between the pipe and the wellbore, the hydrodynamic viscous force between the pipe string and the drilling fluid (Payne and Abbassian 1997).

3.5.1 Drag in straight sections

A straight section is typically weight dominated because friction is only given by the normal weight component. The top force of a straight element is given by Eq. (10), where the cosα-term is representing the weight if the element, while the sinα-term represents the additional friction force required to move the pipe element. The plus sign in Eq. (10) is for pulling while minus is for slacking, and the equation is valid for both the 2D model and the 3D model (Aadnoy 2010).

$$F_2 = F_1 + \beta \Delta L w(\cos\alpha \pm \mu \sin\alpha) \quad (10)$$

3.5.2 Drag in curved sections

In opposite to a straight section, a curved section is seen as a tension dominated process because the normal contact force between the drillstring and borehole is affected by the pipe loading in axial direction. For instance will the tension be much greater than the weight of the string inside bend for a short bend. The equations for axial force is derived by assuming that the pipe is weightless when computing friction, but the weight is rather added at the end of the bend. For curved sections there are different equations for the 2D model and the 3D model, where the first four equations are for the 2D model, and Eq. (15) is for the 3D model (Aadnoy 2010).

Eq. (11) is for POOH and Eq. (12) is for RIH in a drop-off bend.

$$F_2 = F_1 e^{\mu(\alpha_2 - \alpha_1)} + \frac{wR}{1+\mu^2}\begin{bmatrix}(1-\mu^2)(\sin\alpha_2 - e^{\mu(\alpha_2-\alpha_1)}\sin\alpha_1) \\ -2\mu(\cos\alpha_2 - e^{\mu(\alpha_2-\alpha_1)}\cos\alpha_1)\end{bmatrix} \quad (11)$$

$$F_2 = F_1 e^{-\mu(\alpha_2 - \alpha_1)} + wR\,[\sin\alpha_2 - e^{-\mu(\alpha_2-\alpha_1)}\sin\alpha_1] \quad (12)$$

The following two equations; Eq. (13) and Eq. (14), are sequentially for POOH and RIH in a build-up bend.

$$F_2 = F_1 e^{-\mu(\alpha_2 - \alpha_1)} - wR\,[\sin\alpha_2 - e^{-\mu(\alpha_2-\alpha_1)}\sin\alpha_1] \quad (13)$$

$$F_2 = F_1 e^{\mu(\alpha_2 - \alpha_1)} - \frac{wR}{1+\mu^2}\begin{bmatrix}(1-\mu^2)(\sin\alpha_2 - e^{\mu(\alpha_2-\alpha_1)}\sin\alpha_1) \\ -2\mu(\cos\alpha_2 - e^{\mu(\alpha_2-\alpha_1)}\cos\alpha_1)\end{bmatrix} \quad (14)$$

For the 3D model Aadnoy investigated a symmetric relationship between the upper equations of the 2D model, and managed to reduce them into two equations; one for POOH and one for RIH, where the plus sign is for pulling while minus is for slacking (Aadnoy et al. 2010):

$$F_2 = F_1 e^{\pm\mu|\Delta\theta|} + \beta\Delta L w\left(\frac{\sin\alpha_2 - \sin\alpha_1}{\alpha_2 - \alpha_1}\right) \quad (15)$$

3.6 Torque

The moment required to rotate the drillstring and the bit is expressed by torque. This moment is needed to overcome the rotational friction against the wellbore, known as frictional torque, the viscous force between drillstring and drilling fluid, called dynamic torque, and the bit torque (Payne and Abbassian 1997). Following aspects are often deciding the magnitude of the torque (Bennetzen et al. 2010):

- Tension or compression in the drillstring
- DLS
- Sizes of the drillstring and hole
- Weight of the string
- Directional changes of the wellbore (inclination and azimuth)
- Lubricity or friction factor

The same principle as for drag situations also applies for the rotating friction, the torque, where there are different equations to model straight and curved sections.

3.6.1 Torque in straight sections

The applied torque is normal moment multiplied with the friction factor, seen in Eq. (16), and is valid for both the 2D and the 3D model.

$$T = \mu r w \Delta s \sin\alpha \quad (16)$$

From Eq. (16), a vertical bend (α equal to zero) would give no torque, while a horizontal section (α equal to 90 degree) applies the maximum torque. For the case with only rotation, axial friction has no effect, and the direction of the motion plays no role on the torque.

3.6.2 Torque in curved sections

Torque without axial motion with the 2D model in a drop-off bend is presented by Eq. (17), while torque based on the 2D model in a build-up bend is given by Eq. (18).

$$T = \mu r\,(F_1 + wR\sin\alpha_1)(\alpha_2 - \alpha_1) - 2\mu r w R(\cos\alpha_2 - \cos\alpha_1) \quad (17)$$

$$T = \mu r\,(F_1 + wR\sin\alpha_1)|\alpha_2 - \alpha_1| + 2\mu r w R(\cos\alpha_2 - \cos\alpha_1) \quad (18)$$

Eq. (19) is valid for calculation on torque with the 3D model when not pulling or lowering the string.

$$T = \mu r F_N = \mu r F_1|\theta_2 - \theta_1| \quad (19)$$

3.7 Combined axial and rotational motion

The effect of combined axial and rotational motion is not unknown, but the industry is rather familiar with the effect for this situation. For instance has experience from the field showed that drag is reduced when the drillstring is rotating (Allen et al. 1997). The above equations for torque & drag must be modified for combined motion, but will not be further elaborated in present report.

3.8 Method to model friction with selected model

Mainly two different approaches exist for friction modeling, the soft string model and the stiff string model, where the soft string model is the most common to use, and is also the one applied in present report (Mitchell and Samuel 2009). The soft string model is simpler because it, unlike the stiff string model, assumes that the drillstring is behaving like a cable. This implies that it neglects the stiffness of the string, and ignores the bending effects, which are caused by the radial clearance of the drillstring and stiffness of the pipe. For situations with smooth well path, the soft string will give a good approximation of forces and contact loads. However for cases with stiff drillstring, for instance the BHA (bottomhole assembly) with many stiff components, or complex well profiles govern by a lot of tortuosity, the soft string approach can create significant errors and be a source for misinterpretation of drilling problems (Menand et al. 2006). For a case where rotation is generating friction, the pipe has a tendency to move upwards the borehole wall, seen in Fig. 5. This will lead to less contact forces than if the pipe is placed on the low side of the wellbore, which is assumed in the soft string model. Fig. 6 presents the different orientations the drillstring can have in a wellbore. A disadvantage with the soft string model is that the model cannot predict such diverse positioning. From research the soft string has a tendency to overestimate torque & drag prediction although it underestimates the bending effects.

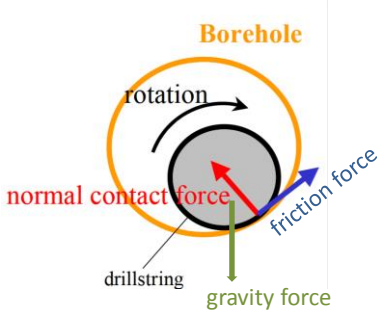

Fig. 5- Forces on the drillstring in contact with the borehole when rotating (Menand et al. 2006).

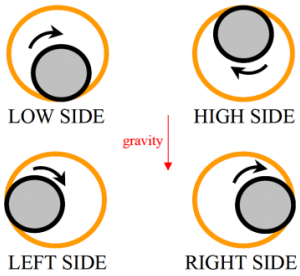

Fig. 6- Four different positions of drillstring in the wellbore (Menand et al. 2006).

As earlier mentioned the well geometry determines which model (2D or 3D model) to apply for friction analysis. The 2D model is considered accurate enough for a well that is drilled in a single plane, meaning that the azimuth change is negligible (small DL) and the trajectory is made by change in only inclination. For this case, force calculations on top of an element can be applied with either the 2D model, containing Eq. (11) to Eq. (14), or the 3D model can be applied, with Eq. (15), where the DL becomes equal to inclination. Studies have showed that either procedure should give approximately the same solution (Mirhaj et al. 2011). However, if it is unavoidable to keep the azimuth constant, for instance when drilling to target and it is necessary to bypass a challenging formation without touching it, it would be more relevant with the 3D model. Fig. 7 shows forces acting in a side bend, and the general rule of thumb is that the friction is considered higher for more side-bends throughout the wellbore trajectory (Mirhaj et al. 2010).

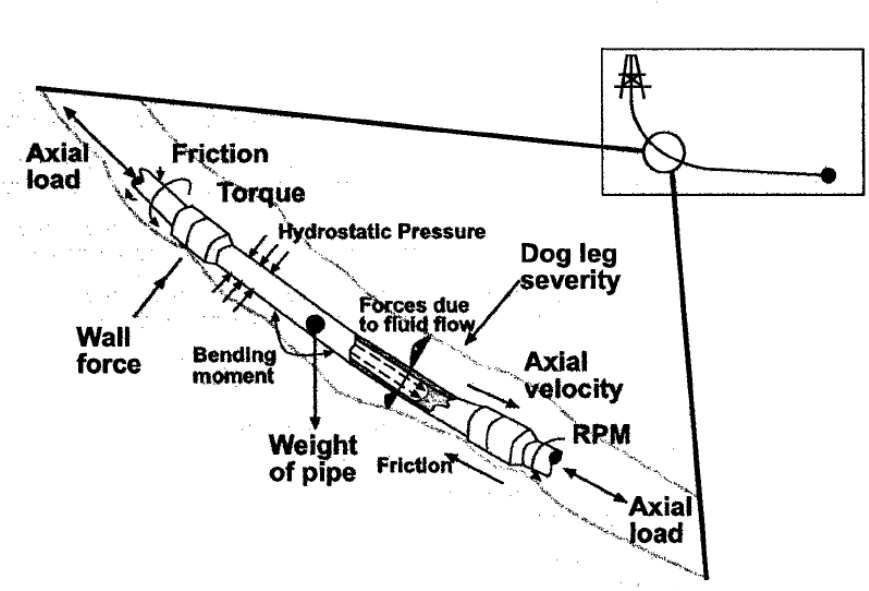

Fig. 7- Forces acting in a downhole bend (Anston et al. 1998).

Table 3 and Table 4 present possible wellbore sections for respectively the 2D model and the 3D model. In the tables sign "+" denotes increasing in an angle, "-" denotes decreasing, while "constant" means that the current angle does not change.

Table 3- Characterizing different sections in the 2D model (Ismayilov 2012).

Type of section	Inclination	Azimuth
Straight/vertical	"Constant"	"Constant"
Build-up	"+"	"Constant"
Drop-off	"-"	"Constant"
Side bend	"Constant"	"+" or "-"
Horizontal	"Constant"	"Constant"

Table 4- Characterizing different sections in the 3D model (Ismayilov 2012).

Type of section	Inclination	Azimuth
Build-up with right side bend	"+"	"+"
Build-up with left side bend	"+"	"-"
Drop-off with right side bend	"-"	"+"
Side bend with left side bend	"-"	"+"

Fig. 8 shows an overview over equations in the 2D model for the different situations. To summarize, the model contains equations for three operations; axial motion, rotation, and combined. There are two sets of equations applied to model the well; one for straight well sections and one for arbitrary well orientations, see Fig. 9 and Fig. 10 (Aadnoy et al. 2010). The side force or normal force is acting between the pipe string and the wellbore, in a direction perpendicular to the incline surface. The weight of the string is pointing downwards in the direction of gravity, while the drag force always acts in the opposite direction of where the pipe is moving.

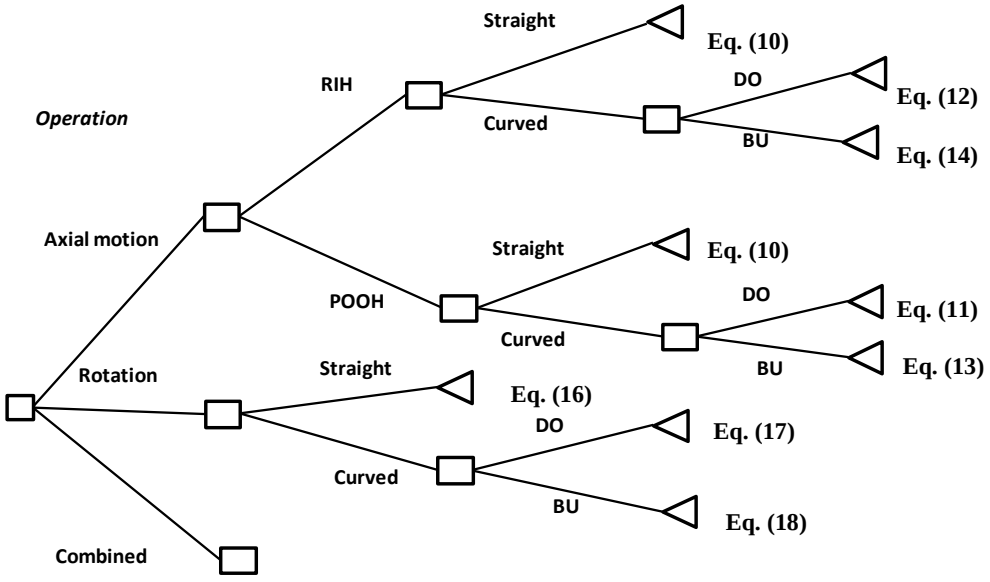

Fig. 8- Summary of equations in the 2D friction model.

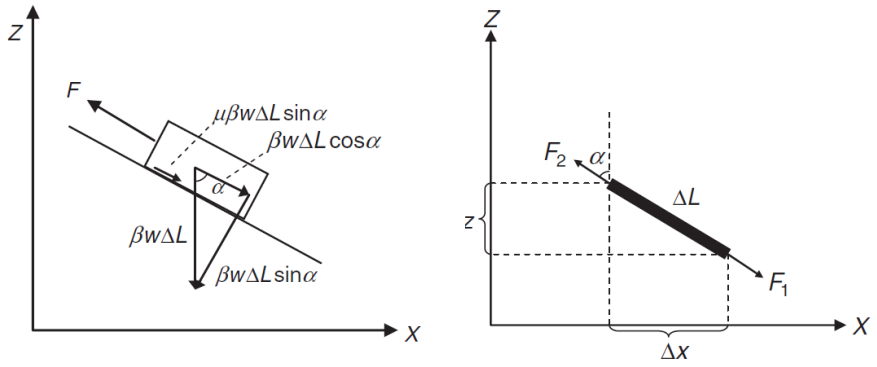

Fig. 9- Forces on an element in a straight section (Aadnoy et al. 2010).

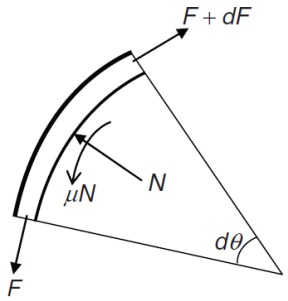

Fig. 10- Element being pulled along curved surface, where Coulomb friction is assumed (Aadnoy et al. 2010).

Fig. 11 shows a flow diagram for the procedure applied in all operations modeled in present work. Bottom-to-top calculation is done to find the resultant force on the surface, where the well is first divided into sections, which depends on the size and unit weight of the drillstring, and on the geometry of the wellbore. This is entered into the model, with the drillstring design, mud properties and a friction factor. The method is called bottom-to-top calculation because the calculation starts from the bottom and are summed up to the top of the well. The friction factor can be found by matching this modeled force on the top, which is depending on the friction factor, with the measured force from real time data. A common practice is to manually find a proper friction factor, and repeat the bottom-up calculation of the drillstring with different friction factors until the calculated surface loads match measured values. This is a trial and error method.

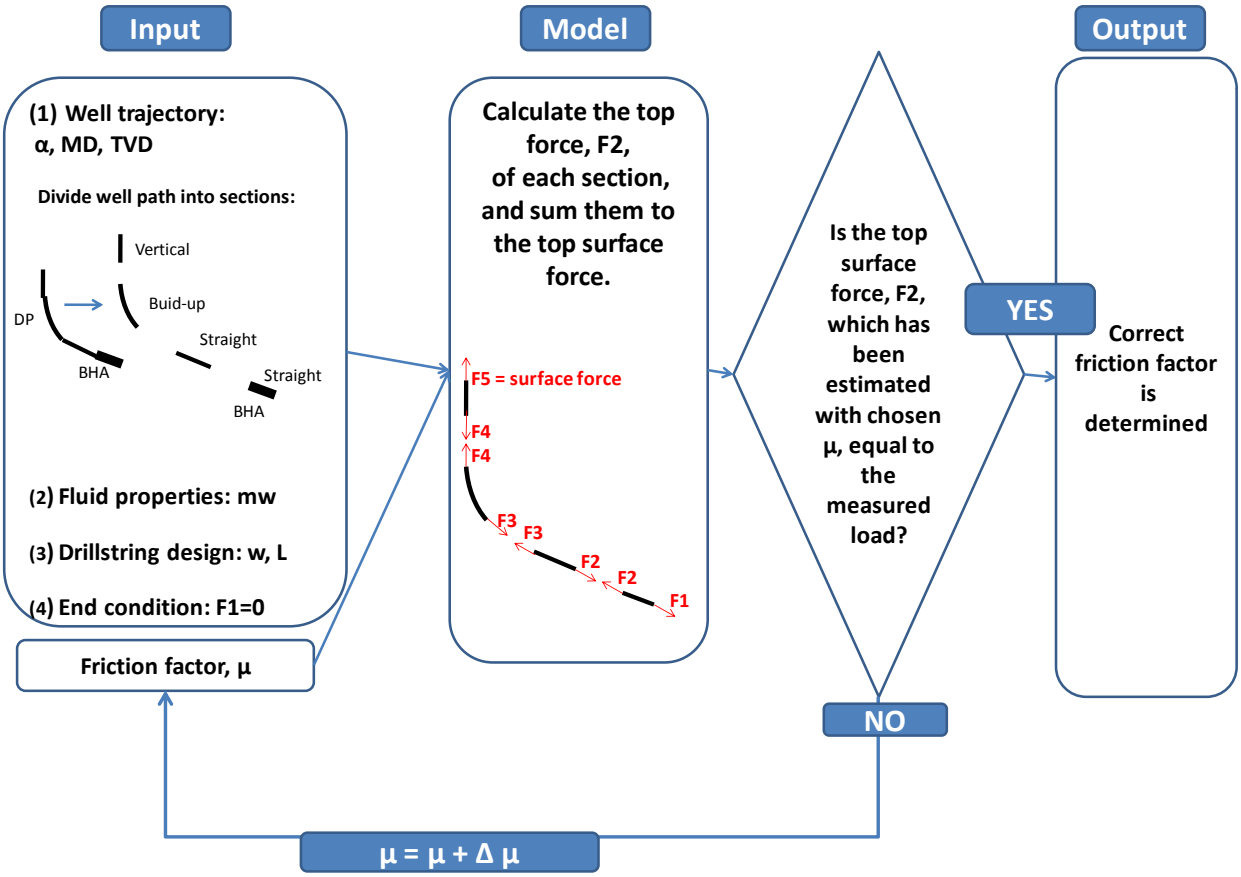

Fig. 11- Flow diagram for finding a proper friction factor that match the estimated surface load with the measured surface load.

3.8.1 Input data to the friction model

Required input data to the friction model, includes:

General data:

- Rig data (travel block weight) [tons]
- Fluid properties (mud weight) [S.G]

Drillstring configurations:

- Drillpipe unit weight [g/cm3]
- Drillpipe length [m]
- Tool joint (TJ) radius [m]
- BHA unit weight [g/cm3]
- BHA length [m]

- Largest radius on the BHA (bit radius) [m]

Well profile data/survey:

- measured depth [m]
- measured inclination [rad]
- measured azimuth [rad]
- Casing shoe depth [m]

Real time data/sensor values:

- Bit depth [m]
- Real time hook load [tons]
- Real time torque [kNm]

In the analysis, a good balance between some degree of conservatism and excessive design should be obtained. This applies particularly in the choice of values for parameters that are not known, such as the friction factor.

3.8.2 Methodology of the friction modeling demonstrated with example 6.4 from the book Mechanics of Drilling

This section presents example 6.4 in the book Mechanics of Drilling (Aadnoy 2006) to demonstrate how the friction model is built in Excel developed by present author. The example is also applied to verify that the Excel tool gives expected modeled friction factor, because the friction factor is already known and given for the specific hook load in the book.

The well in example 6.4 is a S-shaped well with 5” drillpipe placed down to the bottom end of the drop section, and a 500 kN BHA is installed to bottom. The unit weight of the drillpipe is 0,294 kN/m, and is assumed to be corrected for buoyancy. The radius required to model torque is assumed to be 0,0635 m for this example, which is the same as the radius of the drillpipe. The blue writings in the following tables are input data. Table 5 is listing properties of mud weight and drillstring design, which are entered into the friction model. Fig. 12 and Table 6 show the trajectory involved, which are also put in to the model. In addition the measured hook loads, presented in Table 7, for the different situations are input data needed to find a proper friction factor for the well.

Table 5- Input values applied in the Excel tool to model the S-shaped well.

	DP	TJ	BHA		
mw	w	r	w	length	
s.g	kN/m	m	kN/m	mMD	mTVD
0	0,294	0,0635	-	-	-

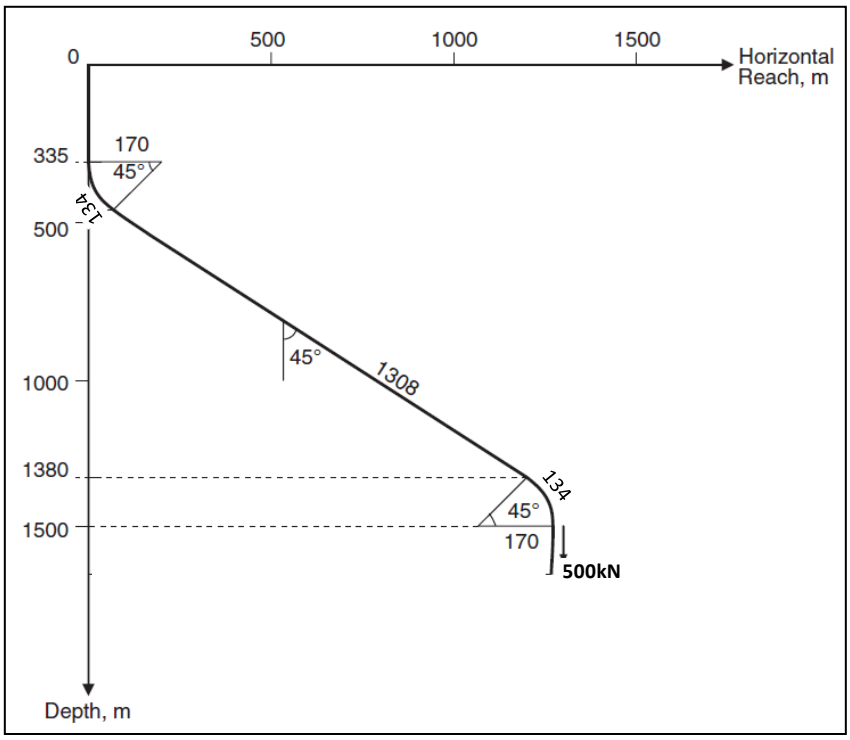

Fig. 12- Geometry of the S-shaped well (Aadnoy 2006).

Table 6- The S-shaped well divided into different sections depending on the trajectory.

Well section -bottom to top	MD1 mMD	MD2 mMD	Length m	α1 deg	α2 deg	Φ1 deg	Φ2 deg
Drop off	1911	1777	134	0	90	0	0
Inclined-Tangential	1777	469	1308	90	60	0	0
Build up	469	335	134	60	60	0	0
Vertical	335	0	335	60	0	0	0

Table 7- Measured hook loads for static drillstring, POOH and RIH for the S-shaped well.

	TD		Load	
	m TVD	m MD	tons	kN
Static	1500	1911	96	941
RIH	1500	1911	73	715
POOH	1500	1911	128	1255

The simplest case is the static weight, which is measured at the surface in a free-rotation mode of the drillstring (the rotational friction term is dominating), defined as the buoyed unit string weight multiplied by the projected vertical depth, seen in Eq. (20). The derivation of Eq. (20) is included in Appendix, and known as the projected height principle. Then the friction factor (in axial direction) is then close to zero and in the modeling assumed to be zero, even though it in theory never becomes exactly zero. Table 8 shows that the surface static load is modeled to be 941 kN with zero friction factor, which is equal to the sum of the weight of each element, as expected. This can also be applied as a quality control on the model.

$$w(\alpha) = \frac{w}{L}TVD \tag{20}$$

Next, friction factor for RIH is found by using the function goal seek, which is a built-in tool in Excel that uses methods based on numeric approximation to "back solve" for an input value to a system of formulas when a desired output value is entered into it. The tool is applied to find the friction factor which puts the estimated hook load on the surface equal to the measure hook load on the surface, which is 715 kN for RIH, as seen in Fig. 13. Fig. 14 shows how goal seek is applied to find a friction factor that gives a estimated hook load equal to the measured hook load of 1255 kN at the surface for POOH. Also for a case with torque, goal seek is applied to find the friction factor that results in a estimated torque equal to the measured cumulative torque at the surface. For the S-shaped example well, the estimated torque must be equal to the measured torque of 17,58 kNm, seen in Fig. 15.

Table 8- Data from the Excel tool showing the calculation sheet for modeling friction. With given trajectory and drillstring design of the S-shaped well, the static weight on the surface is calculated to be 941 kN (assumed zero friction factor).

	α1	α2	α1	α2	MD1	MD2	TVD1	TVD2	ΔMD	ΔTVD	mw	w	F1	R(BU)	R(DO)	bf	wb	Static weight	μ	F2(s)	F2(BU)	F2(DO)	F2
	deg	deg	rad	rad	m	m	m	m	m		s.g	kN/m	kN	m	m		kN/m			kN	kN	kN	kN
								1500										500					500
DO	0	45	0,00	0,79	1911	1777	1500	1380	134	120	0	0,29	500	0	171	1	0,294	35	0,0	0	0	535	535
S	45	45	0,79	0,79	1777	469	1380	456	1308	924	0	0,29	535	0	0	1	0,294	272	0,0	807	0	0	807
BU	45	0	0,79	0,00	469	335	456	336	134	120	0	0,29	807	171	0	1	0,294	35	0,0	0	843	0	843
S	0	0	0,00	0,00	335	0	336	0	335	336	0	0,29	843	0	0	1	0,294	99	0,0	941	0	0	941
																		941					

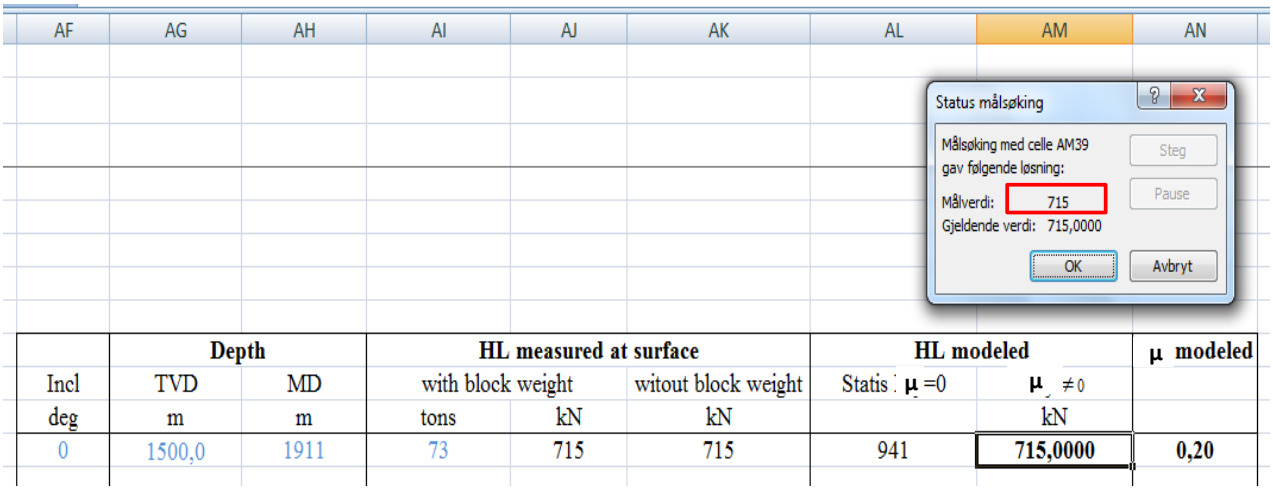

	Depth		HL measured at surface			HL modeled		μ modeled
Incl	TVD	MD	with block weight		witout block weight	Statis] μ =0	μ ≠0	
deg	m	m	tons	kN	kN		kN	
0	1500,0	1911	73	715	715	941	**715,0000**	**0,20**

Fig. 13- Demonstration of how the Excel spreadsheet is applied on the S-shaped example well to find an appropriate, modeled friction factor when RIH.

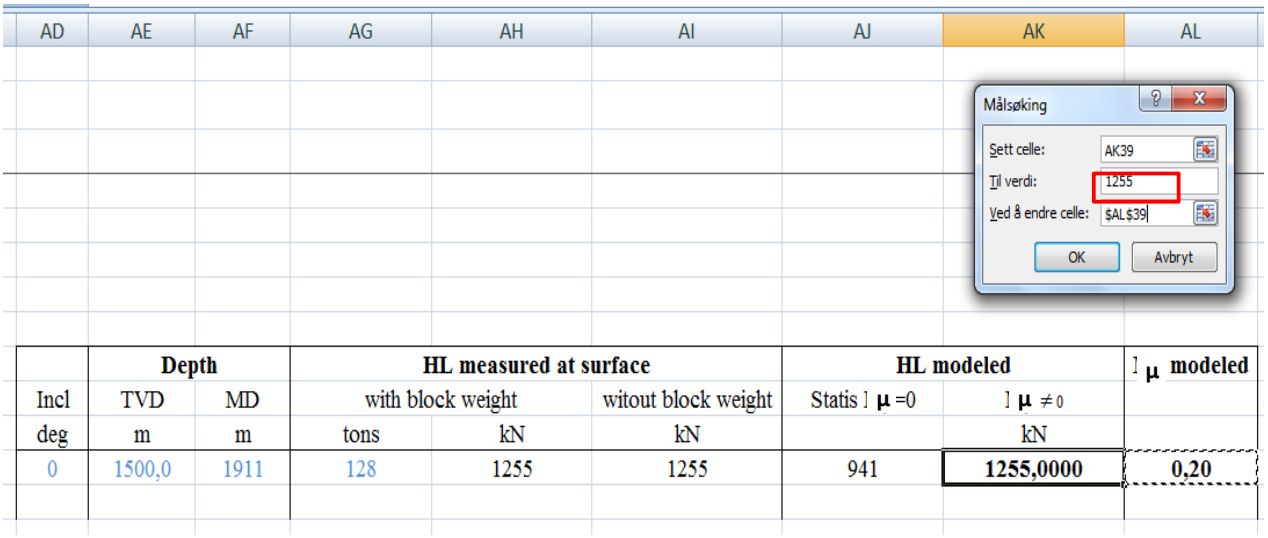

	Depth		HL measured at surface			HL modeled		] μ modeled
Incl	TVD	MD	with block weight		witout block weight	Statis] μ =0	] μ ≠0	
deg	m	m	tons	kN	kN		kN	
0	1500,0	1911	128	1255	1255	941	**1255,0000**	**0,20**

Fig. 14- Demonstration of how the Excel spreadsheet is applied on the S-shaped example well to find an appropriate, modeled friction factor when POOH.

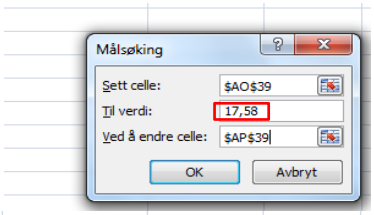

	Depth		TRQ measured at surface			HL modeled		μ modeled
Incl	TVD	MD	with block weight		witout block weight	Statis μ =0	μ ≠ 0	
deg	m	m	tons	kNm	kN		kN	
0	1500,0	1911	2	17,58	17,58	941	17,5800	0,20

Fig. 15- Demonstration of how the Excel spreadsheet is applied on the S-shaped example well to find an appropriate, modeled friction factor for known cumulative torque.

The result in Table 9 and Table 10, and the graphical presentation of the result in Fig. 16 and Fig. 17, show loads along the well path of the S-shaped example well with modeled friction factor. The modeled friction factor became 0,2 for RIH, POOH and for the case with torque when matching the estimated with the measured loads. It is then possible to calculate the loads at other depths along the well path using the same friction factor, for specific depths, operations, drillstring weights and trajectories. For instance is the green curve in Fig. 16 showing loads along the drillstring when POOH with a 0,2 friction factor and 500 kN BHA at the bottom, where the loads are estimated to be 626 kN at the end of the drop off section (1380 mTVD), 953 kN at the stop of the sail section (456 mTVD), 1156 kN at the end of the build-up section (336 mTVD) and 1255 kN is measured at the surface (0 mTVD). The blue graph, showing the static weight, is a linear graph with the unit weight of the drillstring as the slope. The maximum load (at the surface) is showing 941 kN static weight. Fig. 16 also clearly shows that the friction is increased in the bends.

Table 9- Data from the Excel spreadsheet tool showing results for a static case, RIH and POOH for a TD of 1500 mTVD of the S-shaped well. The upper table shows modeled friction factor and the lower table shows estimated loads along the well path.

	μ
Static	0
RIH	0,2
POOH	0,2

Depth m TVD	Static kN	RIH kN	POOH kN
1500	500,0	500,0	500,0
1380	535,3	462,8	626,7
456	806,9	680,3	953,0
336	842,2	617,0	1156,5
0	941,0	715,5	1255,0

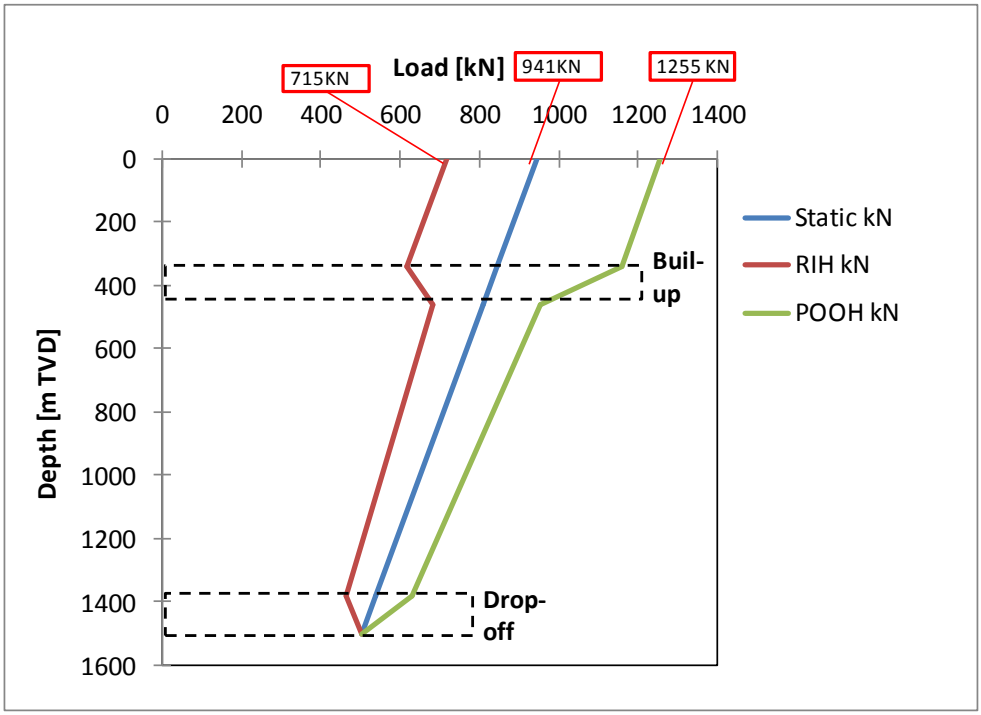

Fig. 16- Estimated loads plotted along the drillstring depth for 1500 mTVD of the S-shaped well.

Table 10- Data from the Excel spreadsheet tool showing results for a static case and modeled torque for a TD of 1500 mTVD of the S-shaped well. The upper table shows modeled friction factor and the lower table shows estimated loads along the well path.

	μ
Static	0
torque	0,2

Depth m TVD	Static (cummulative) kN	Torque kNm
1500	500	0,00
1380	535	5,47
456	807	9,00
336	842	17,58
0	941	17,58

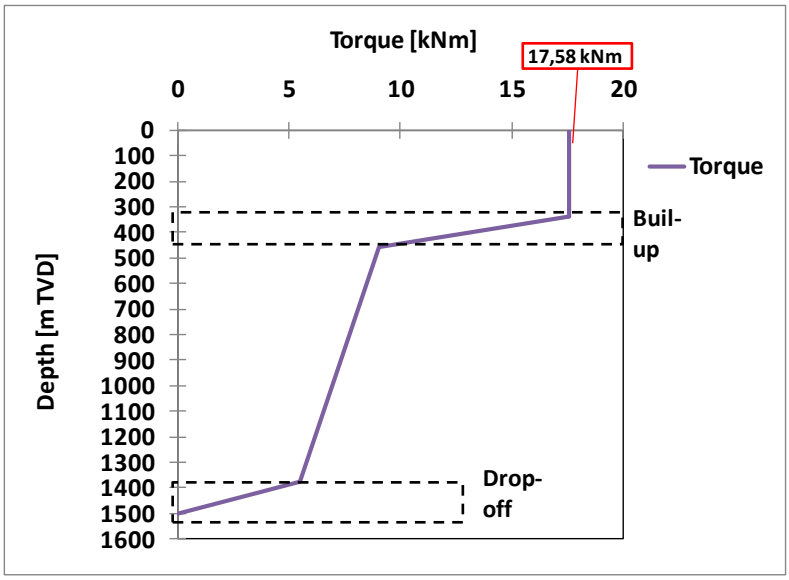

Fig. 17- Estimated torque plotted along the drillstring depth for 1500 mTVD of the S-shaped well.

3.8.3 Quality control

To check if the model is correct and for quality control of field data, tripping in and tripping out are commonly compared with the static weight of the drillstring (Fazaelizadeh et al. 2010). In such a comparison the field data related to tripping in and tripping out should always be greater than static weight because of friction between the drillstring and the wellbore. The static weight, also recognized as the free rotating weight, equal to the weight of the drillstring when no friction is applied to the drillstring movement, and is similar to the buoyed pipe weight multiplied by the projected vertical height of the well, independently of the orientation of the well. A second check is to ensure that the static string weight found from the projected height principle, which is explained in Appendix, is equal to the hook load when putting the friction coefficient to zero in the friction equations in the model. Measured free rotating weight should match perfectly with the model.

3.8.4 Concerns in calculations

The most important assumptions in calculations in the model are summarized in the following list:

- The wellbore is assumed to be smooth over the entire wellbore length, where shallow DLs and tortuosity are not considered.

- The wellbore has constant build-up rates and drop-off rates for the curved sections.
- The friction factor modeled does not account for local variations.

The division of the well path can be challenging because actual wellbore survey in general are vague which makes it difficult to accurately distinguish well sections. In the model it is assumed a smooth well path, while a real wellbore contains serve DLs and other irregularities. To have the highest possible accuracy in the model, it is therefore important to carefully divide the wellbore into sections and subsections as precise as possible. The benefit with this is that the model would be more sensitive to DLs and wellbore irregularities. The friction factor modeled is an average friction factor through the well from depth on the bottom of the string to the surface. This means that the value of the modeled friction factor does not account for local variations, for instance going from an open hole to a casing. However it is expected a lower average friction factor for the sections where the whole drillstring is in the casing, than the sections where the lower part of the drillstring is in the open hole and the upper part is in the casing. These assumptions will be further discussed in chapter 6.

Part B: Application field data to verify model of friction factor

In this part the friction model is applied on real wells. First relevant data of the applied wells are presented, followed by results from modeling friction. The last sections of part B includes evaluation of the result, where limitations and suggestions for future work are mentioned, and a conclusion.

4 Field data background

Three wells; well C47, well A12/A12 T2 and well A5, will be presented with relevant field data to run the friction model.

4.1 Field data of well C47

The presented dataset of well C47 is taken from the final well report from Statoil and real time field data from drilling and completion of the well. Well C47 is an oil producer and water injector in the Gullfaks Field in the North Sea, and was completed in 158,8 days to a TD of 4337,63 m measured depth (MD).

Fig. 18 shows pressure plot of well C47, where the relevant curves for present report includes gradient curves along the well for pore pressure (dark blue curve) and mud weight (light blue curve). The blue short lines are representing two zones with shallow gas sands (1084 mMD to 1090 mMD and 1492 mMD to 1508 mMD).

Next figure, Fig. 19, presents the well trajectory in terms of TVD plotted with inclination (blue curve) and azimuth (red curve) in degrees. The kickoff point (KOP) is positioned approximately at 600 mTVD, followed by a build-up section. Then there is a sail section with an inclination of approximately 60 degrees, before dropping into the reservoir section with an inclination of 70 degrees at 2073 mTVD. An adjustment of the well path was done during drilling because the geology was not as predicted. At 3835 mMD it was decided to drop 14 mTVD from 2080 mTVD to find the Statfjord 2 formation. The inclination was dropped from 91 to 81 degree with a controlled ROP. The main target was

at 3810 mMD, but because of unexpected faulting, this was 40 m deeper than thought (Christophersen et al. 2007). Well C47 can be assumed to be a 2D well because of negligible DL (almost constant azimuth).

Fig. 20 is presenting the different casings, hole dimensions and depths along the well path with vertical section and TVD. Well C47 has a standard casing program with standard hole sizes, and the additional length drilled in the 12 ¼" section is from approximately 2379 mMD (1730 mTVD) to 2787 mMD (1905 mTVD). Table 11 shows the depths and the angles that are describing the different wellbore sections.

Also block weight and drillstring design must be known to be able to make a torque & drag analysis. However, properties for the drillstring above the BHA are missing values for the modeled wells. Even though a lot of research and sending of requests to Statoil have been done, it was not possible to get the values, so the missing values were assumed. Length with drillpipe above the BHA was found by subtracting the BHA length from the total length of the section. For simplicity, the string is divided in lower part with BHA, and the rest of the string is consisting of 5" drillpipe. API dimensions have been applied (Petro materials 2012) to find the inner diameters of the pipes, while the weights are calculated by assuming steel density of 7,85 kg/cm^3. Average values for BHA is applied for calculations, while an actual BHA consists of different components with different shapes, weights and lengths. Table 12 and Table 13 summarize the values for the weights and lengths used in the model for the 17 ½" section and the 12 ¼" section of well C47, while Appendix in present report contains examples of the calculations behind the values. For well C47 also the block weight was missing and assumed to have a reasonable value of 30 tons.

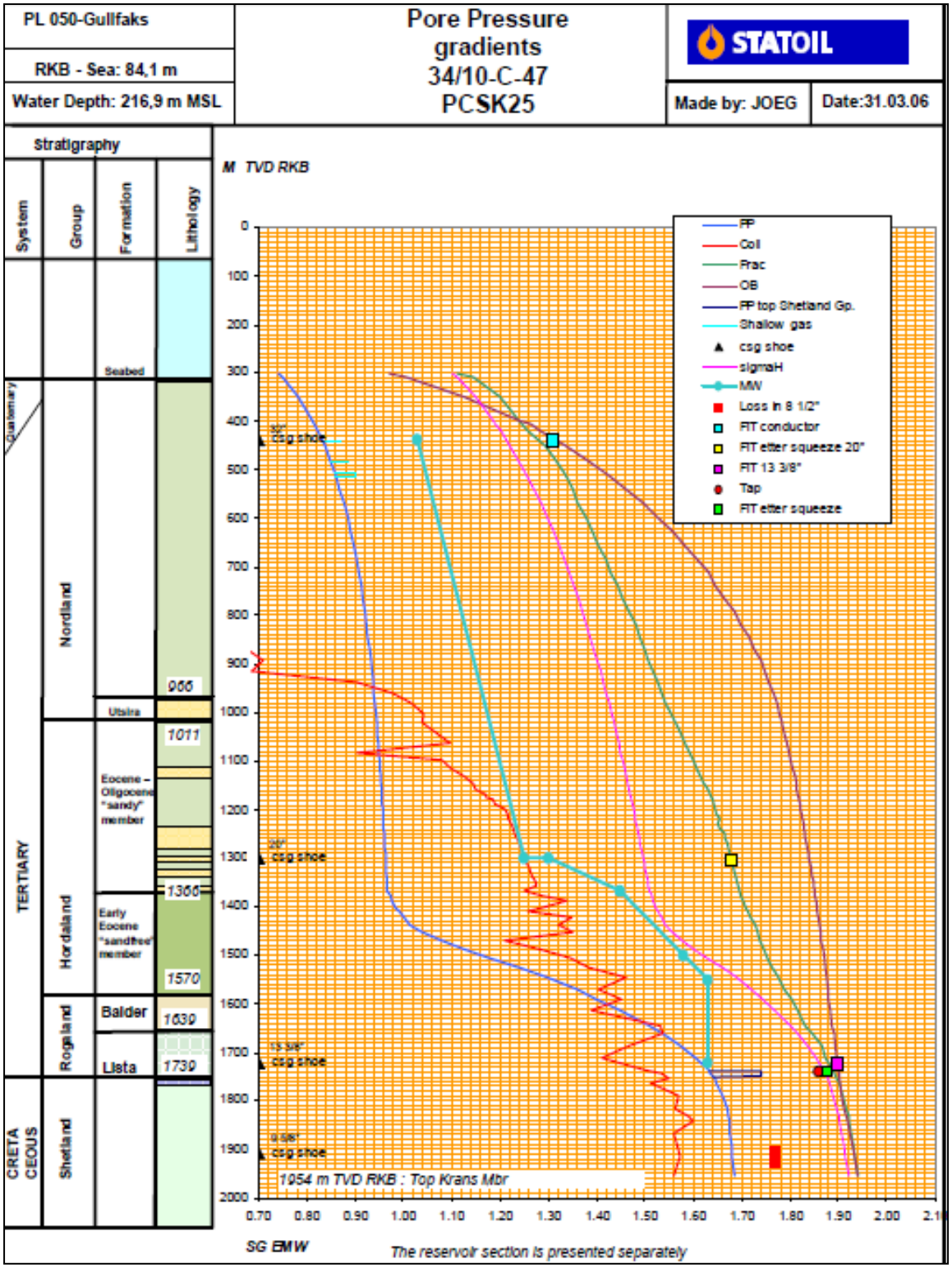

Fig. 18- Pressure plot of well C47 (Christophersen et al. 2007).

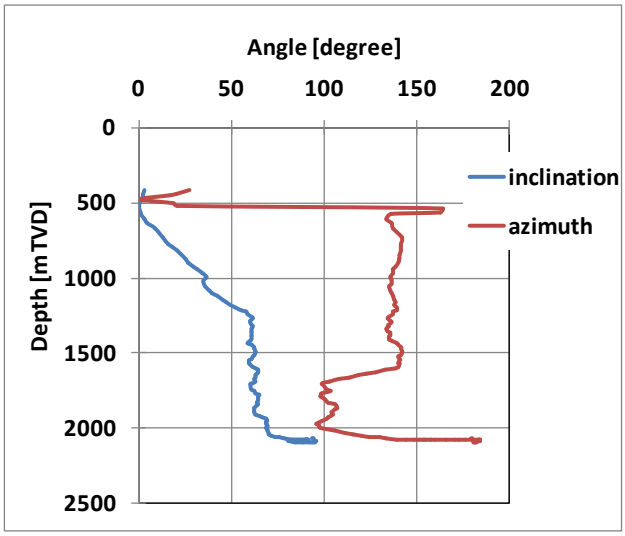

Fig. 19- TVD versus inclination and azimuth of well C47 (based on data from Statoil).

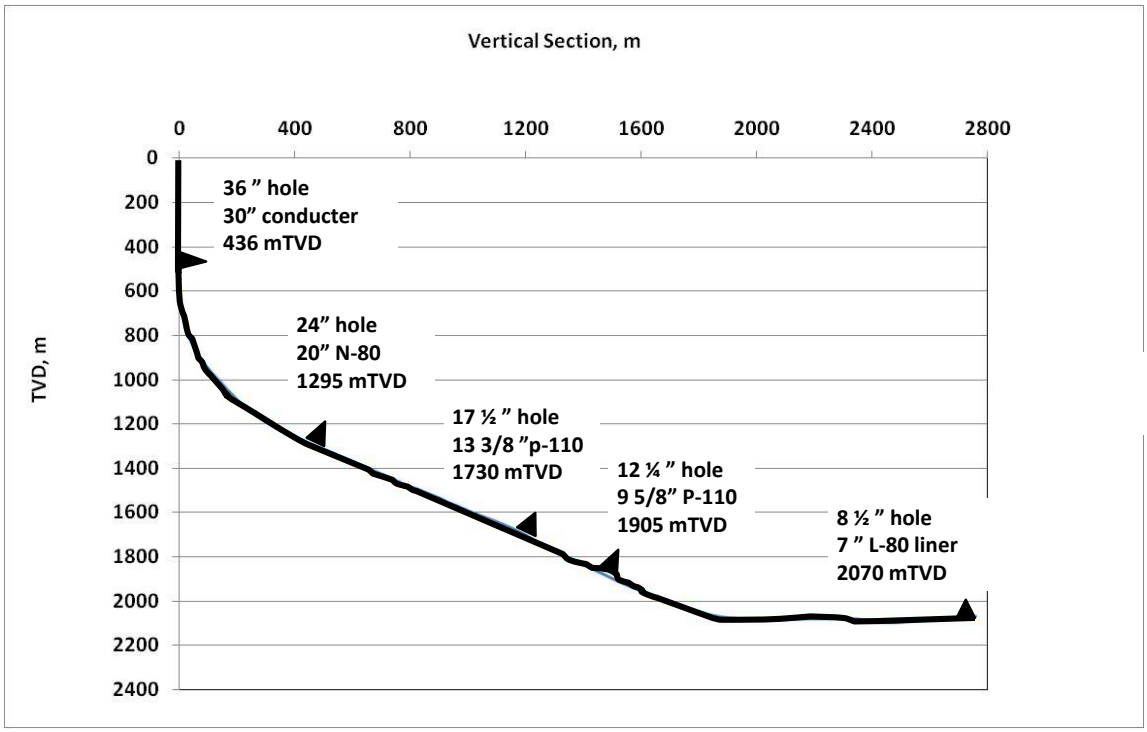

Fig. 20- Vertical well profile and casing program of well C47 (based on data from Statoil).

Table 11- Well profile divided into different sections from the geometry of well C47 (based on data from Statoil).

Well section -bottom to top	MD1 mMD	MD2 mMD	Length m	α1 deg	α2 deg	Φ1 deg	Φ2 deg
Horizontal	4338	3375	963	90	90	0	0
Build up	3375	2101	1274	90	60	0	0
Inclined-Tangential	2101	1408	693	60	60	0	0
Build up	1408	640	768	60	0	0	0
Vertical	640	0	640	0	0	0	0

Table 12- Drillstring design and fluid properties applied for the 17 ½" section of well C47 (based on data from Statoil).

Section	WBM	DP	TJ	BHA			Travelling block	
	mw	w	r	w	lenght		w	
Inch	sg	kN/m	m	kN/m	mMD	mTVD	tons	kN
17 1/2	1,30	0,28467832	0,0635	1,926	192	96	30	264

Table 13- Drillstring design and fluid properties applied for the 12 ¼" section of well C47 (based on data from Statoil).

Section	OBM	DP	TJ	BHA			Travelling block	
	mw	w	r	w	lenght		w	
Inch	sg	kN/m	m	kN/m	mMD	mTVD	tons	kN
12 1/4	1,76	0,2847	0,0635	1,1782	142	71	30	264

Fig. 21 shows an example of one of the data files with real time data of well C47. The data file is required to interpret field data, and contains information on nine items distributed over four plots with a time index. The plot to the left is showing weight on bit (WOB) in unit tons, bit position (DBTM) and hole depth (DMEA) given in measured meters. The second plot gives hook load (HKL) in tons and block position (BPOS) in meters. Next is presenting the stand pipe pressure (SPP) in bar and the mud flow (MFl) in liter per minute. The last plot to the right shows the torque (TRQ) in kNm and revolutions per minute or average rotary speed (RPMB) in c/min.

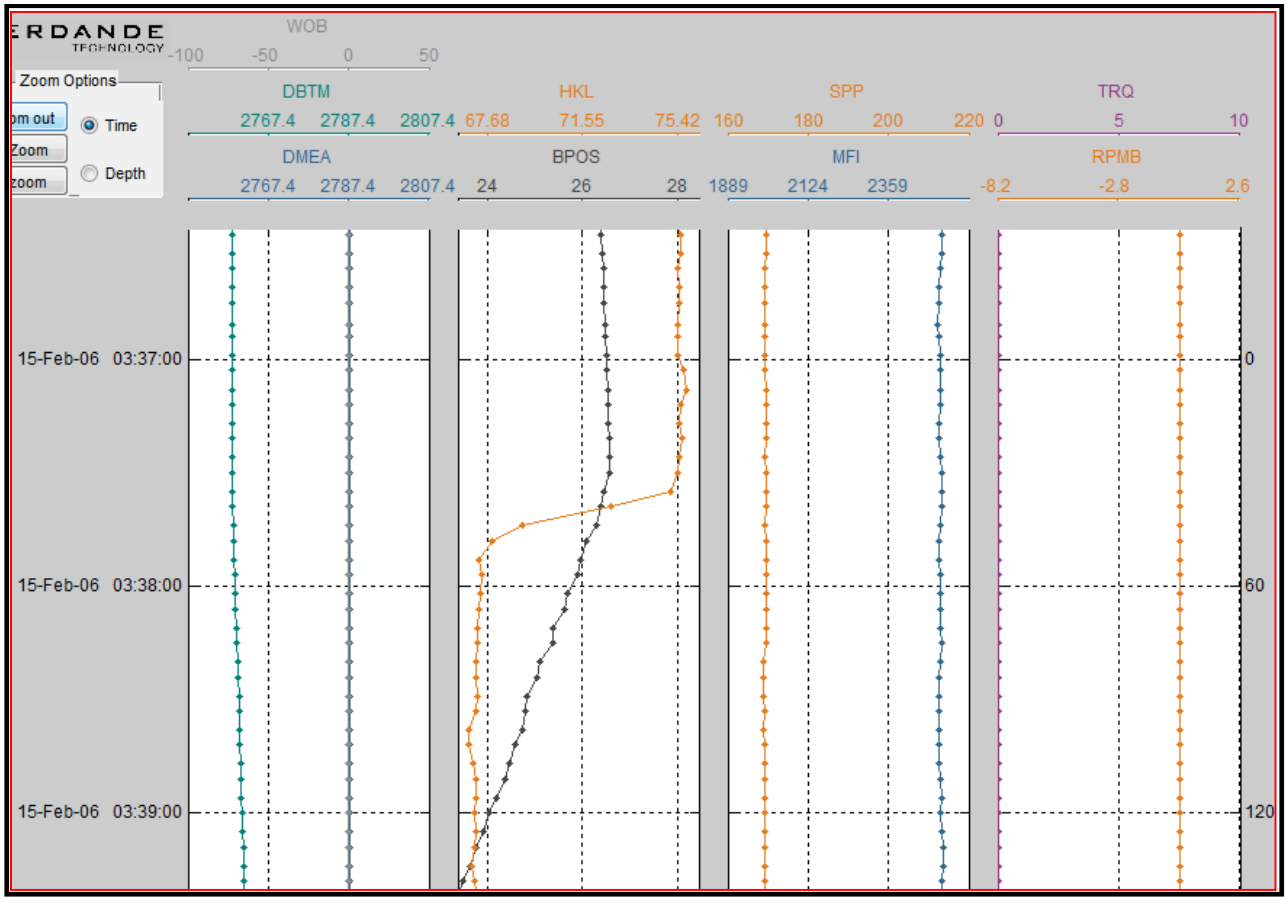

Fig. 21- Real time data of 17 ½" section for well C47 plotted with a time index (Data from Statoil via Verande Technology).

Most of the data that are entered into the model are not exact values, but average data. For instance is the real time data entered into the model average values found over a time interval with an average depth and average recorded hook load, during lowering or rising of one stand. Fig. 22 presents an example of real time data from 1 January 2006 of the 17 ½" section of well C47. The interesting time interval is between 16:43:00 to 16:45:30, where the pipe is lowered from 2039 mMD to 2066 mMD, resulting in an average depth of 2052,5 mMD. Simultaneously the hook load is varying between 69,59 tons and 73,81 tons, which results in an average value of 71,7 tons. The same is for the properties of the trajectory, which is entered as end points of each section modeled. The entered real time data are corrected for block weights, which are 30 tons for well C47, 45 tons for well A12/A12 T2 and 50 tons for well A5.

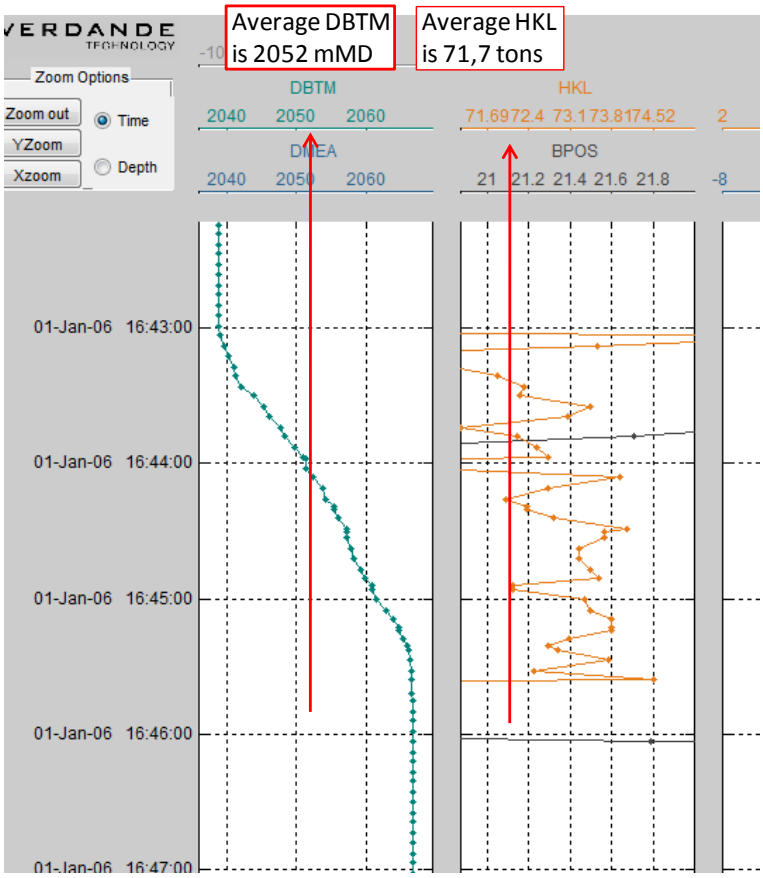

Fig. 22- Example of real time data reading of the 17 ½" section of well C47 1 January 2006 (Data from Statoil via Verande Technology).

4.2 Field data of well A12/A12 T2

This section contains a description of another well applied with the model, well A12/A12 T2 (well 15/3-A-12). Well A12/A12 T2 is a development well drilled from 15 October 2011 to 16 September 2006 in the Gudrun Field. First well A12 was drilled, and then A12 T2 was drilled as a sidetrack, and together they make the complete well A12/A12 T2. The Gudrun Field is an oil and gas field which is located outside Stavanger in the North Sea, approximately 50 kilometers north of the Sleipner East and West. The sea depth is approximately 110 meters and the reservoir lies from 4000 to 4760 meters deep. The production is planned to start in 2014.

Fig. 23 shows the inclination in degree plotted with depth, where it starts to build angle at approximately 453 mTVD. An almost constant inclination of 60 degrees is held from around 2500 mTVD to 3200 mTVD, before dropping to 4000 mTVD and entering the reservoir vertically. Well A12/A12 T2 can be assumed to be a 2D well because of negligible DL (almost constant azimuth).

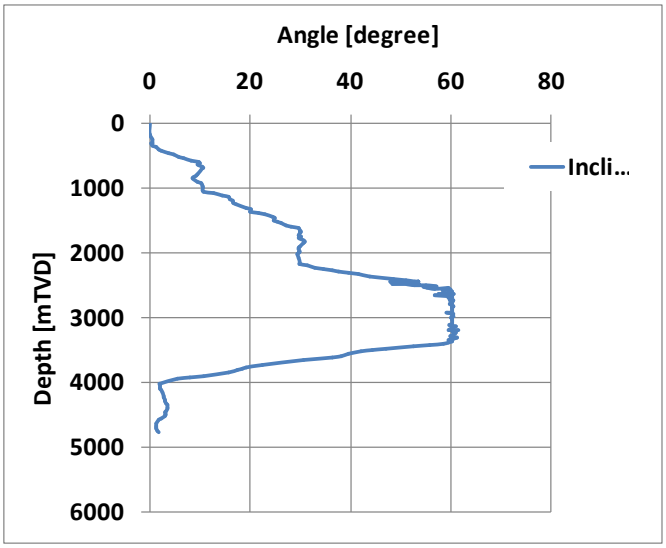

Fig. 23- Inclination plotted along the TVD of well A12/A12 T2 (based on data from Statoil).

Fig. 24 is presenting the well profile of well A12/A12 T2 in terms of horizontal departure (HD) and mTVD, where the dark blue part is the vertical section, followed by a red build up section, a green sail section, drop off section in purple, and a light blue vertical section at the end.

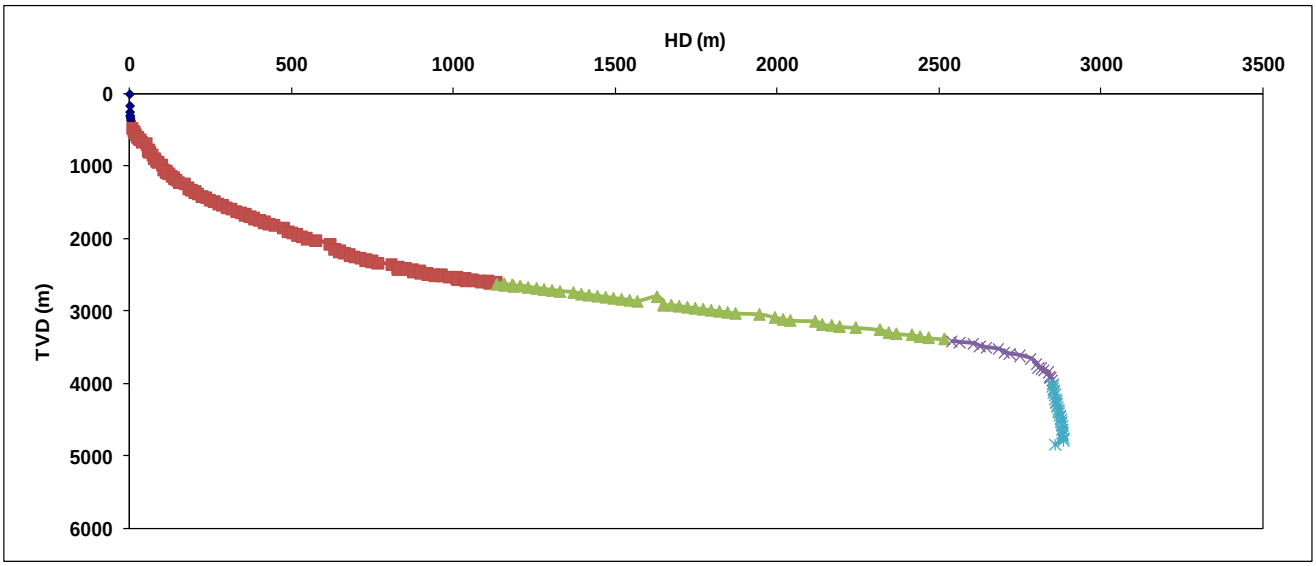

Fig. 24- Well profile in HD versus TVD of well A12 /A12 T2 (based on data from Statoil).

In Table 14 the well profile is divided into five section from bottom to top, where the upper row is the straight (vertical) section at the bottom of the well, the second row is the

drop-off, the third row is the sail section with 60 degrees inclination, the fourth row is build-up section, and the last row is the upper straight (vertical) section of the well. The second column in Table 14 shows the MD at the start of the section, while the third column shows MD at the end of the section. The next column is total length of the section, and the two last columns are inclination in degree at the start depth and at end depth of the section.

Table 14- Well sections of well A12/A12 T2 (based on data from Statoil).

Well section -bottom to top	MD1 mMD	MD2 mMD	Length of section m	α1	α2
Straight	6119	5227	892	0	0
Drop off	5227	4518	708	0	60
Inclined-Tangential	4518	2965	1554	60	60
Build up	2965	453	2512	60	0
Vertical	453	0	453	0	0

Table 15 shows a summary of properties for the 17 ½" section of well A12/A12 T2, where also here the drillstring above the BHA needs to be assumed the same way as for well C47. The radius of the TJs above the BHA, which are needed for the torque calculations, are assumed to be 0,08414 m, while the radius applied in the BHA section is 0,0635 m when the diameter for the bit is 17 ½" (API 2013).

Table 15- Drillstring design and drilling fluid applied for the 17 ½" section of well A12/A12 T2 (based on data from Statoil).

Section	OBM	DP	TJ	BHA						Travelling block	
	mw	w	r	w	lenght		D	r		w	
Inch	sg	kN/m	m	kN/m	mMD	mTVD	m	m	inch	tons	kN
17 1/2	1,4	0,2847	0,06	2,0285	212	106	17 1/2	8 3/4	0,222	45	396

4.3 Field data of well A5

Well A5 (well 15/3-A-5) is a development well which is also drilled in the Gudrun Field. Fig. 25 shows the well trajectory of well A5, where the blue curve is inclination and the red is azimuth in degrees. The well can be assumed to be a 2D well because the azimuth is almost constant through the well path. Fig. 26 is representing the well profile of well A5 with depth on the vertical axis and HD on the horizontal axis. Table 16 presents the same information as Fig. 26 in a table form. It shows that well A5 first consists of a vertical part from 0 mMD to 405 mMD, followed by a build-up section from 405 mMD

to 2506 mMD. Next section is a straight section going from 2506 mMD to 4220 mMD, then a drop-off section to 5485 mMD, and finally ending in a straight section to TD of 5919 mMD. The average values for the drillstring design and the BHA are summarized in Table 17. The measured hook loads are corrected for a travelling block of 50 tons. Fig. 27 combines the well profile of well A12/A12 T2 and well A5, because the wells are going to be compared in the following sections. It can be seen that the profiles are very similar in the upper sections, but starts to deviate more and more with depth after 2800 mTVD.

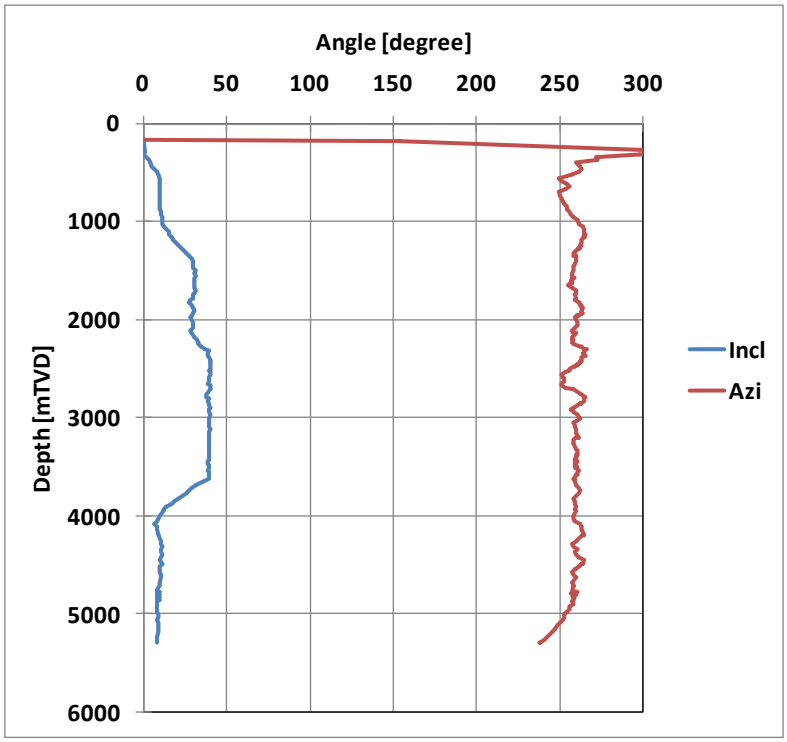

Fig. 25- Inclination versus azimuth in degrees of well A5 plotted against depth (based on data from Statoil).

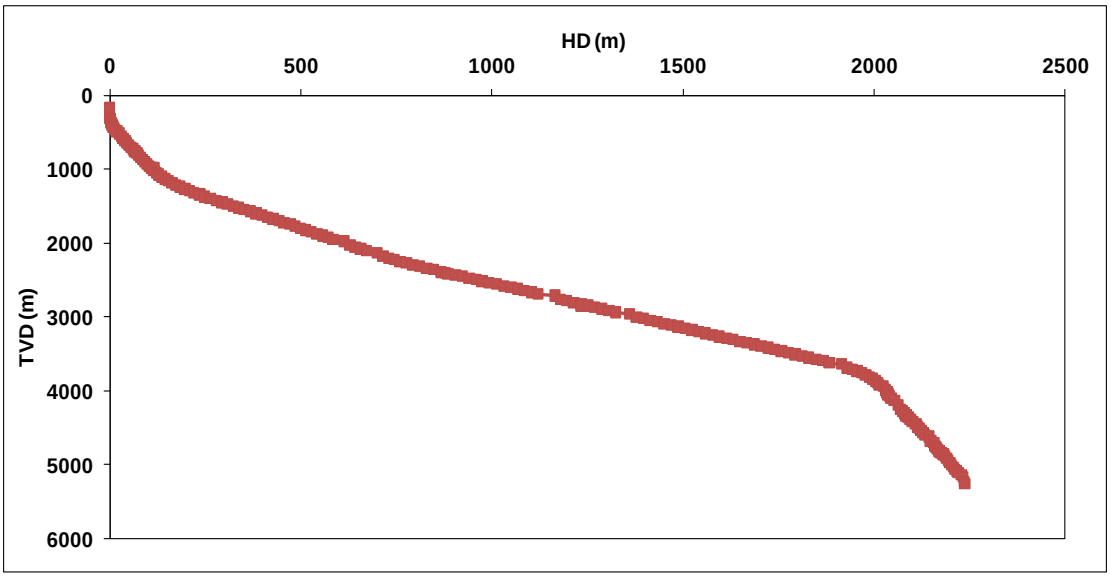

Fig. 26- Well profile of well A5 with HD versus TVD (based on data from Statoil).

Table 16- Well sections of well A5 (based on data from Statoil).

Well section -bottom to top	MD1 m MD	MD2 m MD	Length of section m	α1 deg	α2 deg
Inclined-Tangential	5919	5485	435	10	10
Drop off	5485	4220	1264	10	60
Inclined-Tangential	4220	2506	1714	40	40
Build up	2506	405	2101	40	0
Vertical	405	0	405	0	0

Table 17- Drillstring design and fluid properties applied in the model for the 17 ½" section of well A5 (based on data from Statoil).

Section	OBM	DP	TJ	BHA						Travelling block	
	mw	w	r	w	lenght		D	r		w	
Inch	sg	kN/m	m	kN/m	mMD	mTVD	inch	inch	m	tons	kN
17 1/2	1,44	0,285	0,0635	2,116625	225	172	17 1/2	8 3/4	0,222	50	441

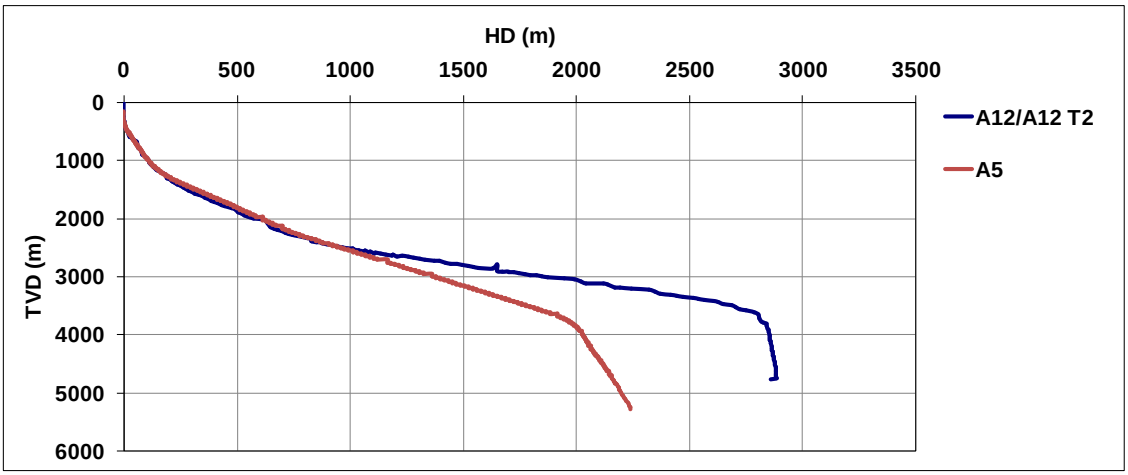

Fig. 27- Combining the well profile of well A12/A12 T2 and well A5 (based on data from Statoil).

5 Results of selected friction model

This chapter contains results from field cases with the selected friction model. The same procedure as applied in the example S-well in chapter 3.8.2, is applied to model friction factor for the field wells; well C47, well A12/A12 T2 and well A5.

5.1 Drag results from the 17 ½" section and the 12 ¼" section of well C47

Fig. 28 shows modeled friction factor versus depth plotted between 390 mMD and 2748 mMD, but the depth interval between 1100 mMD to 2748 mMD should rather be applied for evaluation. The reason for this is that the model is more sensitive to change in measured data for small inclinations and shallow depth with little drillstring downhole and can give misleading result, which will be further demonstrated in chapter 6. The blue curve in Fig. 28 shows modeled friction factor with depth when POOH 31 December 2005 in the 17 ½" section, while the red curve presents modeled friction factor with depth when POOH 10 February and 12 February 2006 in the 12 ¼" section. The friction factors modeled is average values for the complete hole, and the case depends on how far out the drillstring has been pulled at that time. For instance is the 20" casing shoe positioned at approximately 1500 mMD, which means that when POOH during drilling of the 17 ½" section, the entire drillstring will be in contact with the casing if the drillstring is being pulled out of the hole above this depth. On the other side, if the drillstring is being pulled out of the hole from a depth below the casing shoe, the modeled friction factor will be for a case where the upper part of drillstring is in contact with the casing, while the lower part is in contact with the open hole, as demonstrated in Fig. 29. The average friction factor is modeled to be approximately 0,25 for the case when the entire drillstring is contact with the 20" casing during drilling of the 17 ½" section, while it is around 0,37 for the case when the parts of the drillstring is contact with the 20" casing and parts of the drillstring is in contact with the 17 ½" open hole. The red curve, which presents the friction factor plotted with depth when drilling the 12 ¼" casing, shows that the friction factor is in average 0,15 for the case when the drillstring is in contact with the 13 $^{3}/_{8}$" casing over its entire length, and also 0,15 for the case when it is in contact with both the 13 $^{3}/_{8}$" casing and the 12 ¼" open hole.

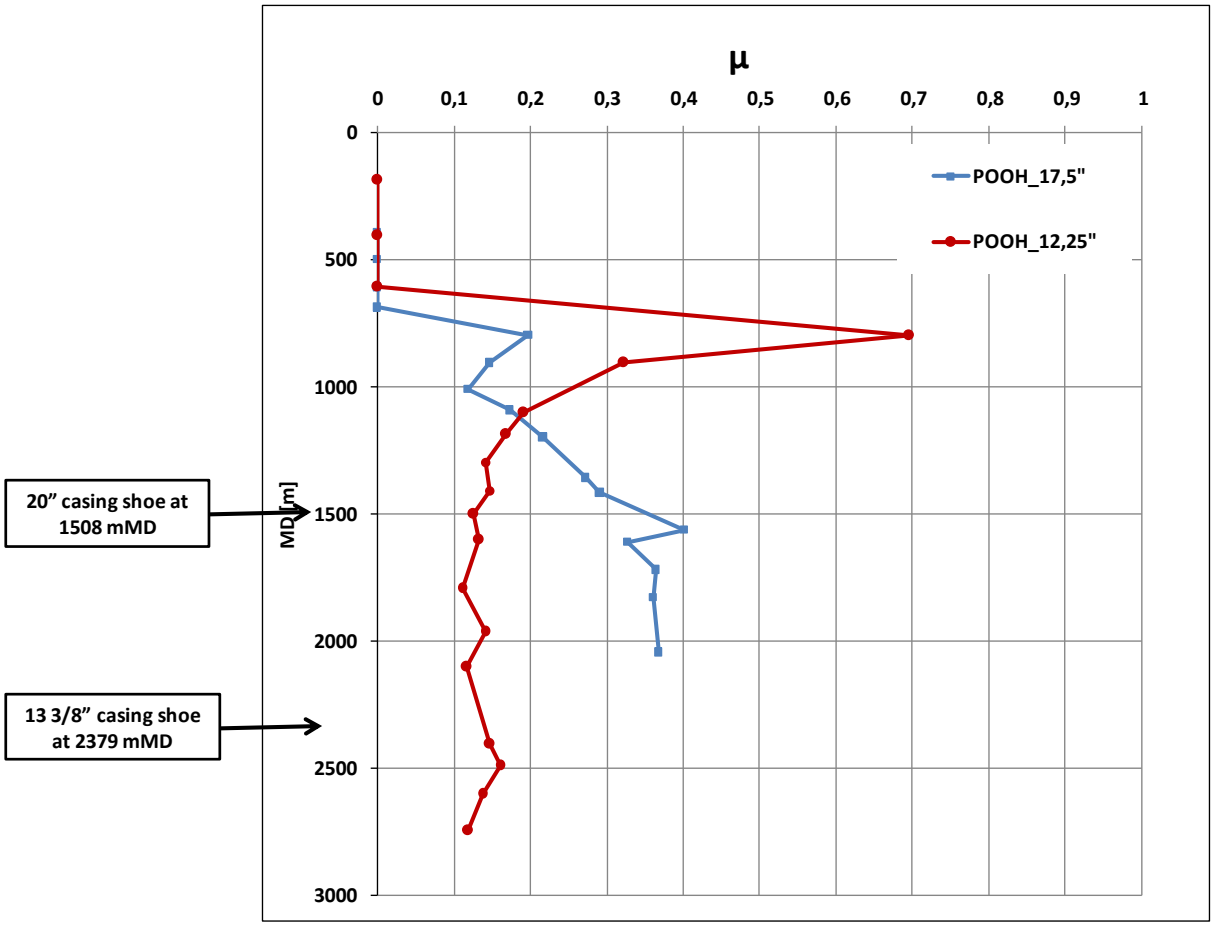

Fig. 28- Graph of friction factor versus depth when POOH for the 17 ½" section and the 12 ¼" section for well C47.

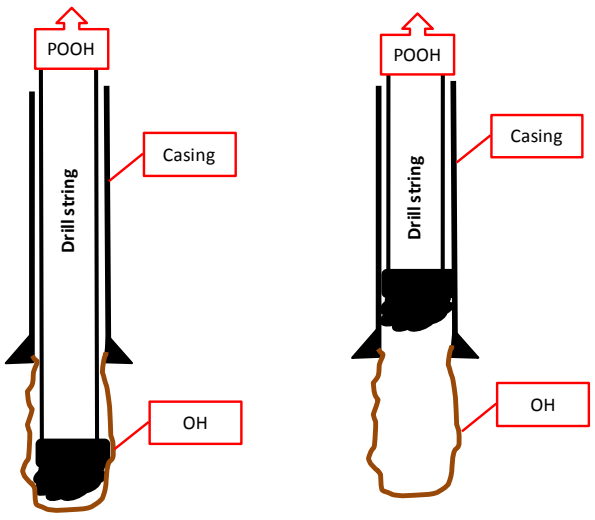

Fig. 29- Left sketch: The drillstring in contact with both the open hole and the casing.

Right sketch: The entire drillstring is in contact with only the casing.

Table 18 shows the result of modeled friction factor and estimated loads for different depths along the well path at total depths of 1546 mTVD (RIH) and 1568 mTVD (POOH) for the 17 ½" section of well C47. For POOH from 1568 mTVD, the friction factor was modeled to be 0,3678, while for RIH from 1546 it was modeled to be 0,2071, and with these values the loads farther downhole are calculated. Fig. 30 has the same information showed in Table 18, but in a graphical presentation. It shows clearly that bends and changing from lower to higher weight of the drillstring result in increased friction.

Table 18- Data from the Excel spreadsheet tool showing results for a static case, RIH and POOH for a TD of 1546 mTVD (RIH) and 1568 mTVD (POOH) for the 17 ½" section of well C47. The upper table shows modeled friction factor and the lower table shows estimated loads along the well path.

	μ
Static	0
RIH	0,2071
POOH	0,3678

RIH			POOH		
Depth m TVD	Static kN	RIH kN	Depth m TVD	Static kN	POOH kN
1546	0,0	0	1568	0,0	0
1450	154,6	99	1472	154,6	253
1260	201,8	129	1260	207,5	340
640	352,6	257	640	358,3	721
0	504,6	409	0	510,3	873

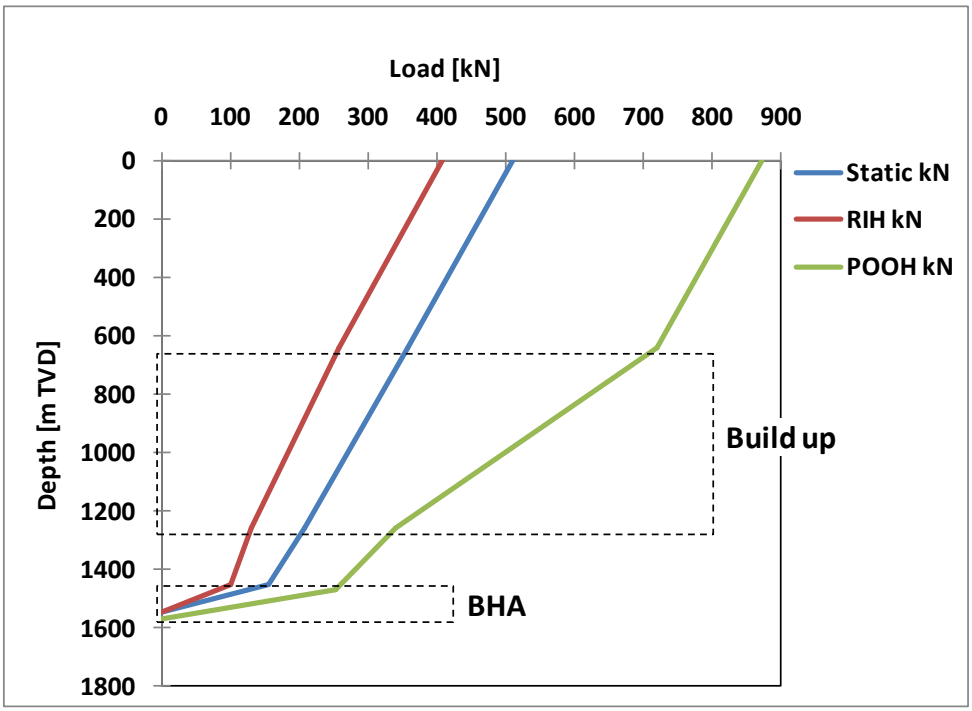

Fig. 30- Estimated loads and modeled friction factor in the 17 ½" section of well C47. For POOH at 1568 mTVD the friction factor was modeled to be 0,3678, and for RIH at 1546 m the friction factor was 0,2071.

5.2 Drag results for the 17 ½" section of well A12/A12 T2

Table 19 is presenting result from modeled friction factor with depth when POOH 15 June 2012 in the 17 ½" section of well A12/A12 T2. The two first columns are mMD along the well and measured hook load at surface. The following column is hook load at the surface when the friction factor is assumed to be zero. The fourth and fifth column are estimated hook load when the friction factor is put first to 0,69 and then to 0,39. Modeled friction factor as a function of drillstring length downhole is presented in the sixth column. The average friction factor when POOH in the 17 ½" section of well A12/A12 T2 is 0,69, while it is 0,39 when POOH in the 17 ½" section of well A5. Note that the measured loads found from real time data are already corrected for block weight of 45 tons. Fig. 31 is presenting the same case in a graph from a depth of 1186 mMD to 2773 mMD. The average modeled friction factor is represented by the red graph and is showing 0,69 for the depth interval in the 17 ½" section of well A12/A12 T2. The 20" casing shoe setting depth is at 1021 mMD.

Table 19- Result from modeling when POOH 15 June 2012 in the section 17 ½" of well A12/A12 T2.

Measured Depth	Measured Load	Estimated Load μ=0	Estimated Load μ=0,69	Estimated Load μ=0,39	μ Modeled
m	kN	kN	kN	kN	
2773	1407	779	1619	1150	0,56
2600	1273	800	1441	1094	0,55
2491	1292	804	1344	1057	0,64
2407	1255	794	1298	1032	0,64
2294	1202	777	1239	998	0,65
2212	1169	761	1206	974	0,64
2098	1120	735	1171	944	0,62
2013	1089	719	1135	918	0,63
1900	1069	693	1103	889	0,64
1815	1025	676	1067	863	0,63
1700	1000	656	999	821	0,69
1585	958	643	919	778	0,77
1501	912	628	877	750	0,77
1414	876	613	830	721	0,81
1300	830	594	761	678	0,93
1186	778	571	728	651	0,88

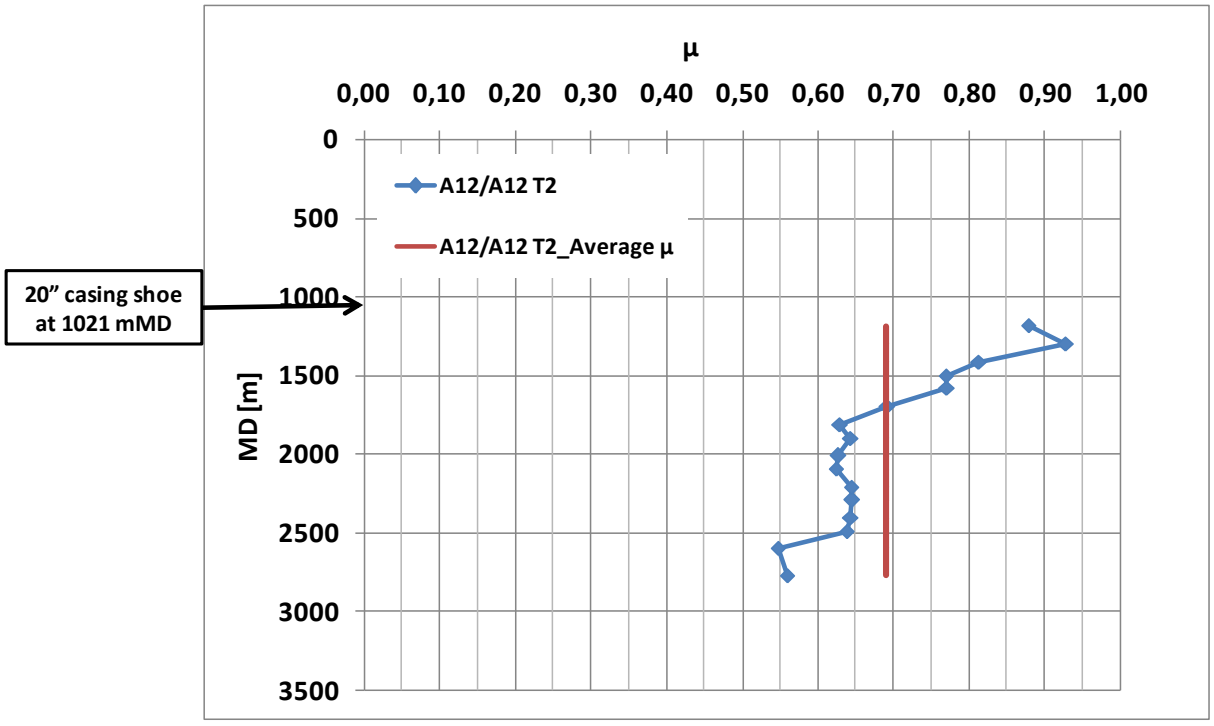

Fig. 31- Graphical presentation of modeled friction factors for different drillpipe lengths when POOH 15 June 2012 in the 17 ½" section of well A12/A12 T2.

5.3 Drag results for the 17 ½" section of well A5

Table 20 is presenting result from modeled friction factor with depth when POOH 4 January 2012 in 17 ½" section of well A5. The two first columns are depth and measured hook load at surface. The following column is hook load at the surface when the friction factor is assumed to be zero. The fourth and fifth column are estimated hook load based on a friction factor of 0,69 and to 0,39. Modeled friction factor as a function of drillstring length downhole is presented in the sixth column. Note that the measured loads found from real time data are already corrected for block weight of 50 tons.

Fig. 32 is presenting the same case in a graph from a depth of 1493 mMD to 3044 mMD, where the red graph is showing an average friction factor of 0,39 for the 17 ½" section of well A5 in the interval modeled. The 20" casing shoe setting depth is at 1024 mMD.

Table 20- Result from modeling when POOH 4 January 2012 in section 17 ½" of well A5.

Measured Depth m	Measured Load kN	Estimated Load μ=0 kN	Estimated Load μ=0,69 kN	Estimated Load μ=0,39 kN	μ Modeled
3044	1288	897	1726	1276	0,38
2904	1230	872	1662	1234	0,37
2819	1231	857	1623	1208	0,39
2702	1187	842	1556	1170	0,39
2590	1152	834	1469	1129	0,39
2505	1138	832	1400	1099	0,42
2390	1104	820	1332	1064	0,42
2306	1076	804	1298	1040	0,42
2182	977	779	1252	1005	0,33
2099	1010	764	1217	981	0,41
2014	980	734	1222	965	0,39
1899	945	720	1151	926	0,40
1813	919	699	1128	904	0,39
1694	880	674	1085	871	0,39
1608	849	657	1054	847	0,37
1493	820	644	970	802	0,41

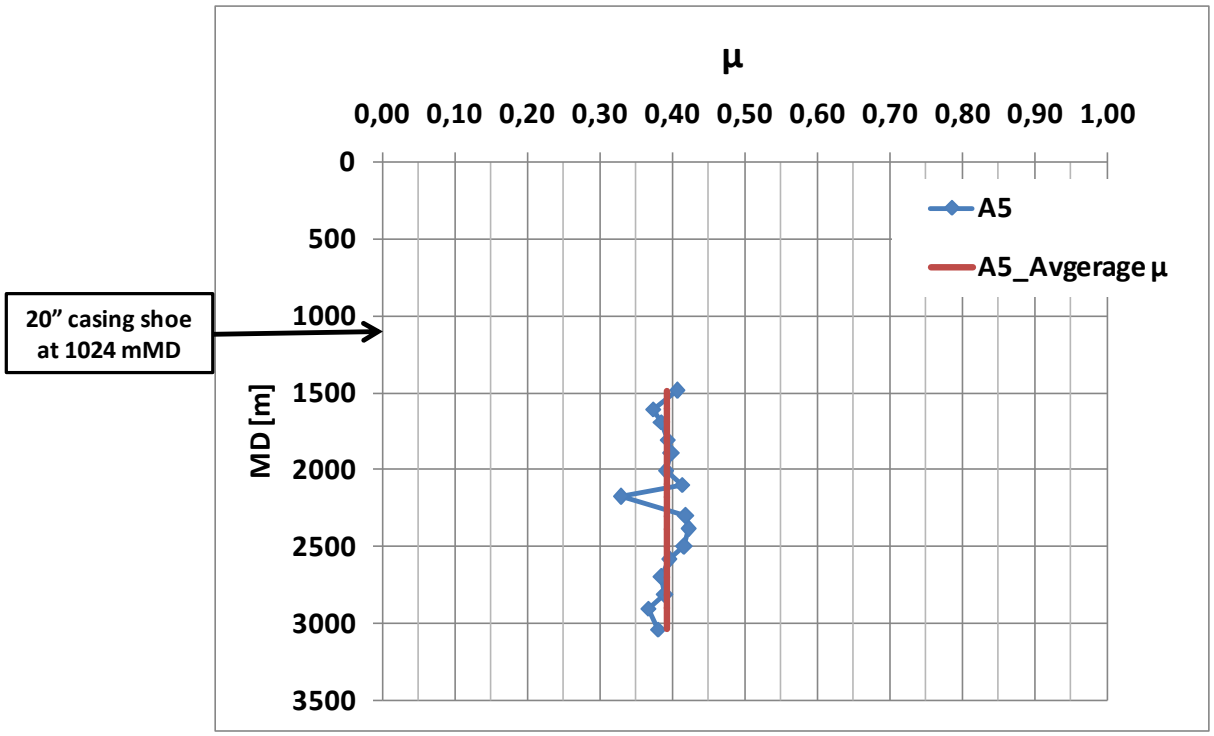

Fig. 32- Graphical presentation of modeled friction factors for different drillpipe lengths when POOH 4 January 2012 in the 17 ½" section of well A5.

6 Evaluation of selected friction model

To evaluate the friction model, the result from the field cases will in this chapter be discussed. First an assessment of the result from modeling well C47 is presented, and then results of well A12/A12 T2 and well A5 are evaluated. There are mainly two reasons for why there would be a deviation between measured data and modeled result for a specific case; either the model is built on wrong assumptions, or it might indicate a potential problem in the wellbore. For instance if there is a small diversity between two subsequent friction coefficients, it means stable borehole condition with no problems of moving the string downhole. However, detection of a current measured friction larger than the reference friction can indicate that the downhole condition no longer is optimal, and an immediate remedial action should be considered. Therefore, sensitivity analysis of friction coefficient could be useful in predicting any problem during drilling operations (Fazaelizadeh et al. 2010).

The subchapters in the last part of chapter 6 contain limitation with the model and suggestion on how to eliminate it. The friction model is built on the basis of fundamental physics, and does not include very complex physical effects, such as the listed limitations and assumptions with the model. It is not possible to ensure correct prediction under any circumstance because there always are some uncertainties in input data, or even effects that are poorly modeled or not modeled at all. The chapter ends with a discussion around some additional future work.

6.1 Evaluation of result from well C47

6.1.1 Compare modeled and expected friction factor of well C47

In this chapter it has been looked at the possibility of applying the result from the friction model to detect whether certain parameters connected to the drilling process, in this case the friction factor, start to deviate from their expected values. The purpose is to investigate the opportunity to find abnormal conditions by take several symptoms into account in such an analysis. This is often referred as early warning detection if applied in real time mode. Table 21 shows expected friction factors that are based on analysis of relevant offset data, such as historical well data, and can be compared with modeled data. The first column is containing three different mud types; WBM (water-based mud), OBM (oil-based mud) and brine. The next two columns are friction factors for subsequently cased hole and open hole. The table is showing a typically lower friction factor for OBM in a cased hole. The left table in Table 22 is comparison between expected and modeled

friction factor in open hole and cased hole for the 17 ½" section when applying WBM, while the right table is comparison between expected and modeled friction factor in open hole and cased hole for the 12 ¼" section when applying OBM

Table 21- Default friction factors based on historical well data (Payne and Abbassian 1997).

Mud type	Cased hole Friction factor	Open hole Friction factor
WBM	0,24	0,29
OBM	0,17	0,21
Brine	0,30	0,30

Table 22- Summary of modeled and expected friction factors for the 17 ½" section and the 12 ¼" section of well C47.

Hole section	17 1/2	
	C	OH
Depth [m MD]	1508	2379
Actual/modeled μ with WBM	0,25	0,37
Expected μ with WBM	*0,24*	*0,29*

Hole section	12 1/4	
	C	OH
Depth [m MD]	2379	
Actual/modeled μ with OBM	0,23	
Expected μ with OBM	*0,17*	*0,21*

Expected friction factor for a cased hole with WBM is 0,24, which is not too far from the modeled friction factor of 0,25 in the 17 ½" section. In the open hole the friction factor seems to be 0,37, which is further away from the expected value of 0,29 with WBM.

Several causes for high friction experienced in the 17 ½" section of well C47 have been discussed in "Model hook load and interpretation of real time data for well C47" (Frafjord 2012). The following list contains a summary of the most important issues:

- Many BHAs were applied in the 17 ½" section, which might have been stiffer than the one used in the 12 ¼" section. Restrictions in the borehole can occur if a stiff BHA is moved through a bend.

- Drilling in an overpressured shale zone with application of a mud which was insufficient.
- A broken circulation was experienced in the 17 ½" section.
- Occurrence of possible DLs in the 17 ½" section because of problems with the steerable downhole tool.

The rise in friction seems to start around the start of the sail section, which is just approximately 100 m above the 20" casing shoe. As discussed in "Model hook load and interpretation of real time data for well C47" (Frafjord 2012), this might be an effect of a bad arrangement drillstring design when POOH in a specific interval in the well path. Combination of changes in wellbore direction together with stiffness of the BHA and arrangement of tools, such as stabilizers, will affect the friction and might result in difficulties with passing the drillstring through a specific wellbore section. Fig. 33 shows an example of a DL, which can be explained as a "bend" in the wellbore that makes an unnatural direction for the drillstring to follow. Regular hole-deviation surveys usually detect significant DLs, and in the 17 ½" section it is suspected because of extra torque and force needed to move the pipe caused by restriction of pipe movement at a specific depth. If no remedial action is performed, DLs can moreover lead to borehole problems including formation of keyseats and ledges, presented in Fig. 33, which in turn can result in more severe problems such as stuck pipe and pipe failure (Hawker et al. 2001). Another theory for why the friction factor increases a small distance above the casing shoe is because of possibilities for a bad cleaning of the well after cementing the 20" casing, where the cement can then act as a restriction.

In the 17 ½" section the BHA has been changed five times, while no change of BHA were performed in the 12 ¼" section (Christophersen et al. 2007). It is common to change the BHA to continue a straight section of the well after drilling a deviated build interval with the possibility of DLs, by using a specific assembly for building angle. The changed BHA can be stiffer and not flexible enough to run through certain sections, seen in Fig. 34. Also stabilizers in the assembly contribute to hang up the string in opposing sections of the wellbore, preventing movements of the drillstring. It is not a good solution to force down the drillstring if register down-weight when entering this section, but a recommended remedial action is to ream carefully and open up the bottom section of the hole to the full-hole size (Hawker et al. 2001).

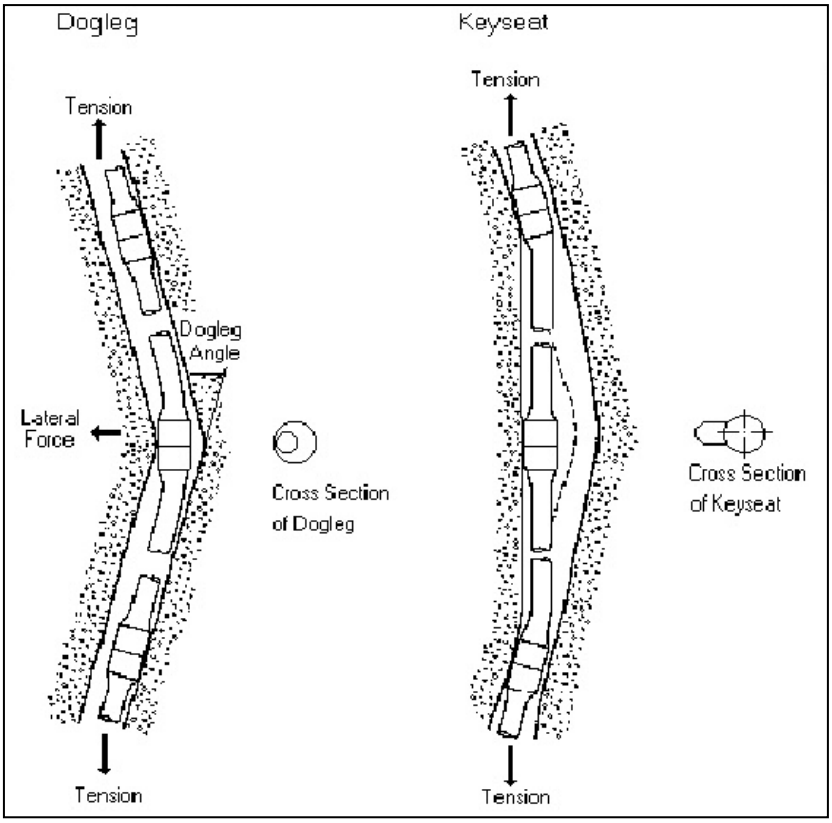

Fig. 33- The figure show two different seats where the drillstring can be hung up; DL seat to the left and keyseat to the right (Hawker et al. 2001).

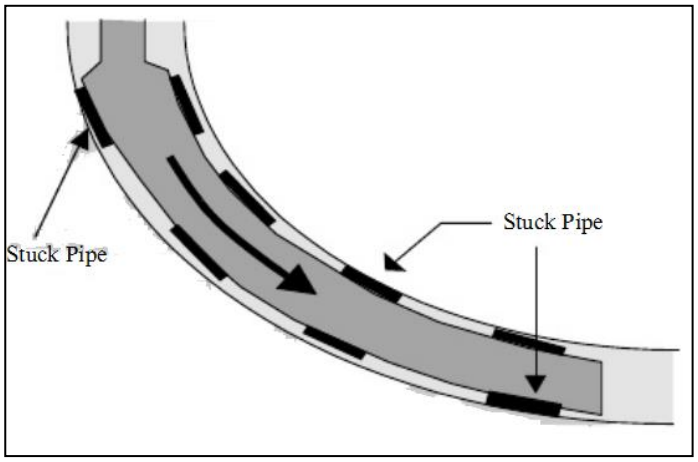

Fig. 34- The sketch shows typical location in wellbore with risk for getting stuck pipe (Hawker et al. 2001).

"Model hook load and interpretation of real time data for well C47" also contains a discussion around benefits of detecting issues, mentioned above, causing undesirable borehole conditions as early as possible to prevent problems before they are getting

critical. Some remedial actions in the case with the 17 ½" section, include actions to improve the hole condition by improve hole cleaning, with reaming, proper hole circulation and change of mud type. However, the final well report for well C47 indicates that these actions probably not were made in right time, because there have been registered downhole problems, which probably were caused by insufficient hole cleaning as main factor. Some of the problems reported in the 17 ½" section are pack off, high overpull and sticky cuttings in return on the shaker. In the well report it was mentioned that the mud applied, Ultradrill WBM, was not considered suitable and resulted in high concentration of packed cuttings that was not removed from the hole with the mudflow and circulation used while drilling (Christophersen et al. 2007).

With basis in this discussion it was concluded that issues experienced in the 17 ½" section may have contributed to a high bore hole friction, which can be underlined by a higher modeled friction factor than expected in the open hole.

Because the 12 ¼" section was drilled with OBM, the expected friction factor in the OH is reduced to 0,21, while the modeled friction factor was only 0,15. Also for the cased hole the friction factor was modeled to be 0,15, which is lower than the expected friction factor of 0,17 for this case. There is no severe downhole problems registered during drilling of the 12 ¼" section, which is supported by the low modeled friction factor that indicate a stable borehole condition.

6.1.2 Compare the friction factor in the 17 ½" section and the friction factor in the 12 ¼" section of well C47

The friction factor modeled in the 17 ½" section is greater compared with the friction factor modeled 12 ¼" section. For the 17 ½" section the friction factor is 0,37 in OH, while for the 12 ¼" section it is only 0,15 in the OH.

One theory for why the friction factor has decreased in the 12 ¼" section is reaming and circulation of the well (26 January 2006) in the time interval between drilling the 17 ½" section and the 12 ¼" section. Circulation and reaming improve hole cleaning because solids in the borehole are removed, and the borehole might become more even with less DLs leading to reduced friction. Also displacing the well to OBM in the 12 ¼" section (27 January 2006) will help to reduce the friction in the borehole. In general WBM has less lubricate effect than OBM, leading to higher bore hole friction when applying WBM. A second disadvantage with WBM is that it is less inhibitive than OBM. This means that the mud easier reacts with the surrounding formation, such as salt and shale, where the

result can be swelling and sloughing shale leading to tight hole and increased borehole friction.

6.1.3 Compare friction factor for POOH and RIH in the 17 ½" section for well C47

Table 18 shows that the friction factor is modeled to be 0,3678 when POOH from 1568 mTVD to 0 mTVD (31 December 2005), while it is modeled to be 0,2071 when RIH from 0 mTVD to 1546 mTVD (1 January 2006) during drilling of the 17 ½" section of well C47. When the drillstring is being POOH from a depth that is deeper than the 20" casing shoe, the average modeled friction factor is for a case where the upper part of the drillstring is in contact with the 20"casing, while the lower part is in contact with the 17 ½" open hole. On the other side, when the drillstring is being POOH from a depth that is shallower than the 20" casing shoe, the average modeled friction factor is for a case where the entire drillstring is in contact with only the 20" casing. When studying the activities registered in final well report for well C47, it is mentioned that the well was circulated clean in the time interval between POOH 31 December 2005 and RIH 1 January 2006. This might be the reason for a lower modeled friction factor when RIH after circulation.

Fig. 30 shows that the static weight curve has a constant slope regardless of inclination, where it changes when the unit weight of the string is increasing from drillpipe to BHA. It is clear that the build-up bend leads to increase in well friction.

6.2 Evaluation of result from well A12/A12T2 and well A5

The result from well A12/A12 T2 and well A5 is in this chapter applied to evaluate application, reliability and constrains of the friction model. This section contains result from both wells because they are not only looked at separately, but also combined to do an evaluation. As a part of the evaluation, two tests; test 1 and test 2, have been used to check the reliability of the friction model. Test 3 is for quality control by comparing the theoretical and measured static weight, as mentioned in chapter 3.8.3.

6.2.1 Evaluation of the friction model to model shallow sections

When evaluating the result from well A12/A12 T2, the friction factor seems to be overestimated for shallow sections. A change in the trend of the modeled friction factor can be observed when studying modeled friction factor with depth during POOH from

2773 mMD 15 June 2012 in the 17 ½" section of well A12/A12 T2. Fig. 31 shows that the modeled friction factor is ranging around 0,60 in the deepest depth interval (1800 to 2800 mMD). However, as the drillstring is being pulled out of hole, and the drillstring is mostly in the upper, vertical section, the friction factor seems to increase to unreasonable values, towards the value one. Also when comparing the friction factor modeled with the expected friction factor for the well, the friction factor seems to be overestimated. Since the drillstring is mostly pulled out of the hole when it is partly in contact with the open hole, and partly in contact with the 20" casing (the casing shoe depth is 1021 mMD) the friction factor is expected to be 0,21 when using OBM in an open hole. This is lower than the modeled one.

The friction factor is not only overestimated in well A12/A12 T2. In Fig. 32 the friction factor seems to almost be constant of 0,39 during POOH of the 17 ½" section of well A5. For this case, the 20" casing shoe is set at 1024 mMD, meaning that also here the drillstring is partly going through cased hole and open hole when POOH deeper than 1024 mMD. A friction factor around 0,37 is also higher than the expected friction factor of 0,21 for pulling out of an open hole with OBM.

A low friction factor is expected during POOH during drilling of the 17 ½" section for both well A12/A12 T2 and well A5 since no downhole problems have been reported in the daily drilling report of Statoil for this section. However, both sections are relatively shallow compared to the total depths of the wells. A possible theory for the development towards high friction factor is therefore appearance of shallow DLs. Another option is inaccuracy in measured load entered into the model. The modeled friction factor is more sensitive to change in measured hook load in sections with little drillstring downhole and small inclinations in the well path. The result from these sections is therefore more uncertain because of the influence of the entered measured loads, which is further discussed in chapter 6.

6.2.2 Reliability test 1 of the of the friction model: Compare observed and estimated hook load of well A12/A12 T2

Test 1 is made to check if the model gives about the same result for observed and estimated hook load for well A12/A12 T2. The estimated hook load is with a modeled friction factor of 0,39. The friction factor is a modeled result from the very similar well A5. The procedure is illustrated in Fig. 35. Fig. 36 shows measured and estimated hook load for well A12/A12 T2. The blue graph is representing the hook load for measured values, while the green graph is estimated hook load with a the modeled friction factor of 0,39 for the whole interval. It can be seen that there is a deviation of approximately 184

kN (18 tons) in average between the two curves. When having in mind that the friction factor is modeled from a nearby well, this is evaluated to be a reasonable difference. Fig. 36 also shows that hook load when POOH (the blue and the green graph) are higher than the static weight (red graph).

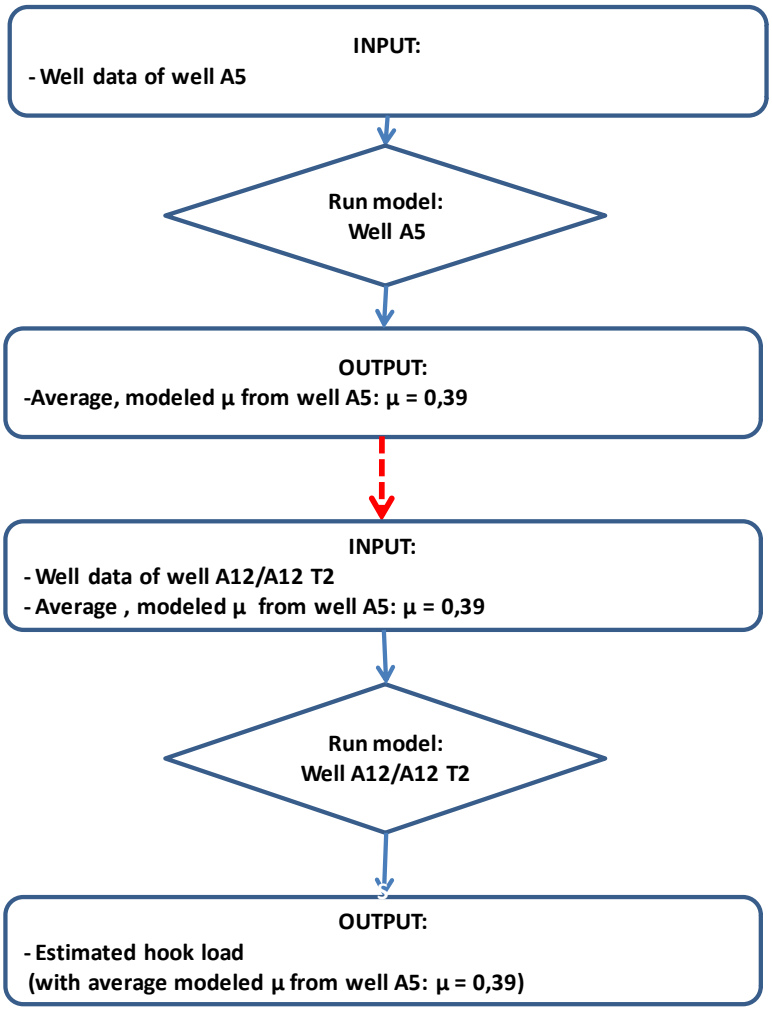

Fig. 35- Process of modeling/observed and estimated hook load for well A12/A12 T2.

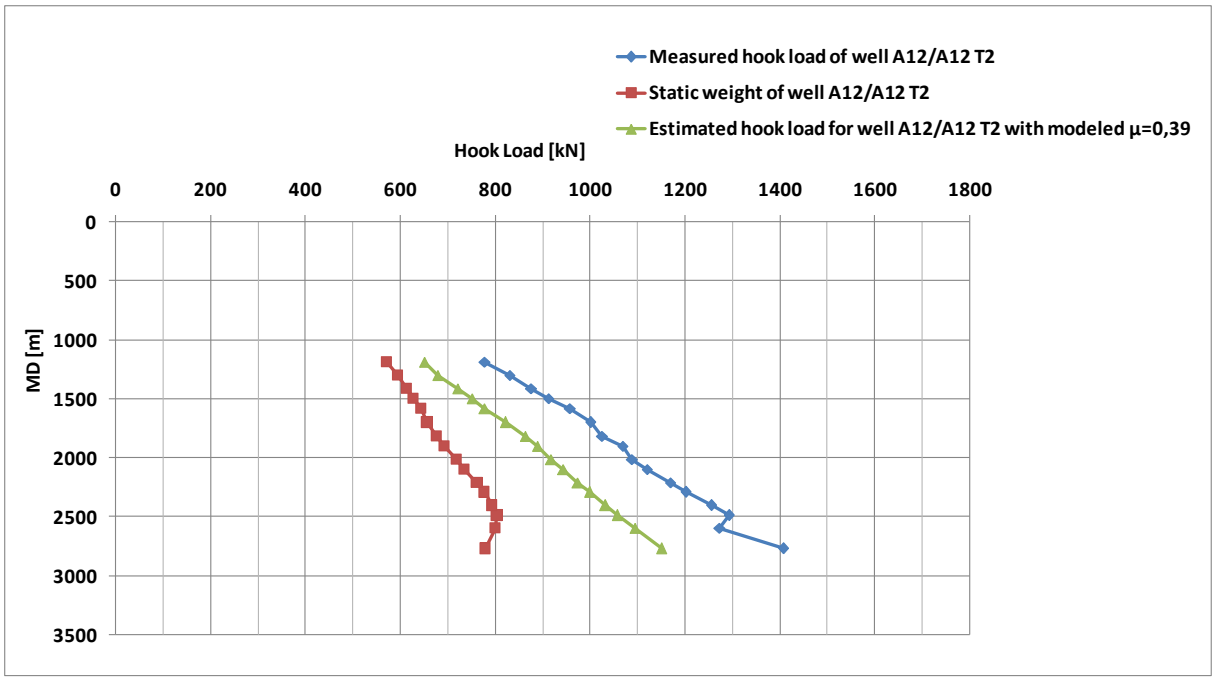

Fig. 36- Comparison of measured and estimated hook load for well A12/A12 T2

6.2.3 Reliability test 2 of the of the friction model: Evaluation of estimated hook load for well A12/A12 T2 and well A5

Test 2 compares estimated hook load for well A12/A12 T2 and well A5, with the modeled friction factor. Fig. 37 shows estimated surface hook load for different drillpipe lengths during POOH when the average modeled friction factor from well A5 of 0,37 is entered into both well A12/A12 T2 and well A5. Because the well profiles of the two wells are very similar, the load estimated is almost overlapping, as expected.

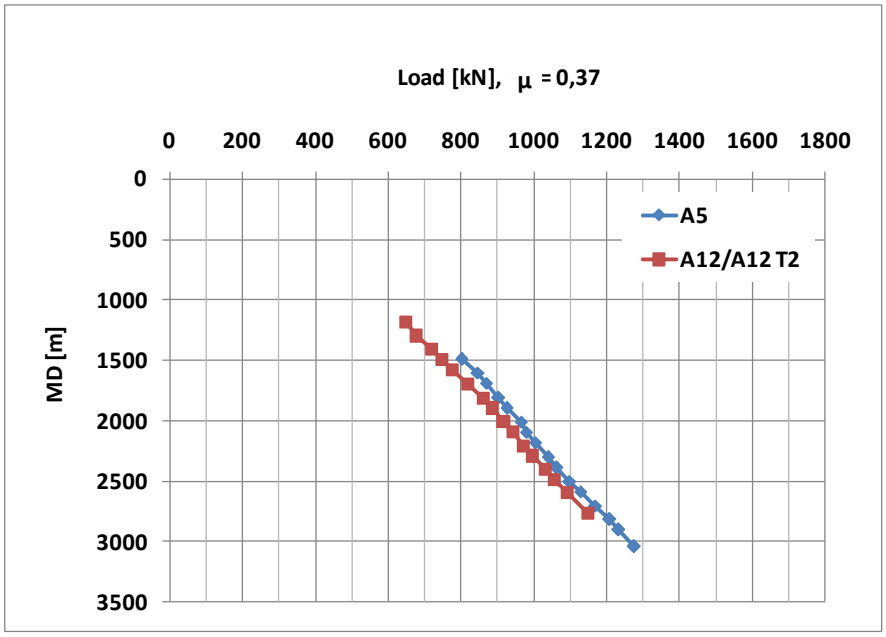

Fig. 37- Estimated hook load plotted for well A12/A12 T2 and well A5 with the same friction factor of 0,37 during POOH of the 17 ½" section

6.2.4 Evaluation of modeled friction factor for cases with torque during reaming in the 17 ½" section of well A12/A12 T2

This section contains results from modeling friction factors during reaming operations (rotating off-bottom) in the 17 ½" section of well A12/A12 T2. To simplify the calculations, the cases with reaming are found when the drillstring is stationary at one depth, meaning that there is only rotational motion without axial movement, illustrated by the red, dotted square in Fig. 38. The first column in the figure shows that the hook load height is constant from 19:01 to 19:08. The bit depth at that time (16 June 2012) is 2121 mMD, while the TD of the hole is 2818 mMD, which means that the reaming operation is stationary almost 700 mMD above the bottom of the hole.

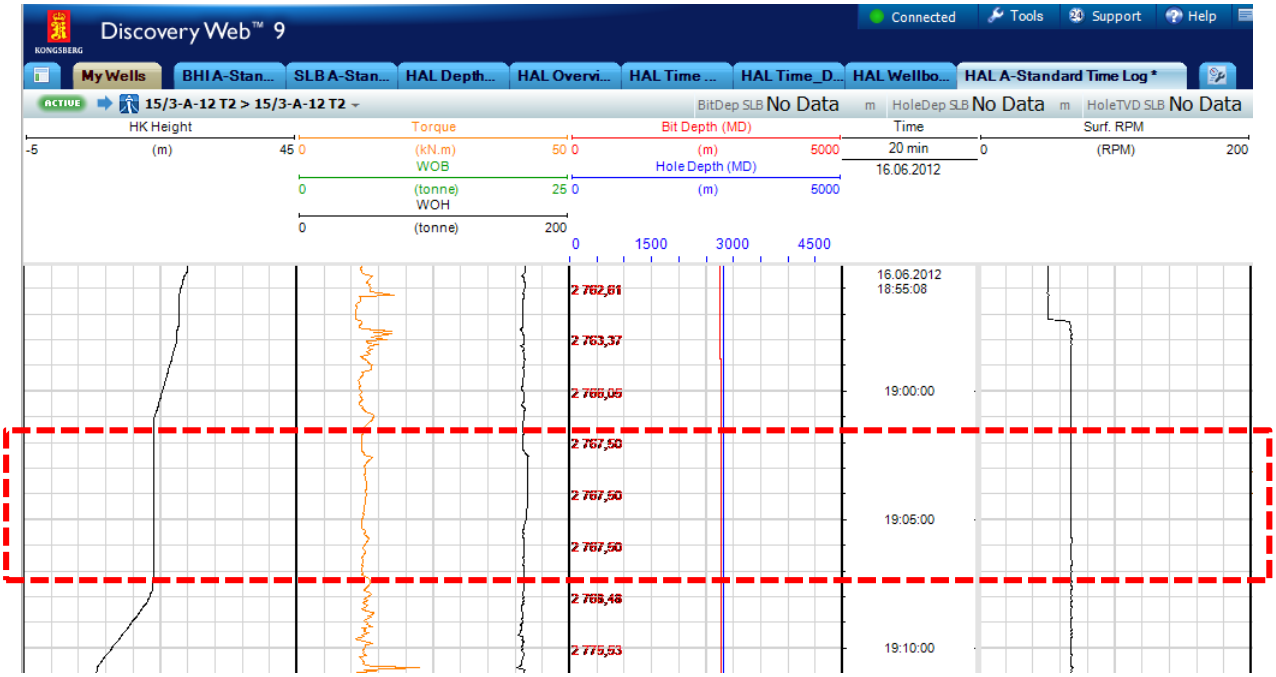

Fig. 38- Real time data showing reaming off-bottom operation at a stationary point in well A12/A12 T2 during drilling of the 17 ½" section (real time data from Statoil via Discovery Web).

Table 23 shows result of modeled friction factors for different depths during reaming in the 17 ½" section of well A12/A12 T2. The fourth coloumn demostrates that the tourqe measured at the surface is increasing for deeper depths with drillstring. The friction factor seems to be 0,23 in average, which is a bit higher than what to expect for a cased well with OBM seen in Table 24. From studying the daily well report of Statoil for drilling of the 17 ½" section, no problems has been reported for this interval, which is also underlined by the low modeled friction factor.

Table 23- Result of modeled friction factors during reaming in the 17 ½" section of well A12/A12 T2.

	Depth		**Torque measured**	**HL modeled**	**μ modeled**
Incl	TVD	MD		Statis μ =0	
deg	m	m	kNm	kN	
55	2539	2818	12,81	774	0,24
52	2498	2755	9,66	772	0,19
30	2013	2121	6,32	734	0,23
25	1467	1498	5,21	625	0,23
17	1211	1226	3,77	576	0,25
			Averarge friction factor		**0,23**

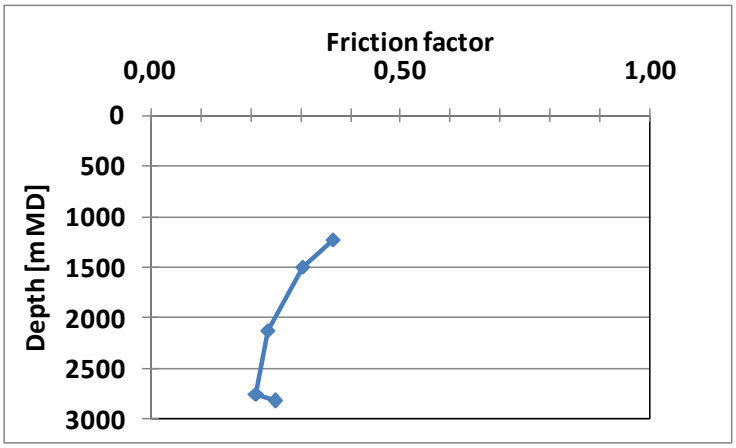

Fig. 39- Modeled friction factor during reaming off-bottom in the 17 ½" of well A12/A12 T2.

Table 24- Expected and experienced (modeled) friction factor during reaming in the 17 ½" section of well A12/A12 T2.

	C	OH
Depth [m MD]	2379	
Actual/modeled μ with OBM	0,23	
Expected μ with OBM	*0,17*	*0,21*

Table 25 and Fig. 40 present values for estimated torque and static weight along the well path for a total drillstring length of 1226 mMD during reaming in the 17 ½" section of well A12/A12 T2. The modeled friction factor in this case was found to be 0,25 by putting the modeled surface torque equal to the measured surface torque of 3,77 kNm. The blue torque graph in Fig. 40 shows highest torque at the surface (3,77 kNm) where most drillstring is downhole and the drillstring weight is maximum. At the bottom there is no mass (and weight) to rotate, and consequently zero torque. The torque is the same along the drillstring to the KOP, and then has a constant slope for the drillpipe in the BU. In the lower BHA part the torque changes more per meter depth than in the drillstring part because more weight needs to be rotated. The red graph, which is representing the static weight in Fig. 40, shows a slope equal to the buoyancy unit weight of the drillpipe for the drillpipe section, while it is equal to the average buoyancy unit weight of the BHA in the lower BHA section.

Another result of loads calculated along the well path is showed in Table 26 and Fig. 41. When setting the estimated surface torque equal to the measured surface torque of 9,66 kNm, the friction factor became 0,19 for a total drillstring length of 2755 mMD. The same trend can be seen in this case, where the torque can be seen as constant for the vertical section, from zero to 453 mTVD, and then decreasing linearly with depth. At the bottom the torque is equal to zero. When comparing the case for a total drillstring length of 2755 mMD, with the case when the total drillstring length is 1226 mMD, it can be observed that the graphs in the two cases have the same trend. However, both torque load and static weight are shifted to higher values for the case with a total drillstring length of 2755 mMD, which has more drillstring downhole, as expected.

Table 25- Values for estimated torque and static weight along the well path during reaming in the 17 ½" section with a modeled friction factor of 0,25 for a total drillstring length of 1226 mMD.

	μ
Static	0
Reaming	0,25

Depth mTVD	Cumm Static weight kN	Torque kNm
1211	0	0,00
1007	340	1,95
453	470	3,77
0	576	3,77

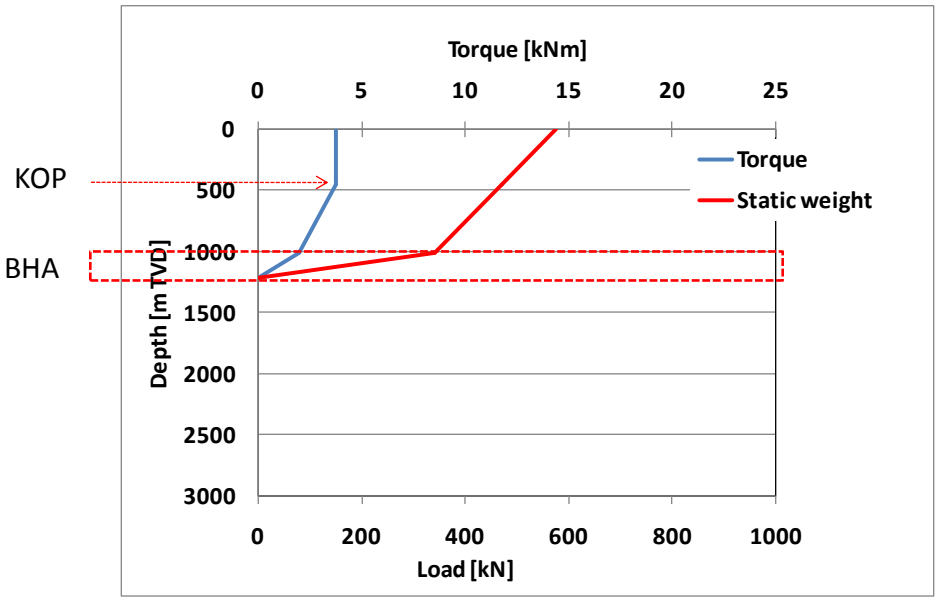

Fig. 40- Estimated torque and static weight along the well path during reaming in the 17 ½" section with a modeled friction factor of 0,25 for a total drillstring length of 1226 mMD.

Table 26- Values for estimated torque and static weight along the well path during reaming in the 17 ½" section with a modeled friction factor of 0,19 for a TD of 2755 mMD.

	μ
Static	0
Reaming	0,19

Depth mTVD	Cumm Static weight kN	Torque kNm
2498	0	0,00
2367	218	1,31
453	666	9,66
0	772	9,66

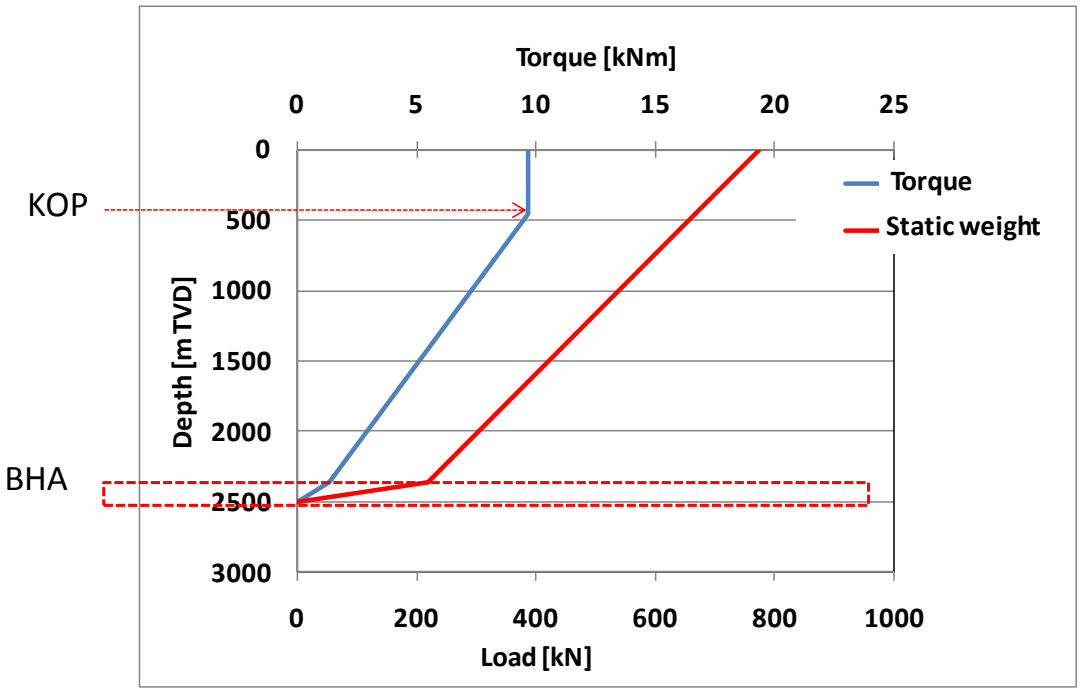

Fig. 41- Estimated torque along the well path during reaming in the 17 ½" section with a modeled friction factor of 0,19 at a TD of 2755 mMD.

6.3 Limitations reported in literature

The listed limitations under this section are common limitations with friction models, which are also recognized in the selected friction model. The discussed concerns and assumptions are made to be as realistic as possible to make the effect on the final modeled result as little as possible. It is also suggested improvements with the friction model for future work.

6.3.1 Tortuosity and micro-tortuosity

Tortuosity can be explained as irregularities in the well path, or the amount by which the actual wellbore differentiate from the planned trajectory (Gaynor et al. 2001). Commonly tortuosity occurs as a result from adjustments of the direction of the drill bit while attempting to correct the actual well trajectory back to the planned trajectory. By definition tortuosity can be divided into macro- tortuosity, which is DL over a length longer than 10 m, and micro-tortuosity, which is tortuosity created in scale between 0,5 meters and 9 meters (Menand et al. 2006). In general it is beneficial with low DL, resulting low torque and drag, instead of high DL, causing high torque and drag (Gaynor et al. 2001).

An actual well path will not be perfectly smooth, as assumed in the soft string model, but will have natural tortuosity. The friction factor is mainly a function of mud type, lubricity, contact force, and interface condition, for instance open or cased hole, but not on touristy in the well. When the tortuosity is masked behind the friction factor, this will then result in a higher friction factor, which needs to be corrected for. Therefore the effect of tortuosity present in the wellbore is a source of error in the modeling of torque & drag. Conventional tortuosity is easy to recognize from survey data, and a tortuosity model can be defined to simulate the effect. At the moment there do not exist any models which account for the smaller drift associated with a spiraled hole, and there are no industry standard for defining the relationship between friction coefficient and tortuosity in the wellbore (Mason and Chen 2007).

Since there are no industry standard for defining exact relationship between friction coefficient and tortuosity in wellbore, the drag values may be either overestimated or underestimated comparing with actual measurements. Taking into account that it is assumed a smooth wellbore profile in the analytical model, and DL and wellbore tortuosity are neglected, an application of slightly higher friction factor could be necessary for future investigation of the model. Otherwise, an option is to consider dividing the well path even more carefully into sections and subsections to increase the sensitivity of the model to DLs and wellbore irregularities. It would also be interesting to find a correlation, if it exists, between micro irregularities in the well path and the friction factor. The tortuosity could then either be accounted for by adding or build in an internal tortuosity model into the friction model, or simply adjusting the friction factor externally for a known tortuosity effect.

6.3.2 Local variations

When doing torque & drag analysis the well is divided into sections and average values are applied, meaning that local variations are not taken into account. A source of error is that the mud weight might not stay constant during the analysis, but will vary within a length because the mud properties are function of factors that changes, such as temperature, cuttings bed and suspended particles. Side forces will be affected, and consequently drag forces will also be changed. This can be considered by using the borehole cutting transport theory, and correct for friction factor over specific wellbore intervals (Samuel 2010; Ismayilov 2012).

6.3.3 Hydrodynamic viscous drag

Hydraulic viscous drag is another effect which is not considered in the calculations. Hydraulic viscous drag is explained as resistance between the pipe and the drilling fluid, and is a function of several parameters, including (Fazaelizadeh et al. 2010):

- Fluid properties
- Tripping velocity
- Flow regime
- Pipe outer diameter
- Wellbore inner diameter

Experience shows that more viscous drag force would be created with more viscous drilling fluid. Also greater viscose drag force would appear for smaller clearance between the drillstring and open hole, compared to large clearance between drillstring and cased hole. The tripping speed is another factor of the hydraulic effect, where the flow regime is commonly ruled by a turbulent regime with increased tripping speed, which will increase the value of viscous drag force. An example is that the friction factor becomes higher when the hoisting speed increases because of pulling full-gauged BHA with higher speed. The extra friction is created because there is too little space for the down moving drilling fluid to pass when the pipe is moving up (Mirhaj et al. 2011).

The hydraulic effect is especially relevant when studying reaming operations, since in a real case the circulation is usually not turned off during reaming. The optimum when doing friction analysis would be to perform friction analysis on cases with no circulation since circulation will affect the drag and momentum because of the pressure difference

between the inside and the outside of the drillstring. Because no reaming operations without circulation was found in the real time data, cases when reaming with very low flow rates were instead used. To demonstrate the influence of fluid flow, Fig. 42 is presenting torque as a function of RPM with different values of mud flows (MF) during reaming in the 17 ½" section of well A12/A12 T2. From the graph it can be seen that it is a reasonable assumption for cases with low fluid flow to consider the torque to be independent of the mudflow. The torque is however more affected by the RPM, where the torque is increasing with increasing RPM.

The influence of fluid flow on the final result of torque & drag modeling is a confusing aspect because many rheological models and options exist, which can give varying results (Mason and Chen 2007). Even though it is known that hydraulic viscous drag has an effect on the friction analysis and should be considered in a friction analysis, no present solution exists to calculate and include this in the friction model[1]. However, a case study has shown that the viscous drag only make up one percent of the total hook load (Aadnoy et al. 2010). Because the hydrodynamic viscous drag results in such a small amount compared to the total hook load, it will necessarily not have a big affect when neglecting this in the torque & drag modeling. This is also a reasonable assumption because the pump pressure and MF is approximately zero in the operations studied in present report. However, for future work the friction model should be improved to enable the possibility to perform a systematic analysis of cases with any flow rate. This would be enabled by implementing a torque & drag model coupled with hydraulic calculations (Cayeux et al. 2012).

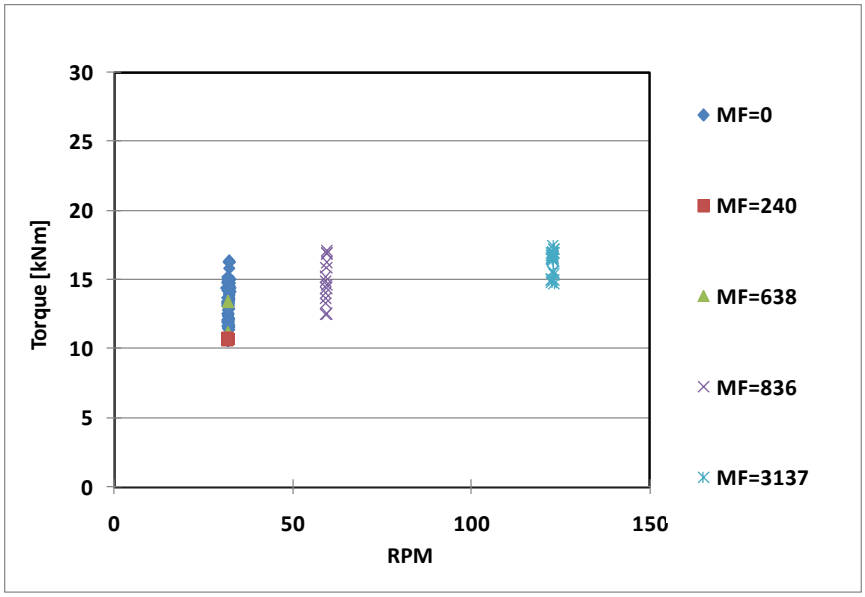

Fig. 42- Graph showing torque for different values of RPM with various MFs during reaming in the 17 ½" section of well A12/A12 T2.

[1] Personal communication with Professor B. S. Aadnoy 2013.

6.3.4 Perfect vertical wellbore

The assumption of a perfectly vertical wellbore with a centered drillstring in the hole, which means no contact between the drillstring and the borehole wall, is also leading to inexact result from the friction analysis. This aspect is essential for calculation of the contact forces because the contact forces are depending on the clearance between the drillstring and the borehole, and the geometry of the well. Fig. 43 shows that a vertical well is not entirely vertical and does not have perfectly smooth well path, but contains local irregularities which creates contact forces. This is also in line with the discussion under chapter 6.3.1.

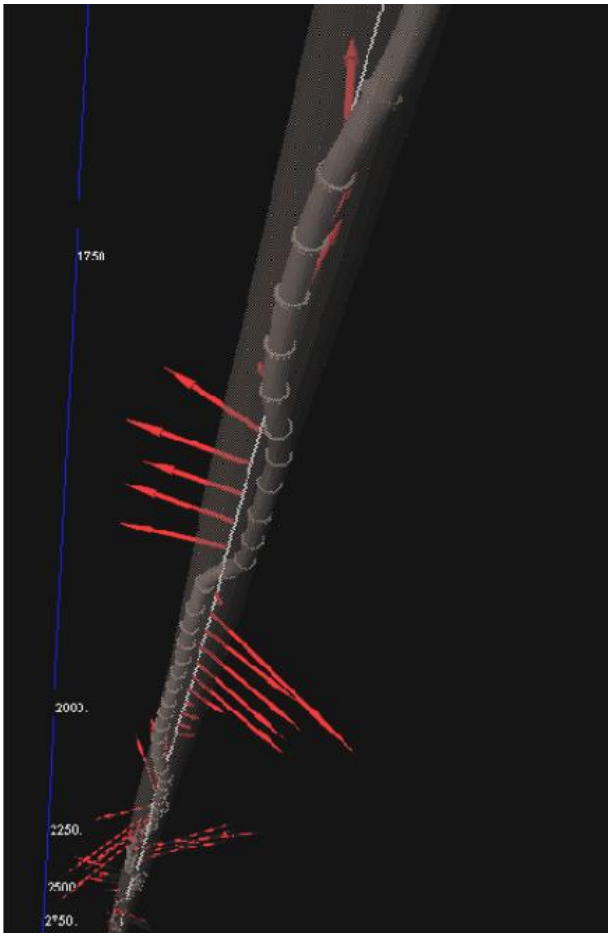

Fig. 43- Contact forces in an actual vertical well (Menand et al. 2006)

6.4 Limitations due to accuracy in field data detected through present work

In present report the quality of the applied field data can be questionable. As a rule of thumb, the model is only as good as the input data. This means that it is essential to have

accurate and reliable input data in a model to obtain precise verification of the model. In this context the quality of the result from a model depends in general on two factors; the quantity or the amount of the data, and the quality of the data used in the model. Firstly lack of data can result in invalid assumptions made and applied in the model. For present report some of the well data missing were assumed, for instance the drillstring design above the BHA for the modeled wells. In addition, lack of available data for deeper sections than the 17 ½" section of well A12/A12 T2 and well A5 is an issue. By apply deeper sections to the model a better impression of the model would be obtained. Also poor data resolutions can result in inaccurate trend lines and lead to misinterpretations. It was challenging to find the exact values for depth (MD and TVD) and trajectory (inclination and azimuth) for specific points in the well path where the hook load was measured because of few existing survey points and limited availability of survey data.

Secondly the correctness of the measuring equipment recording, and adjustments of the recorded values will have an effect on the quality of the measured values. Measured values which can be inaccurate, include measured load and well trajectory. The chance of having inaccurate measured data for low drillstring weight is higher than for more weight on the hook[2]. Fig. 44 can be applied as an explanation for this statement, which is showing measurement uncertainty and minimum weight for a typical weighing instrument. The green, positive sloped line in Fig. 44 is the absolute measured uncertainty, which is described as the uncertainty in the recorded weight expressed as the unit of measurement, and is determined in calibration. The blue line in Fig. 44 is the relative measurement uncertainty, defined as the absolute measurement uncertainty divided by the load expressed as a percentage. By weighting close to the lower limit of the measurement range of the instrument, the relative uncertainty can become so high that the weighing result cannot be trusted anymore. The red region in Fig. 44 is presenting the area which will give inaccurate measurements because the measurement uncertainty of the instrument is larger than the required accuracy of the weighing process. This leads to a specific accuracy limit for every weighing instrument, which is called minimum sample weight, better known as the minimum weight. The minimum weight represents the smallest amount of material that will satisfy the specific weighing accuracy requirement (Fritsch and Quenot 2013). Even though this is conclusions drawn from another industry than the oil industry, it was discussed that this is a general theory of a weight indicator and is also applicable for this case, where the inaccuracy is increasing towards the lower limit of the weight indicator[34]. It is also worth to mention that properties of the drillstring and BHA components are important data to have somewhat exact because hook load weight is very sensitive to these properties.

[2] Personal communication with Professor Sangesland, S. 2013.

[3] Personal communication with Professor Sangesland, S. 2013.

[4] Personal communication with Professor Asheim, H., A. 2013

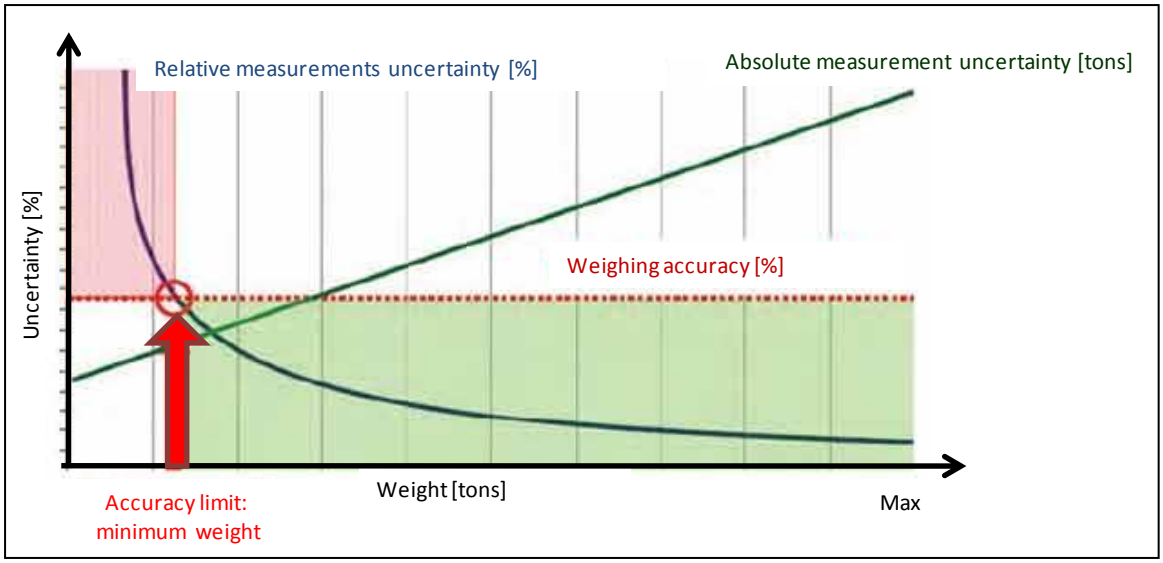

Fig. 44- Measurement uncertainty and minimum weight (Fritsch and Quenot 2013).

6.4.1 Friction loss in the hoisting system affecting the accuracy of the measured load

This subchapter is discussing consideration of friction loss in the hoisting system, which affects the accuracy in measured data. Friction resistance in the hoisting system must be corrected for because only the borehole friction is of interest (Luke and Juvkam-Wold 1993). It is important to distinguish between the hook load measurement and the top of string force. In present report it is assumed that the actual surface hook load data used are based on draw works deadline tension measurements, showed in Fig. 45 and Fig. 46. The measurement of hook load is performed relatively far away from the actual top of string force. Typically, the measurement is made in the deadline anchor, the crown block or the topdrive. Depending on the location of the measurement, there will be additional physical phenomena which interact with the system, such as the length of drill-line, the friction between the drill-line and the sheaves, the tension exerted by the mud hose and umbilical to the topdrive, the additional weight of mud when the pumping is started, the drilling fluid which is filling the mud hose and the topdrive, the misalignment of the travelling block compare to the crown block when the dolly is retracted, and so on. Sheave friction in the friction analysis is a result from passing drilling lines through the sheaves (Mirhaj et al. 2010). Typically the average calculated individual sheave efficiency ranges from 96 % to 99 %. Luke and Juvkam-Wold (1993) have presented many examples of friction losses in the hoisting system, and how it affects the measured hook load. The hook load is considered to be affected by the dead-line tension, the number of lines between the blocks and direction of the block movement (Luke and Juvkam-Wold 1993).

Because the friction losses in the hoisting system can be significant and affect the correctness of the hook load measurements, it is important to compensate for these effects and consider this in the friction analysis (Landmark Wellplan user manual 2004). To do this it is in most cases required some sort of calibration and knowledge about where the measurement is made. Therefore is for instance the assumption that the travelling equipment weight is a constant that is added to the top of string force is an important source of error[5]. One possible source of errors is therefore inaccurate weight of the travel system, which needs to be subtracted from the recorded string weight. In the literature it is also mentioned that hook load measurements at the deadline anchor should be corrected for the weight of the drill-line spooled out of the drawworks, the sheave friction and the tension on the travelling block from the mud hose and topdrive umbilical (Cayeux et al. 2012). An additional solution is to reduce errors in reading of measured values by calibrate the weight indicator with a load cell placed below the kelly and travelling equipment (Johancsik et al. 1984).

The result would therefore be more correct by model torque & drag in software which considers this, such as the Halliburton software Wellplan. Wellplan is a well-known software applied by engineers during the design and operation phase for drilling and other operations, such as well completion and well services. The correction of the sheave friction is often based on Eq. (21) and Eq. (22), and could also be build into Aadnoy`s friction model for improvements (Landmark Wellplan user manual 2004):

$$L_r = \frac{n(e-1)(H_r + W_{tb})}{e(1 - \frac{1}{e^n})} \quad (21)$$

$$L_l = \frac{n(e-1)(H_l + W_{tb})}{(1 - e^n)} \quad (22)$$

[5] Personal communication with Cayeux, E. via Kristensen, E. 2013., H., A. 2013

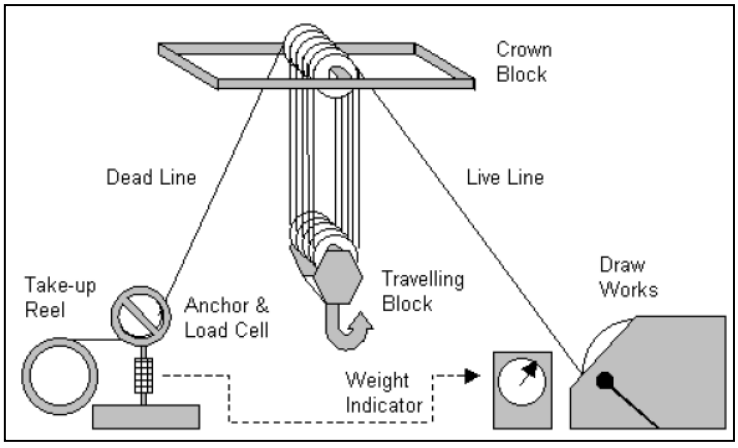

Fig. 45- Typical draw works rig up (Landmark Wellplan user manual 2004).

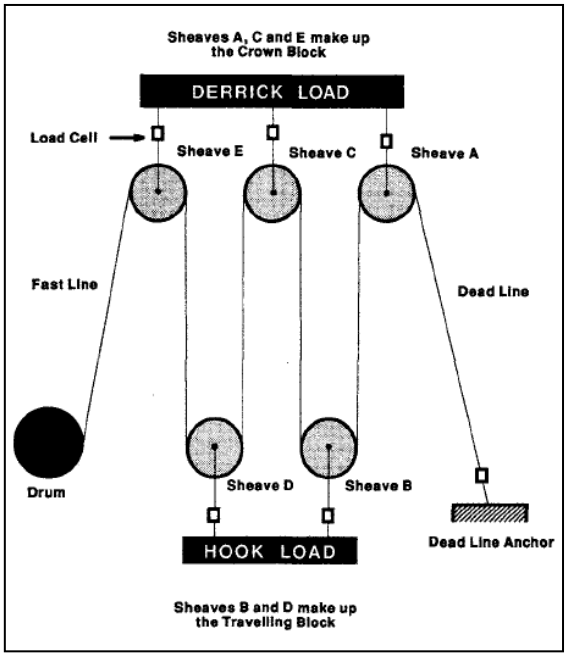

Fig. 46- Illustration showing an example of components in a block and tackle system (Luke and Juvkam-Wold 1993).

6.4.2 Accuracy with depth

Uncertainty in measured data has an effect on the result. The quality control mentioned in chapter 3.8.3, which is here referred as reliability test 3, is one way to make sure that quality of measured data is acceptable (Fazaelizadeh 2010). Reliability test 3 compares free-rotating weight with estimated static weight from the projected height principle for well A12/A12 T2. The red graph in Fig. 47 shows static weight calculated with the projected height principle of the drillstring in the 17 ½" section of well A12/A12 T2. The KOP is at 435 m and the length of the BHA is 210 m, therefore the red graph is

representing the static weight of only the BHA at this depth. The blue graph is recorded free-rotational weight, which was only available in the real time data for the depth entered in the graph in Fig. 47. If there was no inaccuracy in measurements, measured free-rotating weight should match perfectly with the model. However, Table 27 shows that a measured drillstring weight of 157 tons and an estimated static weight of 86 tons give a difference of 72 tons at 2491 mMD, which corresponds to 9 % relative to the theoretical static weight at that depth. This will have a greater importance for low load values of drillstring in the shallow section, than in a deep section if assuming the same uncertainty for shallower depths. For instance when studying Table 19 which shows the load measured during POOH 15 June 2012 in section 17 ½" of well A12/A12 T2, the load was measured to be 779 kN, which is 79 tons. If assuming the same uncertainty of 86 ton between the measured and theoretical loads for this depth, 86 tons uncertainty to 79 tons will make a big difference in the model, and have an effect in the output of the model. So, if there are some inaccuracies in the readings of real time data, or wrong corrections of the measurements, there is a higher chance of getting misleading result for the shallow section with small inclination than for the deeper with more drillstring downhole and higher inclination.

Table 27- Table presentation of inaccuracy in measured hook load for well A12/A12 T2.

Depth		Diffrence in measured HL and theoretical HL	
mMD	mTVDD	tons	%- relative to teoretical HL
2491	2326	72	9
1998	1905	64	9
1527	1493	58	9

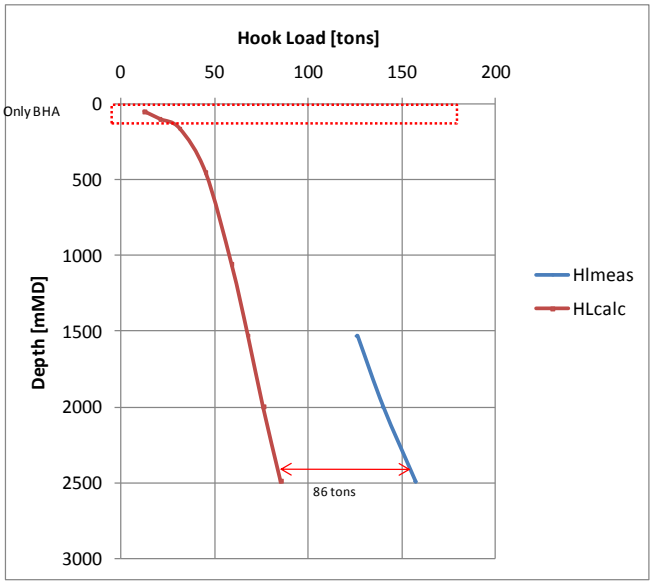

Fig. 47- Graphical presentation of inaccuracy in measured hook load for well A12/A12 T2 (based on data from Statoil).

This section contains a demonstration on how a change hook load has an influence on deep and shallow sections. The model is applied during POOH from three different depths of well A12/A12 T2 to demonstrate the sensitivity in modeled friction factor with changed hook load values. Fig. 48 shows the well profiles of the three depths, where the shallow section has a total hole depth of 1207 mMD and 16 degrees inclination at the end of the section, the middle section has a depth of 2964 MD and inclination of 60 degrees at the end, and the deepest section has a total hole depth of 4518 mMD and inclination of 60 degrees. The analysis was performed by entering the specific depths and inclinations of each of the three sections into the friction model, and then changing the friction factor from 0 to 1 stepwise and reporting the estimated hook load. The result in Fig. 49 shows how the hook load change has an effect on the simulated friction factor for the shallow section (blue graph), medium section (green graph), and a deep section (red graph). Even though the friction factor is ranging between 0 and 1 in Fig. 49, it is not usual to have a friction factor as high as 1 for deep well sections. For a shallow section, however, there can be a higher chance of getting errors in load measurements and having shallow doglegs leading to high friction factor. Fig. 50 has zoomed in on the result of the shallow and deep section. It shows that changing the hook load with five tons (65 to 70 tons) result in an approximately 0,20 (0,30 to 0,50) higher friction factor for the shallow section, while changing the hook load with five tons (110 to 115 tons) result in an approximately 0,02 (0,10 to 0,12) higher friction factor for the deep section. This means that the hook load measurements has a much greater effect on the resulting friction factor for a shallow sections with small inclination, than an change in hook load measurements for a deeper sections with higher inclination. The main difference between the two cases is that the upper, more straight section is typically weight dominated because friction is only given by the normal weight component, while a more curved section is seen as a tension dominated process because the normal contact force between the drillstring and borehole is affected by the pipe loading in axial direction. It looks like the reliability of the method is increasing in longer and more deviated wells. Also the friction is acting on a much larger length for a deep section than a shallow, and therefore the friction has to be higher to make a difference in hook load measured at the surface. After the issue of modeling shallow depths was discovered in present report, the same aspect was detected to be stated by others (Maidla and Wojtanowicz 1987, which therefore strengthens the theory discussed under this section.

In present report the deepest section model is the 17 ½” section because of limited access to real time data, but for better evaluation of the theory and the model also deeper sections with real time data should be modele

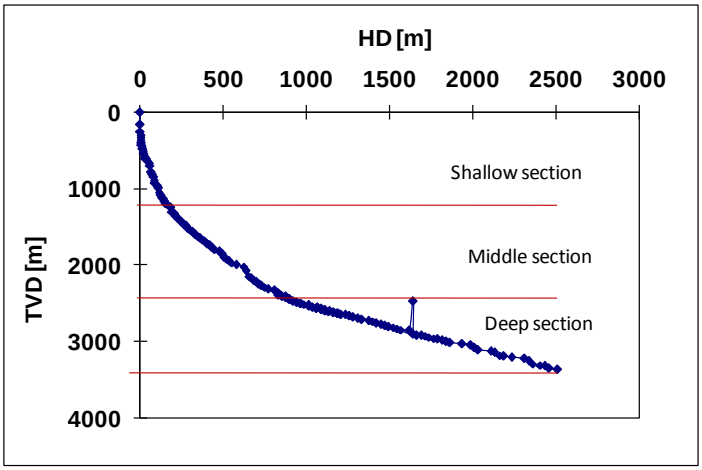

Fig. 48- Well path survey for well A12/A12 T2 (based on data from Statoil).

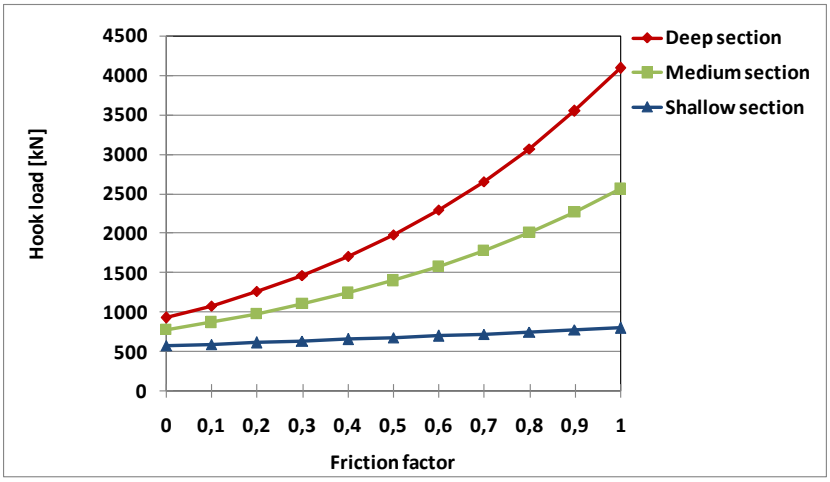

Fig. 49- Sensitivity in estimated hook load versus friction factor for different sections of the well path.

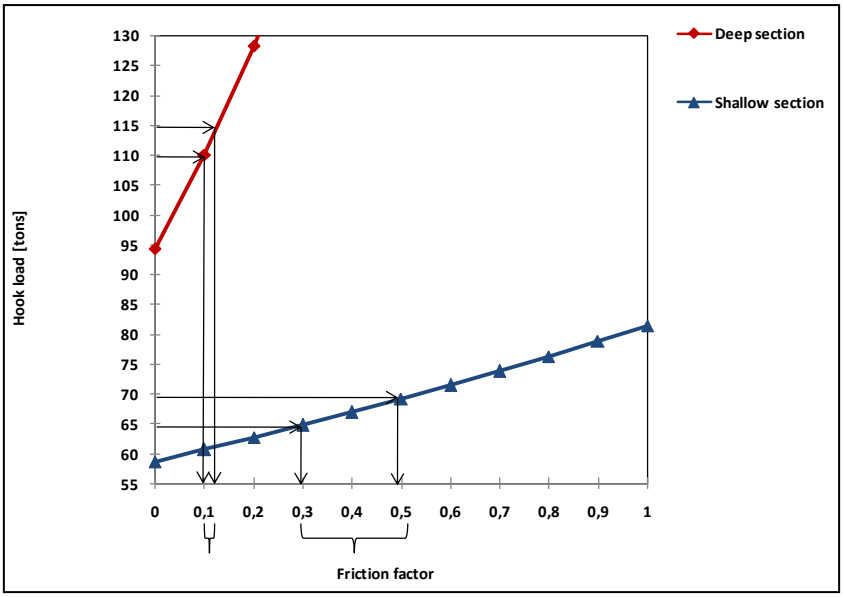

Fig. 50- Sensitivity in estimated hook load versus friction factor for a shallow and a deep section of well A12/A12 T2.

6.4.3 Buckling

Buckling is another aspect that should be considered in torque & drag modeling. Fig. 51 shows two different types of buckling. The first phase, 2D sinusoidal wave of the string, might occur as the drillpipe is put into high axial compression. If the compression forces are increased even more, this can causes the pipe to move up the sides of the wellbore in the shape of a helix, known as 3D helical buckling. Issues, including smooth transfer of WOB and problems with running in casing, are typically resulting because of the high side forces in the wall from buckling. The last and worst situation is lock up, where the additional drag from the wall contact force is high enough to prevent any movement of the string, and can occurs if even more compression is put on the pipe. If unpredicted buckling should be an issue, this would result in unexpected high friction forces that affect the friction factor (Rae et al. 2005). However during calculations performed in present report the drillstring is assumed to always be in tension and it is assumed no occurrence of buckling, because this will be uncertain since no detailed operational report on this is provided.

Buckling is an undesirable situation because of the above mentioned aspects, but if the situation is unavoidable, the additional drag forces should be considered during the modeling. In the consideration of buckling effect, provided knowledge would include prediction of loss of WOB, calculate on the risk for lock up and find the effect of fatigue (Mason and Chen 2007). Formulas, including Eq. (23) and Eq. (24), for critical loads before buckling have been developed.

For a horizontal section the tubulars are in compression because of friction in axial direction, weight on the bit and load on the packer. Then the tubular will sinusoidal buckle when the axial compressive load overcomes the critical load (Wu et al. 1993):

$$F_{cr} = 2\left(\frac{E\, I\, \beta\, w}{r}\right)^2 \tag{23}$$

Eq. (23) becomes Eq. (24) for an inclined wellbore.

$$F_{cr} = 2\left(\frac{E\, I\, \beta\, w \sin\alpha}{r}\right)^{1/2} \tag{24}$$

In some models, like the soft string model in Wellplan, the additional side force from buckling is computed for helical buckling mode with Eq. (25) (Landmark Wellplan user manual 2004).

$$F_{drag} = \frac{r\, F_{axial}^{\,2}}{4\, E\, I} \tag{25}$$

In future work the applied friction model in present report can be upgraded by including features for monitoring the compressive load along drillstring to find the type, beginning point and length of buckling, and then consider the buckling effect in the analysis. More specific the potential buckling should be considered in the model by built features to the model that first automatically check if there is a potential for buckling, including Eq. (23) and Eq. (24), and then calculates the additional force because of buckling by using Eq. (25). This will not only increase the accuracy of the result, but it also enables to gain information on how long it is safe to operate in a buckling mode. Based on this it can be considered if action should be done to manage buckling, and avoid extra costs in engineering unnecessary alternative solutions.

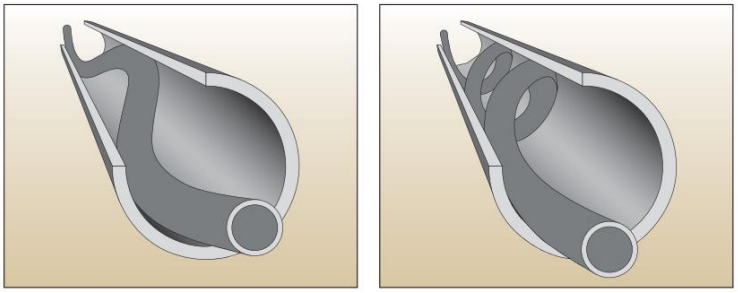

Fig. 51- Sinusoidal buckling of the drillpipe inside a casing in the left sketch and helical buckling of the drillpipe inside a casing in the right sketch (Menand et al. 2006).

6.5 Future improvements

Under each of the above sections it was concluded on how to eliminate the limitations for model improvements. This section contains some additional ideas for future work, and also a summary of improvements of Aadnoy`s friction model:

- Find a correlation between tortuosity and friction, and included it to the friction model.
- Combine the friction model with a hydraulic model to account for hydraulic effects.
- Investigate on the friction losses in the sheaves to subtract it in the calculations in the friction model.
- Evaluate for potential buckling in the well, and then add the effect in the friction model.

If the friction model, which is developed in Excel by the present author, was to be used in an actual well application, it would be time consuming and it would require calculations which make the model disable for real time use. The 3D analytical model in its full power involves an application of the complete solution, which is the main challenge for the model because of the complexity of the full application. To make it possible to automate to the extend mentioned above, the potential to adapt the model to another platform with higher ability to automate, such as matlab, should be examined. For instance could more powerful software than Excel easier couple several models together to considering other factors to the borehole condition, and thereby give a more comprehensive picture of the downhole situation. By combining downhole hydraulic, thermal and mechanics effects during a drilling operation in real time, a better continuously evaluation of the wellbore condition is given. All in all further investigation of the model should be done in a real well with good quality and quantity of measured data.

7 Conclusion

Based on the modeled and evaluated results in present report the following conclusions can be drawn:

- Even though the limitations mentioned in chapter 6 exist, the Excel model, which is developed by present author and based on Aadnoy`s friction theory, has shown to give some reliable results (test 1 and test 2).
- The findings in present work have been used to demonstrate some important applications of the model. One central function of applying the friction theory of Aadnoy is to get insight to the downhole situation by studying the magnitude and trend of the friction factor together with other available data. In well C47 a friction factor was experienced to be higher in the 17 ½" section than in the 12 ¼" section because of hole cleaning issues.
- The limitations revealed in chapter 6 are essential to be aware of when modeling friction to be able to evaluate the result. With this information, more insight to torque and drag applications and issues is given, and after detection of these limitations, awareness is accomplished about what is needed to be improved on the model in future work. Some important discovered issues include:

    - The 2D approach has the tendency to overestimate the borehole friction factor. The cause is most likely shallow DLs. The 2D model should therefore not be used for field applications unless the directional survey shows no presence of shallow DLs.
    - The relative error in the borehole friction factor associated with the unit change in hook load decreases as the total drillpipe length in the hole increases. The reliability of the method applied in present work increase in more deviated holes.
- Many potential improvements of the tool have been suggested to make it more realistic and reduce the limitations. The model should also be adapted to a powerful software to enable real time applications.

8 Nomenclature

8.1 Parameters

α	Wellbore inclination	radians
$\Delta\alpha$	Change in inclination over section length	radians
β	The buoyancy factor	(-)
Φ	Wellbore azimuth	radians
$\Delta\Phi$	Change in azimuth over the section length	radians
θ	Absolute change in direction/ dogleg	radians
ρ_i	Mud density inside of the pipe	kg/m^3
ρ_o	Mud density outside of the pipe	kg/m^3
ρ_{mud}	Mud density	kg/m^3
ρ_{string}	Steel density	kg/m^3
μ	Friction factor	

BPOS	Block position	m
DBTM	Bit position	m
DMEA	Hole depth	m
E	Young`s modulus of elasticity	N
e	Individual sheave efficiency	(-)
F_1	The bottom force of a pipe element	N
F_2	The top force of a pipe element	N
F_{add}	Additional side force calculated	N
F_{axial}	Axial compression force	N
F_{cr}	Critical force before buckling	N
F_{down}	Slacking force	N
F_F	Frictional force	N
F_N	Side or normal force	N
F_{up}	Pulling force	N
ΔF	Difference in F_{up} and F_{down}	N
H_l	Hook load while lowering, calculated in analysis	tons
H_r	Hook load while rising, calculated in analysis	tons
HKL	The hook load	tons [kN]
I	Moment of inertia	N
L	Length of the section	m
L_H	Horizontal projection	tons
L_l	Weight indicator while lowering,	tons
L_r	Weight indicator while rising	tons
ΔL	Length of element	m

MF	Mud flow	l/min
MFl	Mud flow	l/min
n	Number of lines between blocks	(-)
r	Radial clearance between wellbore and work string	m
R	Radius of curvature	m
RPMB	Revolutions per minute or average rotary speed	(-)
Δs	Length of the section	m
SPP	Stand pipe pressure	bar
T	Torque	kNm
TJ	Tool joint	m [inch]
TRQ	Torque	kNm
W	Buoyed weight of the pipe	N
w	Unit weight of pipe	kN/m
W_{tb}	Weight of travelling block	tons

8.2 Abbreviation

2D	Two-dimensional
3D	Three-dimensional
BHA	Bottomhole assembly
bf	Buoyancy factor
BPOS	Block position
DBTM	Bit position
DL	Dogleg
DLS	Dogleg severity
DMEA	Hole depth
ECD	Equivalent circulation density
ERD	Extended reach drilling
ERW	Extended reach wells
HD	Horisontal departure
HL	The hook load. Displayed by the weight indicator
HKL	The hook load. Signature in real time data file
MD	Measured depth
MF	Mud flow. Signature in Excel graph
MFl	Mud flow. Signature in real time data file
NPT	Non-productive time
OBM	Oil-based mud
POOH	Pulling out of hole
PRS	Pickup/rotate/slackoff
RIH	Running in hole
ROP	Rate of penetration
RPM	Revolutions per minute

RPMB	Revolutions per minute or average rotary speed. Signature in real time data file.
SPP	Stand pipe pressure
T	Torque
TD	Total depth
TJ	Tool joint
TVD	True vertical depth
TRQ	Torque. Signature in real time data file
WBM	Water-based mud
WOB	Weight on bit

9 References

Aadnoy, B.S. 2006. Technical limits of long wells. Presented at ONS 2006. http://www.docstoc.com/docs/88876905/Construction-of-Ultra-Long-Wells-Using-a-Catenary-Well-Profile.

Aadnoy, B. S., and Andersen, K. 15 December 2001. Design of oil wells using analytical friction models. *Journal of Petroleum Science and Engineering* **32** (1): 53–71. http://dx.doi.org/10.1016/S0920-4105(01)00147-4.

Aadnoy, B. S., Fazaelizadeh, M. and Hareland, G. October 2010. A 3D Analytical Model for Wellbore Friction. *SPE Journal Paper* **49** (10): 25-36. SPE-141515-PA. http://dx.doi.org/10.2118/141515-PA.

Aadnoy, B.S. and Djurhus, J. 2008. Application of a New Generalized Model for Torque and Drag. Paper IADC/SPE 114684 presented at Asia Pacific Drilling Technology Conference and Exhibition, 25-27 August 2008, Jakarta, Indonesia. http://dx.doi.org/10.2118/114684-MS.

Aston, M.S., Hearn, P.J, and McGhee, G. 1998. Techniques for Solving Torque and Drag Problems in Today's Drilling Environment. Paper SPE 48939 presented at SPE Annual Technical Conference and Exhibition, 27-30 September 1998, New Orleans, Louisiana. http://dx.doi.org/ 10.2118/48939-MS.

Burrow, S.J. 2009. Friction and resistance to sliding in orthodontics: A critical review. *American Journal of Orthodontics and Dentofacial Orthopedic* 135 (**4**): 442–447. http://dx.doi.org/10.1016/j.ajodo.2008.09.023.

Bennetzen, B., Fuller, J., Isevcan, E. et al. 2010. Drilling design and implementation for Extended reach and complex wells. http://www.slb.com/~/media/Files/resources/oilfield_review/ors10/aut10/01_wells.pdf (downloaded 19 February 2013).

Allen, F., Tooms, P., Conran, G. et al. 1997. Extended-Reach Drilling: Breaking the 10-kmBarrier. https://www.slb.com/~/media/Files/resources/oilfield_review/ors97/win97/ex_drilling.pdf (downloaded 15 January 2013).

Cayeux, E., Daireaux, B., Dvergsnes, E.W. et al. 2012. Early Symptom Detection on the Basis of Real-Time Evaluation of Downhole Conditions: Principles and Results From Several North Sea Drilling Operations. *SPE Drilling & Completion* 27 (**4**): 546-558. SPE-150422-PA. http://dx.doi.org /10.2118/150422-PA.

Chrstophersen, L., Gjerde, L. and Valdem, S. 2007. Final well report drilling and completion
34/10-C47. Final well report drilling and completion, Statoil (2007).

Statoil Daily Drilling Reports. 2012. https://partners4.statoil.com (downloaded 6 February 2013).

Drillstring design and implementation for extended reach and complex wells. K&M Technology Group. Third edition 2003.

Fazaelizadeh, M., Hareland, G., and Aadnoy, B.S. 2010. Application of New 3-D Analytical Model for Directional Wellbore Friction. Modern applied science 4 (2): 2-22. http://ccsenet.org/journal/index.php/mas/article/view/4418.

Fritsch, K. and Quenot, J-L. December/January 2013. Good Weighing Practices for the Food Industry. Food Quality magazine.

Frafjord, C. 2012. Model hook load and interpretation of real time data for well C47. Project, Norwegian University of Science and Technology, Trondheim, Norway (December 2012).

Gaynor, T.M., Chen, D., C-K, Stuart, D. et al. 2001. Tortuosity versus Micro-Tortuosity-Why Little Things Mean a Lot. Paper SPE/IADC 67818presented at SPE/IADC Drilling Conference, 27 February-1 March 2001, Amsterdam, Netherland. http://dx.doi.org /10.2118/67818-MS.

Gihselin, D. 2009. Best practices emerging for ERD wells. http://www.varelintl.com/content/includes/best_practices_emerging_for_erd_wells.pdf(downloaded 19 January 2013).

Hawker, D., Vogt, K. and Robinson, A. 2001. Wellsite procedures and operations.

http://www.scribd.com/doc/52900681/212/Hole-Pack-Off-or-Bridge.

Ismayilov, O. 2012. Application of 3-D Analytical Model for Wellbore Friction Calculation in Actual wells MS thesis, Norwegian University of Science and Technology, Trondheim, Norway (July 2012).

Johancsik, C.A., Friesen, D.B., and Dawson, R. 1984. Torque and Drag in Directional Wells Prediction and Measurement. Journal of Petroleum Technology 36 (6): 987-992. SPE- 11380-PA. http://dx.doi.org/10.2118/11380-PA.

K&M Technology Group. 2003. Torque and Drag in ERD Wells, http://www.etechinternational.org/new_pdfs/lessImpact/AttETorqueDragERD.pdf (downloaded 20 January 2013).

TechDictionary. 2008. http://energy.techdictionary.org/Oil-and-Gas-Field-Dictionary/Reamer (accessed 11 January 2013).

Kucs, R., Spoerker, H.F., Thonhauser, G. et al. 2008. Automated Real-Time Hookload and Torque Monitoring. Paper IADC/SPE 112565 presented at IADC/SPE Drilling Conference, 4-6 March 2008, Orlando, Florida, USA. http://dx.doi.org/10.2118/112565-MS.

Landmark Graphics Corporation Wellplan Usermanual 2004. (downloaded 16 February 2013).

Luke, G.R. and Juvkam-Wold, H.C. 1993. Determination of True Hook Load and Line Tension Under Dynamic Conditions. *SPE Drilling & Completio*. **8** (4): 259-264. SPE 23859-PA. http://dx.doi.org/10.2118/23859-PA.

Maidla, E.E., and Wojtanowicz,, A.K. 1987. Field Method of Assessing Borehole Friction for Directional Well Casing. Paper SPE 15696 presented at Middle East Oil Show, 7-10 March 1987, Bahrain. http://dx.doi.org/ 10.2118/15696-MS.

Maidla, E.E., and Wojtanowicz, A.K. 1987. Field Comparison of 2-D and 3-D Methods for the Borehole Friction Evaluation in Directional Wells. Paper SPE 16663 presented at SPE Annual Technical Conference and Exhibition, 27-30 September 1987, Dallas, Texas. http://dx.doi.org/ 10.2118/16663-MS.

Mason, C.J. and Chen, D.C.K. 2007. Changes needed to Modernise T&D Software. Paper SPE 104609 presented at SPE/IADC Drilling Conference, 20-22 February 2007, Amsterdam, The Netherlands. http://dx.doi.org/10.2118/104609-MS.

McCormick, J.E., Evans, C., Le, J. et al. 2011. Practice and Evolution of Torque and Drag Reduction: Theory and Field Results. Paper IPTC 14863 presented at International Petroleum Technology Conference, 7-9 February 2012, Bangkok, Thailand. http://dx.doi.org/10.2523/14863-MS.

McCormick, J.E., Frilot, M. and Chiu, T. 2011. Torque and Drag Software Model Comparison: Impact on Application and Calibration of Field Data. Paper SPE 143623 presented at Brasil Offshore, 14-17 June 2011, Macaé, Brazil. http://dx.doi.org/10.2118/143623-MS.

Menand, S., Sellami, H., Tijani, M. et al. 2006. Advancements in 3D Drillstring mechanics: From the Bit to the Topdrive. Paper IADC/SPE 98965 presented at drilling Conference, 21-23 February 2006, Miami, Florida, USA. http://dx.doi.org/10.2118/98965-MS.

Mirhaj, S.A., Fazaelizadeh, M., Kaarstad, E. et al. 2010. New aspects of Torque-and-Drag Modeling in Extended-Reach Wells. Paper SPE 135719 presented at SPE Annual Technical Conference and Exhibition, Florence, Italy, 19-22 September 2010. http://dx.doi.org/10.2118/135719-MS.

Mirhaj, S.A., Kaarstad, E. and Aadnoy, B.S. 2011. Improvement of Torque-and-Drag Modeling in Long-Reach Wells. *Modern Applied Science* **5** (5): 10-28. http://dx.doi.org/10.5539/mas.v5n5p10.

Mitchell, R.F., and Samuel, R. 2009. How Good Is the Torque & drag Model? *SPE Drilling & Completion* **24** (1): 62-7. SPE- 105068-PA. http://dx.doi.org/10.2118/105068-PA.

Payne, M.L. and Abbassian, F. 1997.Advanced Torque-and-Drag Considerations in Extended-Reach Wells. *SPE Drilling & Completion* **12** (1): 55-62. SPE -35102-PA. http://dx.doi.org/ 10.2118/35102-PA.

Pašić, B., Gaurina-Međimurec, N. and Matanović, D. 2007. Wellbore instability: Causes

And consequences. University of Zagreb, Faculty of Mining, Geology and Petroleum Engineering. http://www.researchgate.net/publication/26494059_WELLBORE_INSTABILITY_CAUSES_AND_CONSEQUENCES (downloaded 13 March 2013).

Petro materials. 2012. http://www.petromaterials.com/pdf/dp01.pdf (downloaded 1 February 2013).

Rae, G., Lesso,W.G. and Sapijanskas., Jr.M. 2005. Understanding Torque and Drag: Best Practices and Lessons Learnt from the Captain Field's Extended Reach Wells. Paper SPE 91854 presented at SPE/IADC Drilling Conference, Amsterdam, Netherlands, 23-25 February 2005. http://dx.doi.org /10.2118/91854-MS.

Redlinger, T.M. and McCormick, J. 23 March 2011. Weatherford International, http://www.drillingcontractor.org/longer-deviated-wells-push-drill-pipe-limits-8779.

Rommetveit, R., Bjørkevoll, K.S., Halsey, G.W. et al. 2007. E-Drilling: A System for Real-Time Drilling Simulation. Paper SPE 106903 presented at Digital Energy Conference and Exhibition, 11-12 April 2007, Houston, Texas, U.S.A. http://dx.doi.org/10.2118/106903-MS.

Samuel, R. 2010. Friction Factors: What are They for Torque, Drag, Vibration, Drill Ahead and Transient Surge/Swab Analysis. Paper ADC/SPE 128059 presented Drilling Conference and Exhibition, 2-4 February 2010, New Orleans, Louisiana, USA. http://dx.doi.org/10.2118/128059-MS.

Townsend, B. 2002. The Physics of Car Collisions. http://ffden-.phys.uaf.edu/211_fall2002.web.dir/ben_townsend/staticandkineticfriction.htm.

Wolfson, L. 2005. Multilateral/Extended Reach. http://www.spe.org/jpt/print/archives/2005/07/JPT2005_07_MER_focus.pdf. (downloaded 3 February 2013).

Xie, L.L., Moran, D., Yan, L. et al. 2012. Innovative Torque & drag Model for Complex Well Operations Increases Operational Efficiency. Paper SPE 152065 presented at SPE Western Regional Meeting, Bakersfield, California, USA, 21-23 March 2012. http://dx.doi.org/10.2118/152056-MS.

A Appendix

A.1 Friction calculation

The Eqs. from (A-1) to (A-6) shows derivation of an expression for friction by using equations for hoisting from Aadnoy`s friction model. Deviation in tension when lowering and pulling the string gives the friction, showed with the following equations:

$$F_{up} = F_1 + \beta\Delta Lw(\cos\alpha + \mu\sin\alpha) \tag{A-1}$$

$$F_{down} = F_1 + \beta\Delta Lw(\cos\alpha - \mu\sin\alpha) \tag{A-2}$$

$$\Delta F = |F_{up} - F_{down}| \tag{A-3}$$

$$\Delta F = [F_1 + \beta\Delta Lw(\cos\alpha - \mu\sin\alpha)] - [F_1 + \beta\Delta Lw(\cos\alpha + \mu\sin\alpha)] \tag{A-4}$$

$$\Delta F = 2\beta\Delta Lw(\mu\sin\alpha) \tag{A-5}$$

$$\frac{\Delta F}{2} = \left|\frac{F_{up} - F_{down}}{2}\right| = \frac{2\beta\Delta Lw(\mu\sin\alpha)}{2} = \beta\Delta Lw(\mu\sin\alpha) = \text{friction term} \tag{A-6}$$

The equations above are for straight sections, but the same theory can be applied for curved sections.

A.2 Projected height principle

For an inclined string, as in Fig. 52, the effective axial load is:

$$w(\alpha) = w \cos\alpha \tag{A-7}$$

The normal force on the borehole wall is:

$$F_N = w \sin\alpha \tag{A-8}$$

An element with a length, L, a projected height of TVD and a horizontal projection of $L_{H,}$ the projected height becomes:

$$TVD = L \cos\alpha \tag{A-9}$$

Inserting this expression into Eq. (A-7), it becomes:

$$w(\alpha) = \frac{w}{L} TVD \tag{A-10}$$

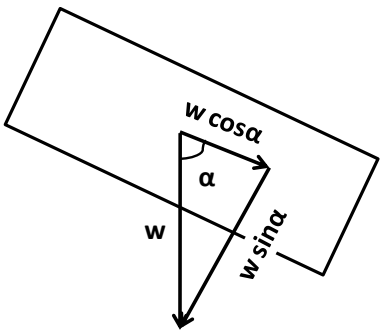

Fig. 52- Axial and normal weight components for an inclined pipe (Aadnoy 2006).

This result is called the projected height principle and is an important result, which shows that the axial pipe weight is equal to the unit pipe weight multiplied by the projected height. The static pipe weight is this way found regardless of inclination or well path. The friction is then assumed to be zero, and must be added whenever there is movement of the pipe (Aadnoy 2006).

A.3 Example of drillstring design calculations

This section contains the calculations for drillpipe and BHA input. Only calculations for the 17 ½" section of well A12 is included in Table 29 to demonstrate the similar procedure to find the weights and lengths applied in the other cases. BHA length of 212 m and unit weight of 2,0285 kN/m are the calculated properties of the BHA which are entered into the friction model and found from Table 28.

Table 28- BHA design of the 17 ½" section of well A12, which is used to calculate the values in Table 29 and applied as input to the friction model (data taken from Daily Drilling Report. Statoil).

Field: GUDRUN
Wellbore: NO 15/3-A-12 T2

Daily Drilling Report
WEST EPSILON

Statoil

Period: 13.06.2012 00:00 - 14.06.2012 00:00

6.2 Bottom Hole Assembly

Run no								
12	**Conveyance:** DP	**Run Type:** Drilling run #8				**BHA description:** 17 1/2" Drilling Assembly for sidetrack		
	String component	Supplier	Quantity	OD inch	ID inch	Length m	Acc length m	Comment
	BIT	Smith Bits		17,500	3,000	0,34	0,34	Sidetracked from A-12 off cement, tagged cement at 2625m.
	STAB SLEEVE			17,400	3,000	0,44	0,78	
	GEOPILOT	Halliburton		9,625	2,375	6,61	7,39	
	MWD	Halliburton		8,000	1,920	2,19	9,58	DrillDOC
	X-O PIN X PIN			9,500	3,000	0,62	10,20	In Line X/O
	EWR	Halliburton		9,500	2,375	3,72	13,92	Resistivity
	IN LINE STAB (ILS)			17,500	3,500	1,24	15,16	
	GAMMA RAY			9,500	2,375	1,54	16,70	Gamma sensor
	PR-SUB			9,500	2,375	1,32	18,02	PWD ECD Sub
	HCIM			9,500	2,375	1,63	19,65	
	TELEMETRY			9,500	4,125	2,81	22,46	P4M
	HOC	Halliburton		9,500	4,000	3,07	25,53	
	ROLLER REAMER			17,500	3,000	2,12	27,65	
	AST			9,500	3,000	3,45	31,10	
	SCREEN			9,500	3,000	1,87	32,97	
	FLOAT SUB			9,375	3,000	0,58	33,55	Solid float valve
	ROLLER REAMER			17,500	3,125	2,30	35,85	
	XO			9,500	3,000	1,15	37,00	
	DC 8 1/4"			8,125	2,813	37,26	74,26	
	JAR			8,125	3,000	9,85	84,11	
	FLEX JOINT			8,000	3,000	2,52	86,63	
	DC 8 1/4"			8,125	2,813	18,67	105,30	
	INTENSIFIER			8,250	3,000	10,39	115,69	
	FLEX JOINT			8,000	3,000	2,65	118,34	
	DC 8 1/4"			8,125	2,813	9,38	127,72	
	XO			8,000	3,000	1,22	128,94	
	HW DRILL PIPE, 5½"			5,500	3,750	83,32	212,26	
	Remarks Timedrilled to sidetrack							

Table 29—Calculation on weights and lengths entered in the friction model for modeling the 17 ½" section from well A12.

	L	OD	OD	ID	ID	Vol	Wt	Wt	Wt	unit wt	Wt
BHA4	m	inch	m	inch	m	m3	kg	tons	N	kN/m	kN
component 1: Bit	0,34	17,50	0,44	3,00	0,08	0,05	402,00	0,40	3944	11,5989	3,94
component 2	0,44	17,40	0,44	3,00	0,08	0,07	514,13	0,51	5044	11,4627	5,04
component 3	6,61	9,63	0,24	2,38	0,06	0,29	2287,43	2,29	22440	3,3948	22,44
component 4	2,19	8,00	0,20	1,92	0,05	0,07	525,40	0,53	5154	2,3535	5,15
component 5	0,62	9,50	0,24	3,00	0,08	0,03	200,37	0,20	1966	3,1704	1,97
component 6	3,72	9,50	0,24	2,38	0,06	0,16	1251,95	1,25	12282	3,3015	12,28
component 7	1,24	17,50	0,44	3,50	0,09	0,18	1450,09	1,45	14225	11,4721	14,23
component 8	1,54	9,50	0,24	2,38	0,06	0,07	518,28	0,52	5084	3,3015	5,08
component 9	1,32	9,50	0,24	2,38	0,06	0,06	444,24	0,44	4358	3,3015	4,36
component 10	1,63	9,50	0,24	2,38	0,06	0,07	548,57	0,55	5381	3,3015	5,38
component 11	2,81	9,50	0,24	4,13	0,10	0,10	818,56	0,82	8030	2,8577	8,03
component 12	3,07	9,50	0,24	4,00	0,10	0,12	906,70	0,91	8895	2,8973	8,89
component 13	2,12	17,50	0,44	3,00	0,08	0,32	2506,60	2,51	24590	11,5989	24,59
component 14	3,45	9,50	0,24	3,00	0,08	0,14	1114,99	1,11	10938	3,1704	10,94
component 15	1,87	9,50	0,24	3,00	0,08	0,08	604,35	0,60	5929	3,1704	5,93
component 16	0,58	9,375	0,24	3,00	0,08	0,02	182,00	0,18	1785	3,0784	1,79
component 17	2,30	17,50	0,44	3,13	0,08	0,35	2712,42	2,71	26609	11,5691	26,61
component 18	1,15	9,50	0,24	3,00	0,08	0,05	371,66	0,37	3646	3,1704	3,65
component 19	37,26	8,13	0,21	2,81	0,07	1,10	8611,24	8,61	84476	2,2672	84,48
component 20	9,85	8,13	0,21	3,00	0,08	0,28	2233,87	2,23	21914	2,2248	21,91
component 21	2,52	8,00	0,20	3,00	0,08	0,07	551,30	0,55	5408	2,1461	5,41
component 22	18,67	8,13	0,21	2,81	0,07	0,55	4314,87	4,31	42329	2,2672	42,33
component 23	10,39	8,25	0,21	3,00	0,08	0,31	2440,92	2,44	23945	2,3047	23,95
component 24	2,65	8,00	0,20	3,00	0,08	0,07	579,74	0,58	5687	2,1461	5,69
component 25	9,38	8,13	0,21	2,81	0,07	0,28	2167,83	2,17	21266	2,2672	21,27
component 26	1,22	8,00	0,20	3,00	0,08	0,03	266,90	0,27	2618	2,1461	2,62
component 27	83,32	5,50	0,14	3,75	0,10	0,68	5364,83	5,36	52629	0,6316	52,63
BHA sum	**212,26**								**430573**	**2,0285**	**430,57**